

1982

Hydrogen storage with zirconium pseudobinaries.

Douglas G. Ivey
University of Windsor

Follow this and additional works at: <http://scholar.uwindsor.ca/etd>

Recommended Citation

Ivey, Douglas G., "Hydrogen storage with zirconium pseudobinaries." (1982). *Electronic Theses and Dissertations*. Paper 2341.

This online database contains the full-text of PhD dissertations and Masters' theses of University of Windsor students from 1954 forward. These documents are made available for personal study and research purposes only, in accordance with the Canadian Copyright Act and the Creative Commons license—CC BY-NC-ND (Attribution, Non-Commercial, No Derivative Works). Under this license, works must always be attributed to the copyright holder (original author), cannot be used for any commercial purposes, and may not be altered. Any other use would require the permission of the copyright holder. Students may inquire about withdrawing their dissertation and/or thesis from this database. For additional inquiries, please contact the repository administrator via email (scholarship@uwindsor.ca) or by telephone at 519-253-3000ext. 3208.

THESES CANADIENNES SUR MICROFICHE



National Library of Canada
Collections Development Branch

Canadian Theses on
Microfiche Service

Ottawa, Canada
K1A 0N4

Bibliothèque nationale du Canada
Direction du développement des collections

Service des thèses canadiennes
sur microfiche

NOTICE

The quality of this microfiche is heavily dependent upon the quality of the original thesis submitted for microfilming. Every effort has been made to ensure the highest quality of reproduction possible.

If pages are missing, contact the university which granted the degree.

Some pages may have indistinct print especially if the original pages were typed with a poor typewriter ribbon or if the university sent us a poor photocopy.

Previously copyrighted materials (journal articles, published tests, etc.) are not filmed.

Reproduction in full or in part of this film is governed by the Canadian Copyright Act, R.S.C. 1970, c. C-30. Please read the authorization forms which accompany this thesis.

THIS DISSERTATION
HAS BEEN MICROFILMED
EXACTLY AS RECEIVED

AVIS

La qualité de cette microfiche dépend grandement de la qualité de la thèse soumise au microfilmage. Nous avons tout fait pour assurer une qualité supérieure de reproduction.

S'il manque des pages, veuillez communiquer avec l'université qui a conféré le grade.

La qualité d'impression de certaines pages peut laisser à désirer, surtout si les pages originales ont été dactylographiées à l'aide d'un ruban usé ou si l'université nous a fait parvenir une photocopie de mauvaise qualité.

Les documents qui font déjà l'objet d'un droit d'auteur (articles de revue, examens publiés, etc.) ne sont pas microfilmés.

La reproduction, même partielle, de ce microfilm est soumise à la Loi canadienne sur le droit d'auteur, SRC 1970, c. C-30. Veuillez prendre connaissance des formules d'autorisation qui accompagnent cette thèse.

LA THÈSE A ÉTÉ
MICROFILMÉE TELLE QUE
NOUS L'AVONS REÇUE

HYDROGEN STORAGE WITH ZIRCONIUM PSEUDOBINARIES

by



Douglas G. Ivey

A Thesis
Submitted to the Faculty of Graduate Studies
Through the Department of Engineering Materials
in Partial Fulfillment of the Requirements for
the Degree of Master of Applied Science
at the University of Windsor

Windsor, Ontario

Canada

1982

© Douglas G. Ivey, 1982

772914

Abstract

Metal hydrides appear to be a promising medium for both energy transmission and storage. Hydrogen can be stored safely and the by-products of combustion consist essentially of pure water. Large quantities of hydrogen can be stored indefinitely and this stored energy can be recovered when needed. A literature survey has revealed that a number of hydrogen storage materials are under investigation, i.e., FeTi, Mg-alloys, LaNi₅, although none of these alloys fulfill all of the requirements of a hydrogen storage medium.

In this study, the author investigated a number of prospective zirconium-pseudobinary compounds of the type $Zr(B_x B'_{1-x})_2$, where B = Fe, Co, B' = Cr, Mn and x = 0.4, 0.5 or 0.6. The twelve alloys all exhibited two phase microstructures, identified as the cubic and hexagonal Laves phases. In all cases, hydrogen absorption increased the size of the lattice parameters and the volume of the unit cells without changing the crystal structure. Hydrogen capacities and hydride stabilities decreased with increasing 'x'. Desorption capacities were of the order of 65-80% of the absorption capacity for each of the alloys tested. The affect of prior oxidation on hydriding properties were variable. Hydrogen capacities were reduced somewhat in most cases, although $Zr(Fe_x Cr_{1-x})_2$, (x = 0.4, 0.5, 0.6), $Zr(Co_{0.4} Cr_{0.6})_2$ and $Zr(Co_{0.4} Mn_{0.6})_2$ demonstrated good resistance to oxidation poisoning, with hydrogen

capacities in the 0.75 - 1.0 H-atoms F.U.⁻¹ range.

ACKNOWLEDGEMENTS

The author wishes to express his sincere gratitude to Dr. Derek O. Northwood for his supervision and guidance throughout the course of this study. The author is indebted to the Atomic Energy of Canada, Chalk River Nuclear Laboratories, and especially to Dr. Graham Carpenter and Mr. Jim Watters, for the use of their vacuum arc furnace. Thanks are also in order to Mr. George Vazsonyi for his assistance in constructing the hydriding/dehydriding apparatus and metallography and to Mr. John Robinson for his help in the SEM and x-ray analysis.

TABLE OF CONTENTS

		<u>Page</u>
ABSTRACT.....		i
ACKNOWLEDGEMENTS.....		iii
TABLE OF CONTENTS.....		iv
LIST OF TABLES.....		vi
LIST OF FIGURES.....		vii
CHAPTER 1	INTRODUCTION.....	1
CHAPTER 2	LITERATURE REVIEW.....	5
2.1	Bonding and Electronic Factors of Metal Hydrides.....	5
2.2	Thermodynamics and Kinetics of Metal Hydrides.....	9
2.3	Hysteresis.....	16
2.4	Storage Criteria.....	18
2.5	Metal-Hydrogen Systems.....	19
2.6	AB ₂ Compounds.....	22
CHAPTER 3	EXPERIMENTAL METHODS.....	29
3.1	Materials.....	29
3.2	Melting and Casting of Alloys.....	29
3.3	Hydriding/Dehydriding Apparatus.....	30
3.4	Calculation of Quantity of Hydrogen Absorbed/Desorbed.....	32
3.5	Hydriding/Dehydriding Procedure.....	36
3.6	Metallography.....	37
3.6.1	Sample Preparation.....	37
3.6.2	Optical Microscopy.....	38
3.6.3	X-Ray Diffraction.....	38
CHAPTER 4	RESULTS.....	39
4.1	Microstructure.....	39
4.2	Hydriding/Dehydriding Characteristics.....	40
4.3	Phase Identification: X-ray Analysis.....	43
CHAPTER 5	DISCUSSION.....	45
CHAPTER 6	CONCLUSIONS.....	51

	<u>Page</u>
CHAPTER 7 FUTURE RESEARCH.....	52
REFERENCES.....	54
APPENDIX A.....	108
APPENDIX B.....	111
APPENDIX C.....	113
VITA AUCTORIS.....	131
PUBLICATIONS.....	132

LIST OF TABLES

<u>Table</u>		<u>Page</u>
1	Summary of Hydriding Behaviour of Metallic Hydride Systems (19).....	59
2	Summary of Hydriding Alloys and Their Properties.....	60
3	Hydrides of Zirconium Binaries and Pseudo-binaries.....	62
4	List of Metals Used, in the Forms and Purities Received.....	64
5	List of Twelve Alloys Utilized in Hydriding Experiments.....	65
6	Typical Results for Volume Calculation of Reactor, Using Ideal Gas Equation ($PV=nRT$), ($R=8.31441 \text{ J.mol}^{-1}\text{K}^{-1}$).....	66
7	Values of 'a' for the Two Calibration Curves of Figure 20.....	67
8	Lattice Parameters for the Twelve Alloys....	68
9	Effect of Hydriding on Lattice Parameters...	69
10	Comparison of X-Ray Results From This Work with Results of Shaltiel et al (55)	70
11	$\Delta H'$ Values for Partially and Totally Occupied Interstitial Sites in AB_2H_y Hydrides (79)	71
12	Comparison of Volume Changes with Final Hydrogen Capacity.....	72
13	List of Maximum Hydrogen Capacities in Terms of H/M Ratios.....	73

LIST OF FIGURES

<u>Figure</u>		<u>Page</u>
1	Schematic representation of the Hydrogen System (1).....	74
2	Summary of methods for hydrogen production (4).....	75
3	Periodic Table showing occurrence of binary hydrides. The underlined compounds cannot be prepared by a direct reaction (16).....	76
4	Electronegativities of the transition metals, the rare earths (RE) and the actinides in relation to hydrogen (19).....	77
5	Pressure-composition-isotherm (P-C-T diagram) showing the relationship between the equilibrium hydrogen pressure and the hydrogen concentration (16).....	78
6	Atomic cells in an intermetallic compound of two metals, A and B, with and without hydrogen present. The atomic cells of hydrogen are indicated by broken lines. Upon hydrogen absorption, the lattice is increased, which is not shown here (22).....	79
7	P-C-T diagram showing hysteresis in a metal-hydrogen system (16).....	80
8	The AB ₅ structure shown in both the hexagonal (right) and orthorhombic (left) lattices. Also shown are tetrahedral (●) and octahedral (■) hydrogen sites and their possible degeneracies (▲) (37).....	81
9	P-C-T plot for the LaNi ₅ -H system (39). Note that hysteresis is small at low temperatures.....	82
10	P-C-T plot for the FeTi-H system (47).....	83
11	P-C-T plot for the Mg ₂ Ni-H system (16).....	84
12	The cubic (C15) Laves phase is shown. The A atoms are shown as open circles and the B atoms as solid ones. The three types of interstitial sites are given: a) B ₄ sites, b) AB ₃ sites and c) A ₂ B ₂ sites (81).....	85

<u>Figure</u>		<u>Page</u>
13	The hexagonal (C14) Laves phase is given. The solid circles represent B atoms and the open circles A atoms. The interstitial sites are shown: a) B ₄ sites, b) AB ₃ sites and c) A ₂ B ₂ sites (81).....	86
14	The calculated heats of formation as a function of the hydrogen concentration are shown for the three types of tetrahedral sites in ZrV ₂ . At the concentration ~2.5, the 2-2 (A ₂ B ₂) and the 1-3 (AB ₃) interstices are competitive with respect to hydrogen occupation (62).....	87
15	Plot of hydrogen concentration against electron concentration (57).....	88
16	Schematic drawing of vacuum arc furnace, showing main components.....	89
17	Photograph of the reactor vessel, surrounded by a tube furnace. The dimensions and description are given in the text.....	90
18a	Schematic drawing of Hydriding/Dehydriding apparatus, illustrating key components.....	91
18b	Photograph of apparatus shown in Figure 18a.	92
19	Photograph of the ceramic (left) and nickel-alloy (right) crucibles utilized in this study.....	93
20	Calibration curves for determining the relationship between pressure, temperature and number of moles of gas in the reactor system. The two curves shown are for the 5th and 6th experimental runs.....	94
21	Optical micrograph of the microstructure of the Zr(Fe _{0.5} Mn _{0.5}) ₂ alloy, showing the two-phase region and the difference in etching. Also evident are elongated grains, characteristic of a cast structure.....	95
22	Optical micrograph of Zr(Mn _{0.5} Co _{0.5}) ₂ alloy illustrating the phase separation.....	96
23	Optical micrographs of a) Zr(Cr _{0.4} Co _{0.6}) ₂ and b) Zr(Fe _{0.5} Cr _{0.5}) ₂ samples, showing the rim structure between the phase separation. The rim structure is composed of the two phases, finely distributed.....	97

Figure

Page

24	P-C-T plot for the $Zr(Fe_{0.4}Cr_{0.6})_2-H$ system...	99
25	P-C-T plot for the $Zr(Fe_{0.5}Cr_{0.5})_2-H$ system...	100
26	P-C-T plot for the $Zr(Fe_{0.6}Cr_{0.4})_2-H$ system...	101
27	P-C-T plot for the $Zr(Co_{0.4}Mn_{0.6})_2-H$ system...	102
28	P-C-T plot for the $Zr(Co_{0.4}Cr_{0.6})_2-H$ system...	103
29	Plots of H/M ratio vs. 'X' for $Zr(B_xB'_{1-x})_2$ where B = Fe, Co and B' = Cr, Mn.....	104
30	P-C-T plots for the $Zr(Fe_xCr_{1-x})_2$ alloys. Note the increase in 'plateau' pressure and decrease in H/M ratio as 'X' increases.....	105
31	Schematic diagram of proposed hydriding system, showing major components.....	106
32	Schematic drawing of reactor design. Dimension are in centimeters.....	107

CHAPTER 1

Introduction

Hydrogen, as a medium for both energy transmission and storage, shows considerable promise. It is essentially non-polluting, the major by-product of combustion being water, and it can be generated from readily available and abundant raw materials and energy sources. Hydrogen has the highest energy density per unit weight of any chemical and can be utilized as an energy medium in a number of ways, ranging from internal combustion engines to fuel cells.

The inevitable decline in production of fossil fuels in the near future and greater environmental awareness require the development of new primary energy sources. The leading candidates include nuclear energy, geothermal energy, tidal power, hydroelectricity, wind power and solar energy (1). Most of these sources produce intermittently, remote from points of use. Thus, the conversion of these energy forms into another transportable energy medium, such as hydrogen, would be a necessity for full exploitation. This hydrogen could then be utilized in the desired manner to produce useful energy. A schematic representation of this so-called hydrogen system is shown in Figure 1 (1).

A number of limitations exist, however, preventing the immediate realization of hydrogen as a fuel. These problems lie in the areas of hydrogen production, utilization and storage.

Hydrogen can be extracted from fossil fuels and from

water (1,2,3,4,5). Fossil fuels are a limited and diminishing resource, while water can be regarded as inexhaustible.

Coal has been proposed as a short-to-medium range source for hydrogen, however, the high sulphur content presents an environmental risk. Water appears to be the obvious ultimate source of hydrogen. The splitting of water into hydrogen and oxygen can be achieved by electrolysis and thermo-mechanical processes (1,4). Neither of these methods is economical or practical at this time, with efficiencies of between 20 and 50 percent (4). Figure 2 summarizes the various methods available for hydrogen production (4).

Hydrogen can be utilized in a number of ways, including internal combustion engines (6), fuel cells (7,8), thermal engines (9), air-conditioning systems (10) and heat exchangers (11). Presently, internal combustion engines and fuel cells appear to be the most important utilization methods. The conversion of conventional gasoline powered internal combustion engines to hydrogen can be accomplished with only a few modifications, thereby providing an immediate to near-future method of utilization. Even now, a number of automobiles and buses have been successfully converted in both the United States and Europe. Fuel cells, though, appear to be the way of the future as their total efficiency exceeds that of internal combustion engines (7). A number of experimental fuel cells have been developed and show some potential, for example, a hydride-air fuel cell (7) and a Ni-H₂ battery (8). Problems still exist in areas such as meeting power requirements, reliability and

battery lifetime (7,8).

The major methods for storing hydrogen are liquid storage, glass microspheres and metal hydrides. Liquid hydrogen is stored in a Dewar flask and the major cost lies in liquefaction (12,13). For a refrigeration cycle that is 33 percent efficient, the energy for liquefaction is estimated at 10 kW-h-kg^{-1} . This quantity is 25 percent of the heat available from combustion of the hydrogen (13).

Microspheres are small glass spheres, 6 to 60 microns in diameter, made from fly ash (12). These spheres are permeable to hydrogen at high temperatures and impermeable at low temperatures. Most of the expense, in this case, is due to the refilling stage where the hydrogen must be compressed and the system heated to 300°C . The energy required for this process is estimated at 3 percent of the energy available during combustion.

Metal hydrides are chemical compounds of metals and hydrogen (14,15). Hence, the hydrogen is stored safely inside the metal itself and the amount of hydrogen stored per volume can exceed that of liquid or gaseous storage methods. Hydrogen is absorbed into the metal by exposing the surface to the pressurized gas at room temperature. The stored hydrogen can be released by heating the hydride to the appropriate temperature. The absorption cycle is exothermic in nature, while the desorption process is endothermic. The heat required to liberate the hydrogen from the hydride can be obtained from waste heat generated in the energy conversion system. The materials that have received the

most interest as solid storage mediums are FeTi, LaNi₅ and Mg (12). However, none of these materials meet all the requirements necessary for storage.

The objective of this study was to investigate the feasibility of hydrogen storage via metal hydrides and in particular zirconium pseudobinary compounds of the form $Zr(B_x B'_{1-x})_2$ where B = Fe, Co; B' = Cr, Mn; and x = 0.4, 0.5, and 0.6. The alloys were produced by melting and casting the pure metals in an arc melting furnace. A hydriding/dehydriding procedure was attempted on each of these melts in an apparatus constructed for this purpose. Changes in the lattice parameters and/or structures between the hydrided and unhydrided alloys were determined by x-ray diffraction techniques. Optical metallography was performed on sectioned, unhydrided samples in an attempt to relate hydriding characteristics to prior microstructure.

Literature Review2.1 Bonding and Electronic Factors of Metal Hydrides

Hydrogen reacts with metals to form three kinds of metal hydrides, namely saline or ionic, metallic and covalent (14, 15). The ionic type bond is made up of metal cations and hydrogen anions. These hydrides are formed by the direct reactions of hydrogen with alkali or alkaline earth metals. The elements are located in groups IA and IIA of the Periodic Table, as shown in Figure 3. The alkali metal hydrides have a sodium chloride type structure, while the alkaline rare earth hydrides exhibit a barium chloride structure. In general, these hydrides are too stable for hydrogen storage applications, with the exception of magnesium which demonstrates some covalency.

Covalent hydrides are made up of beryllium and many of the B group metals of the Periodic Table. The hydrides may be solid, liquid or gaseous and can be quite unstable. None of these hydrides are formed by reacting directly with the metal, which eliminates them in storage applications. The type of bonding exhibited by most potential hydrogen storage hydrides is metallic in nature. Metallic hydrides have a metallic appearance and high thermal and electrical conductivities. They are formed by the reaction of hydrogen with most of the elements of groups IIIA - VIIIA in the Periodic Table (Figure 3). In the past, the metallic bond has been explained by an anionic or protonic model (15). The anionic model assumes charge transfer from

the metal to the hydrogen site, while the protonic model suggests that the electron, from the hydrogen atom, deserts its proton and occupies the d-band of the metal. These models have subsequently been modified and combined (17,18).

There are a number of general observations that can be made concerning metallic hydrides (19):

1) The metal atoms in metallic hydrides are at least trivalent. Orbital overlap necessitates that there be close metal-metal spacing and entering hydrogen should be considered to be metallic;

2) The majority of catalytic properties of transition metal and rare earth hydride systems can be explained in terms of d-electron interaction;

3) Most of the properties of the actinide systems (up to plutonium) can be explained in terms of f-electron interactions;

4) If the d (or f) electrons are tied up in metallic bonding, they will not, in general, be readily available for chemisorption-catalysis. Conversely, if the d (or f) electrons are not involved in metallic bonding, they will usually be available for chemisorption-catalysis.

The type of metals making up the metallic bonds can be divided into three groups, that is the highly electropositive metals, the "less electropositive" metals, and the "still less electropositive" metals (19).

The highly electropositive metals consist of the actinides, the rare earths and the early transition metals.

The basic properties are as follows:

- 1) The difference in electronegativities (Δn) between these metals and hydrogen lie in the range 0.5-1.0 (see Figure 4);
- 2) The heats of reaction and solution are exothermic;
- 3) Hydrogen atoms are found in tetrahedral positions;
- 4) Hydriding reactions tend to be poisoned by electrophilic (electron seeking) molecules.

The "less electropositive" metals are made up of metals such as iron, cobalt, tungsten, etc. and exhibit these properties:

- 1) Hydrides are not formed easily because of high valencies, large cohesive energies, and lattices that are too small;
- 2) The difference in electronegativities (Δn) is in the range 0.5-0.2;
- 3) Heats of solution become endothermic;
- 4) They may cause major electronic effects as alloy additions.

The "still less electropositive" metals include such metals as nickel and palladium. These metals are characterized as follows:

- 1) They form hydrides in a complex manner by adding electrons both to the nearly filled metal d states and also to the new state drawn below the Fermi level;
- 2) Heats of solution and reaction are complex;
- 3) Hydrogen atoms are found in octahedral positions;
- 4) Hydriding reactions tend to be poisoned by electrophobic (electron donating) molecules.

A plot of the electronegativities is shown in Figure 4. The circled metals do not form hydrides while those in brackets can be forced into an unstable hydriding configuration. The differences between the electronegativities (Δn) of hydrogen and a particular metal may be viewed as a driving force of potential for reaction.

Electronic processes in or near the valence-band region can produce large chemical and structural effects (19). The presence of oxide (and/or hydroxide) films, inclusions, grain boundary impurities, etc. may be of major importance in dealing with catalytic properties. In the case of the electropositive metals, it appears that hydride initiation (and poisoning) may occur at such sites, rather than directly on the metals. A summary of hydriding properties is given in Table 1.

In terms of electrons for chemisorption for extremely pure samples of those metals in which the d electrons (e.g., Ti and Zr) or f electrons (e.g., α -U, α -Np, and α -Pa) are almost totally involved in metallic bonding, hydriding is very difficult to initiate. Hydrogen, however, dissociates on the late transition metals almost without an energy of activation. A palladium or nickel flashing or coating over a more electropositive metal may provide an immediate source of dissociated hydrogen and therefore rapid attack. Electrophobic molecules can poison this dissociation by giving electronic charge to the metal levels that would be ordinarily available.

2.2 Thermodynamics and Kinetics of Metal Hydrides

Hydrogen reacts reversibly with the metal by means of the following reaction:



The forward reaction is generally quite exothermic, the heat of formation approaching the heat of combustion of hydrogen in some compounds. The direction of the above equation depends on the hydrogen pressure in the system.

The behaviour of metal-hydride systems can be best represented by a pressure, composition, temperature, (P-C-T) diagram. It is a plot of pressure or composition at various temperatures as shown in Figure 5 (16). The initial steep slope corresponds to hydrogen going into solid solution and this single phase region is usually denoted as the α -phase. Where the curve begins to change slope on the P-C-T diagram denotes the appearance of a metal hydride or β -phase. The solubility of hydrogen in many metals can be quite high, which results in many metal hydrides that are non-stoichiometric. With the formation of the second phase, the hydrogen pressure remains constant and a 'plateau' results, as more hydrogen is added. The concentration of hydrogen in each phase does not change, only the relative amounts of each phase. The plateau continues as long as there are two distinct phases, as required by Gibbs' phase rule (20,21):

$$F = C - P + 2$$

where 'P' is the number of phases, 'C' is the number of components and 'F' is the degrees of freedom. An additional hydride phase, the γ -phase, may also be formed, in which case a second and higher plateau will appear.

The thermodynamics for the formation of a metal hydride can be derived from the van't Hoff isobar (16):

$$\frac{d \ln K}{dT} = \frac{\Delta H}{RT^2}$$

where 'R' is the gas constant, 'T' is the temperature and ΔH is the heat of reaction.

The equilibrium constant (K) is given by:

$$K = \frac{a_{MH_x}}{a_M^f H_2^{x/2}}$$

In this equation, the activities (a) can be considered to be ~1, since we are working with essentially pure phases. The fugacity (f), because of low pressures, is equivalent to the pressure. Assuming ΔH to be constant (over a relatively small temperature range), the van't Hoff isobar can be written as:

$$d \ln \left(\frac{P_{H_2}^{-x/2}}{1} \right) = \frac{\Delta H}{RT^2} dT$$

or

$$\ln \frac{P_{H_2}^{-x/2}}{1} = \frac{2}{x} \frac{\Delta H}{RT} + C \quad (2.2)$$

where 'C' is the constant of integration. If the hydride is stoichiometric and the solubility of hydrogen is small in the α -phase, the standard enthalpy of formation can be determined

from the slope of a plot of $\ln P_{H_2}$ vs. $\frac{1}{T}$.

The free energy change can be determined by the standard relation:

$$\Delta G = \Delta G_f^\circ + RT \ln K$$

where ΔG_f° is the standard free energy change. At equilibrium,

$\Delta G = 0$, which implies that:

$$\Delta G_f^\circ = -RT \ln K$$

or,

$$\Delta G_f^\circ = \frac{x}{2} RT \ln P_{H_2} \quad (2.3)$$

The standard entropy of formation can be determined by:

$$\Delta S_f^\circ = \frac{\Delta H_f^\circ - \Delta G_f^\circ}{T} \quad (2.4)$$

where ΔH_f° is the standard enthalpy of formation.

In systems that are appreciably non-stoichiometric, the standard enthalpy of formation is the sum of three components: the integral heat of solution of hydrogen in the α -phase from zero hydrogen content to saturation, the heat of reaction in going from the hydrogen saturated α -phase to the non-stoichiometric β -phase, and the integral heat of solution of hydrogen in the hydrogen-poor β -phase to the stoichiometric value. This also holds for ΔG_f° and ΔS_f° . In cases where there are large deviations from stoichiometry, the thermodynamic quantities are usually expressed as relative partial molal quantities $(\bar{X}_H - \frac{1}{2}X_{H_2}^\circ)$, where \bar{X}_H is the partial molal enthalpy (or entropy or free energy) of hydrogen atoms in the solid and $X_{H_2}^\circ$ refers

to hydrogen in its standard state as a pure, diatomic ideal gas. To obtain the integral quantities, the partial values are integrated over the entire composition from the pure metal to the stoichiometric hydride (16).

Binary hydrides, i.e., hydrides made up of only one type of metal and hydrogen, are generally too stable for storage application, i.e., require too much energy for hydrogen removal, with the possible exception of MgH_2 . Consequently, most of the storage materials under consideration are binary or pseudobinary alloys. These alloys form ternary hydrides with substantially lower stabilities.

Miedema et al (22,23) have developed a thermodynamical model regarding the formation and dissociation of ternary hydrides. The assumptions entering in and the implications coming out of this model are stated as:

a) The energy effects in alloys of two transition metals, and alloys of transition metals with noble or alkali metals, are mainly nearest neighbour effects.

b) The stability of a hydride can be expressed as a function of ΔH alone. The criterion for a hydride to be stable with an equilibrium pressure at room temperature below 1 atm is:

$$\Delta H = T\Delta S (H_2, \text{ gas}) \sim -9 \text{ kcal/mole } H_2$$

c) Intermetallics, that can absorb large quantities of hydrogen near room temperature, have at least one metallic element that can form stable binary hydrides. Examples are

Sc, Y, La, Ti, Zr, Hf, Th, U and Pu.

d) The heat of formation of a ternary hydride,

$AB_n H_{2m}$, from the binary intermetallic AB_n and gaseous H_2 can be resolved into:

$$\Delta H(AB_n H_{2m}) = \Delta H(AH_m) + \Delta H(B_n H_m) - \Delta H(AB_n) \quad (2.5)$$

For the ternary hydride to be stable at room temperature, with a dissociation pressure of 1 atm., the heat of formation has to be more negative than -9 kcal/mole H_2 .

A schematic representation for ternary hydrides (22) is shown in Figure 6. Metal A is the minority metal in the compound AB_n and attracts hydrogen (hydrides of A are more stable than those of B). The hydrogen atoms primarily surround the A metal atoms. There are contacts between the A atoms and the hydrogen and likewise contacts between the B atoms and hydrogen, while the atomic contact between A and B, that was responsible for the heat of formation of the original compound, is lost. The contact surface area is approximately the same for A-H and B-H, thereby implying that the ternary hydride, $AB_n H_{2m}$, is energetically equivalent to a mechanical mixture of AH_m and $B_n H_m$, so that the heat of formation is given by equation (2.5).

It seems that the negative component of equation (2.5) has the greatest effect and leads to the rule of reversed stability (22). This rule states that the more stable the binary intermetallic compounds one starts with, the less will be the tendency to form stable hydrides. There will only be the formation of a stable ternary hydride if at least

one of the metals (A) forms fairly stable binary hydrides.

For this reason, A is restricted to metals such as Sc, La, Y, Ti, Zr, Hf, Th, U or Pu.

In metal hydrogen systems, the configurational entropy (ΔS) is relatively constant (22,23,24) and is equal to -30.0 ± 6 cal/deg.mole H_2 . This entropy effect is predominantly due to the high entropy of hydrogen as a gas, (31.0 cal/deg.mole H_2 at room temperature), which is lost upon entering the metal. Because of the relatively constant value of ΔS , the enthalpy value is usually considered the more important value. However, Gruen and Mendelsohn (24) show that entropy changes in a number of AB-H systems differ by up to 6.5 eu/mole H_2 leading to differences of about 2 kcal/mol H_2 in the free energies of reactions at 300K. This corresponds to changes of more than one order of magnitude in hydrogen dissociation pressures.

The reaction kinetics of hydrogen absorption and desorption in metal-hydrogen systems is an important consideration in selecting materials for practical storage applications. Kinetics are hard to follow quantitatively because many hydriding reactions have rate constants of the order of a few seconds. Conventional experimental methods cannot follow such rapid changes. A temperature change of a few degrees Celsius is sufficient to alter the kinetics significantly.

The 'plateau' behaviour exhibited by hydride systems is similar to many of the phase transformations of the nucleation and growth type (25).

$$F(t) = 1 - \exp \{-(t/\tau)^n\} \quad (2.6)$$

where $F(t)$ is the fraction of reaction completed at time t ; τ is the reaction rate time constant (relaxation time), and n is an integer or half-integer, the value of which is governed by the geometries associated with the rate controlling process. For the $\alpha \rightarrow \beta$ transformation, the fraction of the reaction completed is given by:

$$F(t) = \frac{W(t) - W_\alpha}{W_\beta - W_\alpha} \quad (2.7)$$

where $W(t)$ is the weight of absorbed hydrogen at time t , W_α is the weight of absorbed hydrogen in the α -phase limit and W_β is the weight of absorbed hydrogen in the β -phase hydride. Problems are usually encountered in relating these theoretical equations to the actual cases. This is due to the fact that most experimental P-C-T diagrams do not exhibit flat, horizontal plateaus. The slope in the plateau indicates that different portions of the hydride material hydrate at different pressures (25). Impurities, inhomogeneities, particle size and stresses could all be factors contributing to this phenomenon.

The majority of work done on hydriding/dehydriding kinetics to this point in time has been qualitative in nature. The kinetics vary depending upon the material in question. Kinetic, as well as thermodynamic, properties can be affected by alloy composition and crystal structure. Poisoning effects must also be considered, as contaminants may affect the rate-controlling processes. Kinetics are

also directly dependent upon the system pressure (26).

The greater the difference between system pressure and equilibrium pressure the faster the reaction rates.

Kinetics can vary from very fast absorption/desorption rates in alloys such as LaNi_5 , where the reaction rate is controlled by heat transfer (27) to extremely sluggish rates in Mg-alloys, which can be governed by dissociative chemisorption and associative desorption (28).

2.3 Hysteresis

In many metal-hydrogen systems, hysteresis has been found. This phenomenon occurs when the transition pressure in the P-C-T curve is higher for absorption than for desorption. An example of hysteresis is shown in Figure 7. The cause of hysteresis is not fully understood. However, lattice expansion on hydriding is believed to be of importance (29,30). The hydride phase seems to cause an irreversible plastic deformation in the matrix. Desorption of a small amount of hydrogen primarily relaxes the residual forces so that the phase is no longer under stress. Therefore, desorption should occur at a lower critical transition pressure. Because of strain sensitivity, the amount and size of impurities as well as processing history have considerable effect on the absorption pressure plateau.

Another explanation for hysteresis is the defect theory by G.G. Libowitz (31). This theory assumes that there are non-stoichiometric vacancies in the lattice. As hydrogen is withdrawn from the stoichiometric hydride,

hydrogen vacancies are formed, and the hydride becomes non-stoichiometric. At the composition where the lattice becomes saturated with vacancies further removal of hydrogen causes the lattice to break down, thus forming a two-phase system. Therefore, the plateau pressure is actually the equilibrium pressure of non-stoichiometric hydride. On hydriding, it is possible, because of the longer time to reach equilibrium, that a rather stable metastable hydride is formed having fewer vacancies (higher hydrogen composition) than the stable hydride. The metastable hydride, because of the lower stability, has a higher dissociation pressure. Since the hydriding phase has fewer vacancies the hydriding curve on a P-C-T diagram extends further to the right than the dehydriding curve, as shown in Figure 7.

Flanagan et al (32) have proposed another approach to hysteresis, based on the solvus behaviour in the palladium-hydrogen system. Large dislocation densities, of the order of $\sim 10^8 \text{ m}^{-2}$, are introduced by the $\alpha \rightarrow \beta$ or $\beta \rightarrow \alpha$ phase transitions. The dislocation density in the $\alpha \rightarrow \beta$ followed by the $\beta \rightarrow \alpha$ transformation is about twice that found in the $\beta \rightarrow \alpha$ phase transition. It, therefore, appears that each phase transition leads to its own characteristic dislocation pattern and the contribution due to the reversal of dislocation motion is negligible. In the previous explanations, the desorption isotherm ($\beta \rightarrow \alpha$ transition) was said to approximate the equilibrium condition, whereas

Flanagan et al show that neither $P_{\alpha+\beta}$ or $P_{\beta+\alpha}$ corresponds to equilibrium, since dislocations, non-equilibrium defects, are generated along each plateau pressure branch.

The degree of hysteresis in a metal-hydrogen system can be affected by the type of testing. Hysteresis is more pronounced in dynamic tests than in conventional static tests (27). This effect could be due to deformation disordering of the metal lattice by cycling through the high capacity range. An effect of this type has been noted in AB compounds, FeTi (27) and ZrCo (33).

Even though a number of arguments exist on the causes of hysteresis, it is generally agreed that hysteresis reduces the efficiency of hydrogen storage systems.

2.4 Storage Criteria

For hydrides to be useful as energy storage media, a number of requirements are necessary. The hydride should:

- 1) be capable of storing large quantities of hydrogen;
- 2) be readily formed and decomposed;
- 3) be as safe as other energy carriers;
- 4) have reaction kinetics satisfying the charge/discharge requirements of the system;
- 5) have the capability of being cycled without alteration in pressure or temperature during the life of the system;
- 6) have low hysteresis;
- 7) have resistance to poisoning from contaminants

such as O_2 , H_2O , CO , etc.;

8) have low cost.

A number of materials have been developed but none of them meet all these requirements.

2.5 Metal-Hydrogen Systems

The metal-hydrogen systems currently under investigation can be divided into five classes, namely, AB_5 , AB , AB_2 , Mg-based and AB_3 and A_2B_7 compounds. Each of these systems will be discussed briefly. Table 2 summarizes the properties of each alloy class as they relate to the storage criteria. Interested readers are referred to publications (34,35,36) for further information.

In the AB_5 system, the majority of work has been done on $LaNi_5$. This material has a hexagonal or orthorhombic structure with a $CaCu_5$ type lattice, as shown in Figure 8 (37,38). Hydrides are formed with plateau pressures of a few atmospheres at temperatures up to $100^\circ C$ (37,38), see Figure 9. The ΔH value is of the order of $-7.2 \text{ kcal-mol}^{-1} H_2$. Attractive properties include high hydrogen capacity, low hysteresis, tolerance to gaseous impurities and ease of activation in the initial cycle (39,40,41,42). $LaNi_5$ also shows good kinetics, the reaction rate being controlled by heat transfer, with nickel serving as a catalyst for the hydrogenating reactions (27,39,40). The major problems, associated with this material, lie in the area of alloy cost and cyclic degradation (43). Alloy cost can be lowered somewhat by substituting Ce, Nd, Gd, Y, Er, Th and Zr for La (22,37,38) and Al, Co, Fe, Cr and Cu for Ni

(22,44,45,46).

The AB alloys store hydrogen at a low cost and exhibit plateau pressures of a few atmospheres at temperatures up to 100°C. Most of the work done on AB compounds has been restricted to FeTi, which has a CsCl type crystal structure (47). The pressure-composition isotherms for the FeTi-H system are shown in Figure 10. Two hydrides are formed, i.e., a monohydride with a tetragonal structure and a dihydride which forms a cubic structure (48). The ΔH value for the monohydride is $\sim 6.5 \text{ kcal-mol}^{-1} \text{ H}_2$. It is necessary to initially activate FeTi before it will react at a practical rate with hydrogen (49,50). Reaction kinetics are considerably slower than in the AB₅ case (27,51) and can be affected severely by contaminants such as O₂, H₂O and CO (42,52,53). Other disadvantages of the FeTi-H system are pronounced hysteresis and the weight of the hydrides (57,54). These problems can be alleviated to a degree by the substitution of various alloying elements, such as Mn and Al for Fe. Manganese assists in providing a reduction in hysteresis and some resistance to poisoning (42,53), while aluminum helps to lower the overall weight of the alloy (47,54).

The AB₂ compounds have a high storage capacity, show good resistance to impurities and exhibit low hysteresis (55,56,57,58). These alloys form one of two Laves phases, either the hexagonal C14 structure (59) or the cubic C15 structure (60). The AB₂ materials of interest have the general formula ZrB₂, where B = V, Mn, Cr, Co, Fe, Mo. The

best sorption characteristics have been observed for ZrV_2 , ~~$ZrCr_2$ and $ZrMn_2$~~ with hydrogen pickup approaching ~ 6 H atoms per formula unit (56,57,58). Hydrogen absorption in all of these binaries results in a lattice expansion. Hydrided AB_2 compounds tend to be quite stable, with ΔH values greater than 12 kcal-mol^{-1} in magnitude. A method of lowering the stability, while at the same time maintaining adequate absorption capacity, is to substitute some of the Mn, Cr, Mo or V with Fe or Co (55,61,62,63). In this way, stabilities can be reduced to acceptable levels. Partial substitution of Ti for Zr can also be employed with the result of reducing the cost of the hydriding alloy (64,65).

Magnesium, as a hydrogen storage material, meets two very important storage criteria. It can store large quantities of hydrogen (6.7wt%), i.e., more than twice as much as either $LaNi_5$ or FeTi, and it is inexpensive. However, on the negative side, the Mg-H system has poor reaction kinetics and the hydride that is produced is too stable for most practical applications (66-72). Elements such as Cu and Ni have been added to Mg either as alloying additions or catalysts (16,28,66-72). Although the absorption capacity is diminished, these elements can improve the reaction kinetics by providing an oxide-free path for hydrogen sorption. The pressure-composition isotherms for the Mg_2Ni -H system are shown in Figure 11. Additions of rare earths (72,73) and transition metals (73) have been somewhat successful in increasing desorption rates of hydrogen in magnesium.

The AB_3 compounds, in general, form hydrides that are quite stable and they exhibit little or no hysteresis (37, 74-77). The A_2B_7 materials are also quite stable, though slightly less stable than their AB_3 counterparts (74,76). A number of AB_3 compounds absorb hydrogen to a H/M ratio equal to or greater than 1.0, namely $ErCo_3$ ($ErCo_3H_{5.5}$), $PrCo_3$ ($PrCo_3H_5$), $CeCo_3$ ($CeCo_3H_4$) and D_YCo_3 ($D_4H_{4.25}$) (37,76,77). Most A_2B_7 compounds don't approach a H/M ratio of 1.0, with Ce_3Co_7 showing the highest capacity at $H/M \sim 0.67$ (76). Very little has been done in the areas of reaction kinetics, cyclability and resistance to poisoning, therefore no results are reported.

2.6 AB_2 Compounds

The AB_2 compounds are the most recent of the storage systems. As mentioned previously, they form hydrides with a high storage capacity and resistance to impurities. However, their high thermal stability has resulted in limited technological developments.

The AB_2 compounds form one of two structures, either the cubic C15 structure (60) or the hexagonal C14 structure (59). These crystal structures are shown in Figures 12 and 13. Both of these structures are Friedel-Laves phases, belonging to a group of lattice types in which all interstices are formed by tetrahedra (62,64,78-81). As a result, hydrogen absorption increases the size of the unit cell without changing the structure. There are three types of interstitial sites; namely AB_3 , A_2B_2 and B_4 , where A and B represent the atoms surrounding the sites.

Shoemaker and Shoemaker (80) have found the total number of interstitial sites per AB_2 unit to be seventeen. This number is made up of four AB_3 sites, twelve A_2B_2 sites and one B_4 site. However, hydrogen absorption never comes close to a value of seventeen hydrogen atoms/formula unit. The primary limiting principle is an electrostatic one. Because hydrogen is more electronegative than the metal atoms, on hydriding the hydrogen atoms become negatively charged. The decrease in enthalpy that accompanies the charge transfer and the resulting electrostatic interactions are important contributions to the enthalpy of absorption. These must overcome the energy of the H-H molecular bond and the considerable entropy decrease on absorption. Consequently, in a stable hydride the charged hydrogen atoms cannot occupy positions too close to one another (80). Shoemaker and Shoemaker (80) have proposed the following exclusion rule: two tetrahedra having a triangular face in common may not both accommodate hydrogen atoms at their centres. By employing this rule, Shoemaker and Shoemaker have deduced a maximum hydrogen occupancy of 6 atoms per formula unit for the C15 structure and $6\frac{1}{3}$ atoms per formula unit for the C14 structure. This calculation is in good agreement with experimental maximum capacities (55-58,79).

Shaltiel (81) and Didisheim et al (57) have attempted to determine which interstitial sites are occupied by hydrogen (or deuterium) atoms. Shaltiel (81) has proposed a modified approach to the rule of reversed stability (22,

23). In order to compare the relative stability of hydrogen atoms in different sites of the metal, a value $\Delta H'$ is assigned to each site, which is the sum of the heats of formation of elementary (imaginary binary) hydrides formed by the surrounding A and B atoms. The heat of formation of these hydrides can be deduced by using the theory of Miedema (22,23), assuming each hydrogen site is equally divided between the surrounding metal atoms (this probably isn't true). The hydrogen will preferably occupy interstitial sites with large negative ΔH values.

Didisheim et al (57) have calculated $\Delta H'$ values for the ZrV_2 -D system and the values are plotted against hydrogen (deuterium) concentration in Figure 14. It is evident that there is a greater tendency for interstices to attract hydrogen as the number of Zr(A) atoms surrounding the site increases. Therefore the A_2B_2 interstices are occupied first. At a critical concentration x' , the $\Delta H'$ values for A_2B_2 and AB_3 holes become equal. At concentrations greater than x' , there should be competition between the two sites and both should absorb hydrogen. The B_4 sites have small $\Delta H'$ values and therefore little or no absorption is expected. These predictions are confirmed experimentally (at least qualitatively) by neutron diffraction studies done on the ZrV_2 -H system (57,79).

Shaltiel's model, although it offers good qualitative agreement, neglects some important contributions to stability (57). One is the weakening of the metal-metal bonds caused by interstitial hydrogen (deuterium) and lattice

expansion. This corresponds to the last term of the rule of reversed stability. The second contribution is the electrostatic repulsion of deuterium atoms, and the third is the loss of stability due to a loss in entropy.

There are a number of zirconium based alloys of the AB_2 classification, that are receiving considerable interest. These alloys have the general formula ZrB_2 , where B equals V, Cr, Mn, Fe, Co or Mo. Hydrogen absorption decreases significantly with an increase in the 3d occupation number of transition elements (B) across the 3d series (55). The maximum absorption capacity of ZrV_2 is ~6 H atoms per formula unit (57,58) while that of $ZrFe_2$ or $ZrCo_2$ is less than 0.2 H atoms per formula (56). ZrV_2 , which absorbs the most hydrogen of the series, is the only intermetallic in the Zr-V system. There are two phases present in the intermetallic, one hexagonal and the other cubic. Both phases take part about equally in the hydriding process and the basic structure is unchanged. Both Zr_2V_2 and ZrV_3 sites are involved in hydriding, although the more favourable site remains that which presents the higher number of Zr neighbours (58). $ZrCr_2$, like ZrV_2 , absorbs large quantities of hydrogen, approximately 1.3 atoms per formula unit (56,58). It also exhibits no hysteresis and has an extremely low equilibrium pressure at room temperature. $ZrCr_2$ has a C15 cubic structure and some of the cubic phase transforms to a C14 hexagonal hydride, when the absorption limit is approached. The majority of hydrogen is contained in the

Zr₂Cr₂ sites with a small amount in ZrCr₃ sites. This could be due to a critical hydrogen concentration (x') being reached at $x' \sim 3.5$, as discussed earlier (57). The intermetallic, ZrMo₂, demonstrates slow absorption and desorption kinetics (56). The amount of hydrogen absorbed at even low temperatures is only ~ 0.26 atoms H/formula unit. As in the other ZrM₂ compounds, no hysteresis is evident. The other three ZrM₂ intermetallics, i.e., ZrMn₂, ZrFe₂, and ZrCo₂, with the exception of ZrMn₂, have hydrogen absorptions that are somewhat lower. The hydrogen absorption in these ZrB₂ compounds can be related to their electron concentrations (56) as shown in Figure 15. The plot shows that hydrogen dissolution contributes to electron concentration to the extent that phases with lower electron concentration accommodate more hydrogen than those with higher electron concentration. There is other evidence present in the literature that substantiates the claim that electronic factors are more important for AB₂ compounds than structural factors. Both Shaltiel et al (62,64) and Mendelsohn and Gruen (63) present evidence of this work done on pseudobinaries with C14 and C15 structures.

For the ZrB₂ compounds, a method of raising the equilibrium pressure while maintaining high absorption levels is by the formation of pseudobinary compounds. Substituting some of the V or Cr with Fe or Co decreases the hydrogen capacity some and significantly increases the plateau pressure (55,62,73,80). Many of the pseudobinary compounds,

i.e., $Zr(Co_x M_{1-x})_2$ and $Zr(Fe_x M_{1-x})_2$ form hydrides suitable for storage. Activation is only necessary in a few cases to initiate absorption. For compounds with $M=V$ or Cr , the crystal structure changes, as a function of 'x', from a cubic C15 structure to hexagonal C14 and back again. For the case where $M = Mn$, there is a change from hexagonal to cubic. Hydrogen absorption causes a lattice expansion in these alloys and the following observations have been made (55,62):

- 1) The value of hydrogen capacity decreases as 'x' increases;
- 2) Compounds containing V show a sharp decrease in hydrogen capacity in the areas $0. < x < 0.5$ and $0.85 < x < 1.0$;
- 3) Compounds containing Mn and Cr do not have the initial sharp decrease as in (2), but there is a sharp decrease for $0.6 < x < 1.0$;
- 4) Comparing absorption capacity of compounds containing Mn with those containing Cr reveals relatively small differences for values up to $x \sim 0.6$;
- 5) Pseudobinaries exhibit hysteresis between absorption and desorption isotherms.

Because of the cost and weight of zirconium, some substitution has been investigated. Two such alloys are $Ti_{1-x}Zr_xMn_2$ (64,65) and $Ti_{1-x}ZrCr_2$.

The following observations have been made:

1) The hydrogen absorption capacity of the $\text{Ti}_{1-x}\text{Zr}_x\text{Cr}_2$ system increases linearly with x from 3.3 H atoms/formula unit at $x = 0.0$ to 4.5 H atoms/formula at $x = 1.0$;

2) Hydrogen absorption increases for $(\text{Zr}_x\text{Ti}_{1-x})\text{Mn}_2$ from 0.3 H atoms/formula at $x = 0.0$ to 3.65 H atoms/formula at $x = 0.4$; from $0.4 < x < 1.0$, hydrogen absorption is ~4.0 H atoms/formula;

3) The $(\text{Zr}_x\text{Ti}_{1-x})\text{Cr}_2$ hydrides do not release all the hydrogen upon desorption;

4) The $(\text{Zr}_x\text{Ti}_{1-x})\text{Mn}_2$ hydrides release all absorbed hydrogen.

A list of various AB_2 type binaries and pseudobinaries are given in Table 3 along with their corresponding hydrogen absorption properties.

CHAPTER 3

Experimental Methods

3.1 Materials

The alloys employed were made from high purity metals which were purchased in the various forms and purities listed in Table 4. The zirconium and iron were received in bulk form and therefore had to be cut into smaller pieces. These pieces were subsequently cleaned of oil and other contaminants by soaking in an agitated bath of acetone followed by an alcohol bath. The appropriate amounts of each constituent were measured out on a microbalance prior to melting.

3.2 Melting and Casting of Alloys

The alloys were melted and cast in a vacuum arc furnace at Atomic Energy of Canada's Chalk River Nuclear Laboratories. A schematic drawing of the apparatus is given in Figure 16. For each alloy the alloying elements in the correct proportions were laid out in the water cooled, copper crucible. A quartz cover was then placed over the crucible and secured. The enclosed chamber was evacuated by pumping down with mechanical and oil diffusion pumps. The chamber was then filled with purified, argon gas at a pressure of approximately 0 kPa gauge. This degassing/gassing procedure was repeated and then the furnace was pumped down to a vacuum of 10^{-6} to 10^{-7} Torr.

The furnace was operated under an argon pressure of -60 to -40 kPa gauge. An arc was struck between the

thoriated-tungsten tipped tungsten electrode and a pad of pure zirconium. The current was adjusted until a molten pool of zirconium was established. The electrode was then moved over to the sample and drawn slowly across its length and back again. The gap between the electrode and the sample was maintained at between 1.25 and 2.5 cm. After melting was complete, the power was shut off and the sample allowed to cool. The sample was then turned over and melted four or five more times in order to obtain a uniform melt. Twelve different alloys were cast, ranging in size from 35 to 50 grams. The chemical formulas for each are given in Table 5.

3.3 Hydriding/Dehydriding Apparatus

A hydriding/dehydriding apparatus was constructed for the purpose of this investigation. The major component was the reactor vessel, Figure 17, which was constructed from a 2.54 cm. I.D. stainless steel tube, 45.0cm. in length, fitted with stainless steel, circular, end plates. Both end plates were 7.0 cm. in diameter and 1.91 cm. in depth. The first end plate had two 0.476 cm. threaded holes drilled, one through the centre of the faces and the other through the edge to the center, from which a thermocouple connection and a copper tubing connection respectively were made. The second end plate had a 2.54 cm. hole drilled through the centre of the circular faces and another 0.476 threaded hole drilled through the edge to the centre. The end plates were brazed to the tubing ends with silver solder. A cover plate was also constructed

and fastened to the second end plate with four bolts. The cover plate's dimensions were the same as those of the end plates. Two O-rings, lubricated with vacuum grease, provided a good seal between the two plates.

The reactor was heated in a horizontal tube furnace, equipped with a variac for temperature control. Hydrogen was fed into the reactor via a stainless steel pressure vessel, separated from the reactor by 0.476 cm. copper tubing and a bellows seal valve. Gas pressures were monitored in both the reactor and the pressure vessel by means of pressure gauges. A vacuum pump and nitrogen tank were connected between the reactor and the pressure vessel. An outlet from the reactor vessel was provided, which was directed into a bunsen burner flame, to provide a safe method of disposing of the used hydrogen. A check-valve was installed just before the burner to prevent back flashing and a flow meter was used to regulate gas flow. All the tubing utilized was 0.476 cm. copper, while the valves and fittings were brass. Threaded joints were sealed either by wrapping with teflon tape or by applying a teflon-based sealant. Copper cooling coils, with water acting as the coolant, were wrapped around the ends of the reactor in order to prevent the temperature at any of the joints from exceeding 150°C, i.e., the maximum service temperature of the teflon sealant. The hydrogen used for the experiment was super high purity, while the nitrogen was commercial grade. The entire hydriding apparatus is shown in Figure 18.

Two types of crucibles were available for use as sample holders. One type was made from a glazed ceramic material, while the other was a nickel-based alloy, see Figure 19. Each crucible had a capacity of ten grams and both were impervious to hydrogen pickup. The nickel-based crucible was selected because of its better heat transfer properties, i.e., heat in the exothermic hydriding reaction could be extracted much more readily.

3.4 Calculation of Quantity of Hydrogen Absorbed/Desorbed

The amount of hydrogen absorbed or desorbed by a sample, was calculated using pressure-temperature relationships. Since hydrogen behaves very nearly like an ideal gas at lower temperatures, the ideal gas law was initially assumed:

$$PV = nRT \quad (3.1)$$

where 'P' is the pressure (Pa) in the reactor, 'V' is the volume (m^3) of the reactor, 'R' is the gas constant and has the value of $8.31441 \text{ J}\cdot\text{mol}^{-1}\cdot\text{K}^{-1}$, 'T' is the absolute temperature (K) of the reactor and 'n' is the number of moles of hydrogen gas contained in the reactor. The above equation was found to be valid at room temperature, where the temperature was uniform throughout the reactor.

Before any calculations could be done, the volume of the reactor system had to be obtained. This was achieved indirectly by utilizing the ideal gas equation. Four different samples of the $\text{Zr}(\text{Co}_{0.5}\text{Cr}_{0.5})_2$ alloy were employed. One of these samples was placed into the reactor.

Following evacuation, a small quantity of hydrogen was released into the reactor and the pressure drop recorded.

After each increment, the crucible and sample were removed and weighed on a microbalance to determine the amount of hydrogen absorbed. This procedure was repeated for the other three samples. From the ideal gas equation, the volume of the reactor could be deduced as:

$$V = \Delta nRT/\Delta P$$

The results of this procedure are shown in Table 6, showing that a reproducible volume of $209.0 \pm 0.2 \text{ cm}^3$ was attainable. This volume determination technique also demonstrates the validity of the ideal gas law for hydrogen at room temperature.

The volume of the reactor will change slightly depending upon sample size and also due to thermal expansion. Both of these effects are small and in fact the volume difference due to sample size variability is considerably less than 1%, (Appendix A). Consequently, a constant volume can be assumed for the reactor system.

The ideal gas law was not applicable at higher temperatures for this system, since there were temperature variations. These variations were due to the fact that the entire reactor system was not contained in the furnace and that cooling coils near the end plates induced temperature gradients. Consequently, an empirical equation relating pressure, temperature and volume had to be derived.

It was assumed that any deviation from ideality was due to a constant change in slope and not to a deviation

from linearity, i.e.,

$$P = a \frac{R}{V} nT + B \quad (3.2)$$

where 'a' is an empirical correction factor and 'B' is the intercept. The validity of this equation was tested. At room temperature, a predetermined amount of hydrogen was let into the reactor, i.e., calculated from the ideal gas equation. The reactor was heated slowly to a maximum temperature of 570 K. At selected intervals both the temperature and the pressure were recorded. This procedure was repeated for a number of different initial pressures and all the results were tabulated, some of which are shown in Table 7. The values for each pressure-temperature experiment were plotted and each graph was found to exhibit a linear behaviour with a slope change at between 415-425 K. Figure 20 shows the plots for two of these curves. The slopes were calculated for every curve and from Equation (3.2), the value of 'a' could be calculated, i.e.,

$$m = a \frac{R}{V} n \quad (3.3)$$

or

$$a = \frac{mV}{nR} \quad (3.4)$$

where 'm' is the slope of the pressure vs. temperature curve. The values for 'a', for the above two curves, are shown in Table 7 and the mean values were calculated to be $0.4415 \pm 5\%$ for the 290 - 420 K temperature range and $0.3532 \pm 5\%$ for the 415 - 580 K temperature range.

In order to complete the derivation of the empirical

relationship, the intercept (B) had to be found. It was observed that there was a distinct relationship between the number of moles (n) and the intercept (B). The ratio of 'n' from one experiment to 'n' from another experiment was equal to the ratio of B's from the same two experiments, i.e.,

$$\frac{n_1}{n_2} = \frac{B_1}{B_2} \quad (3.5)$$

Therefore B' for any instance would be equal to:

$$B = \frac{n}{n_1} B_1 \quad (3.6)$$

Hence,

$$B = 6.767 \times 10^6 n \quad (290 \text{ K} < T < 420 \text{ K}) \quad (3.7.a)$$

or

$$B = 8.088 \times 10^6 n \quad (415 \text{ K} < T < 580 \text{ K}) \quad (3.7.b)$$

Therefore the final empirical relationships relating the pressure, temperature and number of moles of hydrogen gas were:

$$P = (1.756 \times 10^4 T + 6.769 \times 10^6) n \quad (3.8.a) \\ (290 \text{ K} < T < 420 \text{ K})$$

and

$$P = (1.405 \times 10^4 T + 8.088 \times 10^6) n \quad (3.8.b) \\ (415 \text{ K} < T < 580 \text{ K})$$

Both of the above equations were tested with additional experimental runs and the agreement was quite good. It should be noted that these equations are only valid for the heating cycle and cannot be applied during the cooling cycle. Cooling occurs relatively rapidly and

therefore pressure gauge response time can be a factor .

3.5 Hydriding/Dehydriding Procedure

Each of the prospective hydriding alloys was tested for its ability to store hydrogen. Hydriding and dehydriding capabilities were examined on a quantitative basis, while contamination effects were studied qualitatively.

A typical hydriding procedure was initiated by crushing a 2-7 gram sample in a pestle and mortar. Because these alloys are extremely brittle, this was achieved with very little difficulty. The sample was then weighed out on the microbalance and inserted into the horizontal reactor vessel at approximately the centre of the furnace area. The reactor was evacuated down to a pressure of -100 kPa gauge. Nitrogen was subsequently flushed through the reactor (for about 15 minutes) in order to force out any remaining air molecules. The vacuuming and flushing procedure was carried out again before final evacuation. A small aliquot of hydrogen was released into the reactor from the pressure vessel. The initial pressure in the reactor was recorded. Any pressure drop, due to hydrogen absorption, was noted and the final 'equilibrium' pressure was also recorded. This 'equilibrium' pressure was taken as the pressure reading after fifteen minutes had passed with no discernable change in pressure. Additional aliquots were added and the same procedure repeated. The maximum pressure range, available for study was from -100 kPa gauge up to 400 kPa gauge. The amount of hydrogen absorbed in terms of moles of H_2 , hydrogen to metal ratio and weight percent was calculated,

tabulated and plotted on P-C-T diagrams.

In the dehydriding procedure, the reactor was flushed through with hydrogen for 10-15 minutes, after which a hydrogen pressure of 0 kPa gauge remained. This flushing was carried out to further remove any gaseous impurities, as most zirconium alloys are susceptible to oxidation at higher temperatures. The reactor was then slowly heated until the maximum amount of hydrogen could be desorbed. The temperature of initial desorption was noted and the quantity of hydrogen desorbed calculated.

If the prospective alloy absorbed and desorbed hydrogen in the first cycle, other cycles, up to a maximum of fifteen, were attempted. If, however, hydrogen was not absorbed in the first cycle, an activation procedure was tried. This procedure consisted of heating the alloy sample under a hydrogen atmosphere to temperatures of approximately 300°C, for one hour followed by cooling to room temperature. If this failed, another similar activation attempt was made, except hydrogen was flushed through the system at 300°C for one hour.

3.6 Metallography

3.6.1 Sample Preparation

The annealed alloys were sectioned on a low-speed diamond saw and then mounted in cold resin. The specimens were wet polished on silicon carbide papers of 240, 320, 400 and 600 grit followed by polishing on 1.0 micron and 0.05 micron alumina wheels. The samples were also swab etched using a solution of 60 parts H₂O, 30 parts HNO₃.

and 3-4 parts HF. These specimens were then examined using optical microscopy and x-ray diffraction.

3.6.2 Optical Microscopy

Each specimen was examined on the Leitz optical microscope at various magnifications ranging from 50X to 500X. The microstructural characteristics were studied, to determine the effectiveness of the homogenizing heat treatment. The samples were viewed under both bright field and polarized light illumination.

3.6.3 X-Ray Diffraction

A Phillips x-ray diffractometer with a proportional counter detection head was employed for the identification of the phases present in each of the alloys. Either graphite monochromated CuK_α or graphite monochromated MoK_α radiation at 40 kV and 20Ma or 54 kV and 20mA respectively was used. A chart recorder was utilized to record the diffracted beams. Phase identification and lattice parameter calculations were accomplished through data from the ASTM Diffraction Files. Appendix B contains the diffraction file cards relevant to this investigation.

4.1 Microstructure

After annealing, the microstructures of the samples were examined by optical metallography. The microstructures showed features characteristic of a cast structure, i.e., the presence of dendritic grains, suggesting the possible need for some type of thermomechanical homogenization treatment (Figure 21). All of the samples appeared to be two-phase, with dark and light etching regions. The light areas tended not to etch very much. The two phases, according to x-ray analysis, were the cubic and hexagonal Laves phases. The exact amounts of each phase were difficult to determine, due to overlaps of the x-ray diffraction peaks. In some alloys, namely $Zr(Cr_{0.4}Co_{0.6})_2$, $Zr(Mn_{0.5}Co_{0.5})_2$ and $Zr(Fe_{0.5}Cr_{0.5})_2$, there was a distinct separation of the phases in the sample, which may have been due to compositional variations (Figure 22). Limited comparative compositional analysis was done on $Zr(Co_{0.5}Mn_{0.5})_2$, using the SEM and x-ray analysis system. Although no absolute compositions were determined, no discernable compositional variation was detected between the dark and light etching regions. In two of the samples exhibiting the phase separation, a rim structure was present between the two areas (Figure 23). This rim was made up of the same structure as the matrix in the two-phase region and resembled the pearlitic structure obtained in normalized steels.

4.2 Hydriding/Dehydriding Characteristics

Before any hydriding was attempted, the alloys were subjected to a homogenization heat treatment. Because of inadequate evacuation or improper sealing of the quartz tubes, all the samples became oxidized. Therefore, although unintentional, the effect of contamination on the hydriding/dehydriding properties became another factor under consideration in this study.

Of the four groups of alloys studied, the series of alloys of the type $Zr(Fe_xCr_{1-x})_2$ produced the best overall results. These alloys exhibited excellent kinetics, with hydrogen being absorbed quite readily within a few minutes of exposure to the gas. One observation common to all alloys that absorbed any hydrogen was the fracturing of the original coarse particles (1-3 mm in diameter) upon absorption. The result was a very fine greyish-black powder, containing the absorbed hydrogen. The alloy with the highest chromium content ($x = 0.4$) absorbed the most hydrogen of the three, obtaining a maximum capacity of 0.93 H-atoms F.U.⁻¹ after seven hydriding cycles. The P-C-T plot for this system is shown in Figure 24. No signs of cyclic degradation were evident. Once the maximum capacity was realized, the hydrogen capacities obtained during the ensuing cycles remained essentially constant. The other two alloys in this series, i.e., $Zr(Fe_{0.5}Cr_{0.5})_2$ and $Zr(Fe_{0.6}Cr_{0.4})_2$, attained maximum capacities of 0.83 and 0.79 respectively. These maximum capacities were attained

during the initial hydriding cycle for both materials. The P-C-T plots for these alloys are shown in Figures 25 and 26. The $Zr(Fe_{0.5}Cr_{0.5})_2$ alloy displayed signs of rapid degradation, of the order of 50%, during the second hydriding cycle. However, gradual recovery followed in the next five cycles, until 91% of the original capacity was reached (Figure 25). For the $Zr(Fe_{0.6}Cr_{0.4})_2$ sample, gradual degradation occurred after the initial cycle until the sixth cycle, whereupon the sorption decreased rapidly. A reduction in sorption capacity of approximately 40% occurred.

The 'plateau' pressures, for the $Zr(Fe_xCr_{1-x})_2$ system, increased with increasing 'x'.* The desorption capacities for the three materials were in the 75-77% range of the quantity absorbed. This figure was approximately constant regardless of the amount absorbed in the hydriding cycle. It was not possible to measure the exact temperature for desorption, although 90% of the hydrogen was desorbed at temperatures of less than 200°C.

The series of alloys of the type $Zr(Fe_xMn_{1-x})_2$ showed in general, poor hydriding/dehydriding characteristics. A number of samples of each alloy were tested and, in most instances, activation was required before any absorption was obtained. The maximum hydrogen capacities for $Zr(Fe_{0.4}Mn_{0.6})_2$, $Zr(Fe_{0.5}Mn_{0.5})_2$ and $Zr(Fe_{0.6}Mn_{0.4})_2$ were 0.243, 0.150 and 0.118 H-atoms F.U.⁻¹, respectively. The kinetics of these materials were very sluggish even after a number of cycles. The desorption capacity was about 80%

*'Plateau' pressures are not true plateau pressures in the sense that a two phase region is obtained. A 'plateau' in this work refers to a relatively flat portion of the P-C-T curve.

of the absorption capacity. Upon examining each sample on removal from the reactor, two distinct particle sizes were evident. Part of the sample consisted of a fine powder, which was the hydrided portion. The remainder of the sample was made up of the original coarse particles, suggesting that the activation procedure was only partially effective. In a number of instances, upon removal from the reactor the samples ignited, leaving a yellowish-black residue after combustion.

The group of alloys of the type, $Zr(Co_xMn_{1-x})_2$, demonstrated a substantial decrease in hydrogen capacity with increasing 'x'. The material, $Zr(Co_{0.4}Mn_{0.6})_2$, achieved a maximum capacity of 0.91 H-atoms F.U.⁻¹, while $Zr(Co_{0.5}Mn_{0.5})_2$ and $Zr(Co_{0.6}Mn_{0.4})_2$ only realized maximum capacities of 0.39 and 0.28 H-atoms F.U.⁻¹ respectively. The $Zr(Co_{0.4}Mn_{0.6})_2$ sample exhibited excellent kinetics, absorbing hydrogen within a few minutes of exposure to the gas. The maximum hydrogen capacity was attained after five hydriding cycles and the capacity remained relatively constant with further cycling. Desorption capacities were approximately 75-77% of the amount absorbed and most of this quantity could be desorbed at temperatures between 150 and 175°C. The kinetics of the other two alloys was quite sluggish while the amount desorbed was substantially less than 50% of the absorbed quantity. The two alloys ignited upon removal from the reactor in the same manner as mentioned previously.

The fourth group of alloys, namely the $Zr(Co_xCr_{1-x})_2$

type, yielded results similar to the $Zr(Co_xMn_{1-x})_2$ system. The $Zr(Co_{0.4}Cr_{0.6})_2$ sample (the lowest 'x' value) showed excellent kinetics and reached a maximum hydrogen capacity of approximately 1.0 H-atoms F.U.⁻¹ after five cycles. The P-C-T plot for this sample is shown in Figure 28. A number of specimens were tested because of inconsistent results. All the specimens absorbed large quantities of hydrogen; however, some specimens exhibited signs of cyclic degradation. Desorption capacities for this sample were low in comparison to the other high hydrogen capacity alloys. A maximum value of 65% desorption was obtained. Most of the hydrogen was released at temperatures under 200°C. The other two alloys in this series, i.e., $Zr(Co_{0.5}Cr_{0.5})_2$ and $Zr(Co_{0.6}Cr_{0.4})_2$, in general, demonstrated no affinity to hydrogen even after 2-3 activation attempts. A number of specimens of both alloy types were tested, and, in all cases but one, no hydrogen was absorbed. In one instance, the $Zr(Co_{0.6}Cr_{0.4})_2$ alloy absorbed hydrogen to a maximum capacity of 0.370 H-atoms-F.U.⁻¹ with an 80% desorption rate.

4.3 Phase Identification: X-Ray Analysis

The alloys studied were all two phase materials. These phases, as determined by x-ray analysis were cubic and hexagonal Laves phases. The lattice parameters of the two structures were calculated for each of the alloys and are listed in Table 8. The calculated 'd' spacings and the corresponding diffraction planes, for each alloy, are given in Appendix C.

The five alloys, which had high hydrogen capacities ($H/M > 0.75$), were also examined using x-ray analysis. All five materials exhibited increases in lattice parameters with no apparent phase changes. The lattice parameters for these hydrided alloys, along with their original lattice parameters are shown in Table 9. This table also lists the percent change in the original lattice parameters. The calculated 'd' spacings for these hydrided alloys are given in Appendix C.

All of the alloys, as reported previously in the sections concerning microstructure and x-ray analysis, are believed to be two-phase. These phases are the cubic and hexagonal Laves phases. There is some degree of uncertainty in identifying the phases present because of x-ray diffraction peak overlap. However, it appears certain from the optical micrographs that two phases do indeed exist. Shaltiel et al (55), the only authors to report data concerning the crystal structures of these alloys, have also detected more than one phase in these compounds. Shaltiel's crystallographic data for single phase materials (those employed for hydrogen storage studies) compare well with those calculated in this study for one of the two phases present in each sample; Table 10. A two-phase microstructure could result because:

- 1) Most AB_2 compounds are allotropic (84,85). A number of AB_2 compounds can exist as either the cubic or hexagonal phase at room temperature, e.g., $ZrCr_2$. Also, some phase transformation to the other Laves phase may have occurred during the homogenization treatment, leaving a two-phase microstructure;
- 2) Compositional variations exist within the samples. An abundance of one element, in an area of the sample, may cause the preferential formation of a specific phase.

Of these two reasons, the first, i.e., sample allometry, appears to be the more likely since compositional variations are minimal, with each sample having been melted at least five times. The limited compositional analysis done on the $Zr(Co_{0.5}Mn_{0.5})_2$ sample shows no discernable compositional variation between the two phases. Compositional variation is also ruled out because of the good overall agreement with Shaltiel et al's results (55). The selection of material allometry as the overriding cause for a two-phase structure agrees with other work on pseudobinary compounds (55-63) and hydride stability (22,23,62,79,81) which will be discussed in the following paragraphs.

The rule of reversed stability, as proposed by Miedema (22,23), states that, the more stable the binary intermetallic compound one starts with, the less will be the tendency to form stable hydrides. This rule of reversed stability has been extended to individual interstitial sites in ZrB_2 compounds (62,79,81). There are three types of interstitial sites in the AB_2 lattice, i.e., A_2B_2 , AB_3 and B_4 , although only the A_2B_2 and AB_3 sites have been found to take up hydrogen (77,78). The site names are derived from the atoms immediately surrounding the site. Shaltiel et al (79) have calculated local heats of formation ($\Delta H'$), based upon Miedema's rule of reversed stability, for each different interstitial site, by summing the heats of formation of the elementary

(imaginary binary) hydrides, formed by the A and B atoms surrounding the site. A list of these $\Delta H'$ values for relevant AB_2 compounds, $ZrCr_2$, $ZrMn_2$, $ZrFe_2$ and $ZrCo_2$, are given in Table 11 (79). It should be noted that the calculation does not include the heat of formation of the initial compound, (i.e., the negative component of the rule of reversed stability). As is evident from Table 11, the $\Delta H'$ values in all instances are lower in magnitude for $ZrFe_2$ and $ZrCo_2$ than for $ZrCr_2$ and $ZrMn_2$. This leads to the conclusion that hydrides are formed more readily with $ZrMn_2$ and $ZrCr_2$ compounds, with lower 'plateau' pressures, than with either $ZrFe_2$ or $ZrCo_2$ compounds. If some of the Cr(Mn) is substituted with Fe (or Co), a lower $\Delta H'$ value (in magnitude) would result for any interstitial position. This lower value would correspond to a higher 'plateau' pressure, and probably a lower hydrogen capacity.

In addition to the above, it has been suggested, that hydrogen capacity is mainly a result of zirconium local environment (62,79,81). This local environment is the nearest neighbours of the type B or B' for a pseudo-binary with the formula, $Zr(B_x B'_{1-x})_2$. The crystal structure, either cubic or hexagonal, would have no effect on hydrogen absorption, since the number and type of nearest and second nearest neighbours are the same and the Zr-B and Zr-B' distances are essentially constant.

The crystal structure, as predicted above, does not

appear to have much effect upon hydrogen capacity of the alloys studied. Upon hydriding, hydrogen occupies interstitial sites, causing an increase in the lattice parameters. The volume changes resulting from hydriding are approximately the same, for both the hexagonal and cubic lattices (Table 12) and, in general, increase with hydrogen capacity. The addition of Fe (or Co) to Cr (or Mn) decreases hydrogen capacity and increases the plateau pressure (Figures 29 and 30 and Table 13). This, again, is in qualitative agreement with the predictions of the modified rule of reversed stability. These results also lend some credence to the reasoning that the two-phase microstructure is due to sample allotropy. The two crystal structures, because of constant volume expansion upon hydriding, must be of approximately the same composition. This idea would also fit in with the prediction that hydrogen capacity is not dependent on crystal structure, but on zirconium local environment. The zirconium local environment would be the same for both the cubic and hexagonal Laves phases, if the compositions are the same for each crystal structure.

The maximum capacities, reported here, did not compare quantitatively with those reported elsewhere, Table 13 (55,79). In all cases, the maximum capacities were lower than those reported in the literature. The oxidation that occurred during homogenization more than likely had some poisoning effect upon hydriding properties. The degree of poisoning depended on the alloy. The $Zr(Fe_xCr_{1-x})_2$ alloys demonstrated good resistance to poisoning, with hydrogen capacities approaching those found in the literature. The other alloy

groups, in general, appeared to be severely affected by oxidation, except for two compounds, i.e., $Zr(Co_{0.4}Cr_{0.6})_2$ and $Zr(Co_{0.4}Mn_{0.6})_2$. These latter two materials exhibited hydrogen capacities of the order of 1.0. Evidence of poisoning is shown clearly for the $Zr(Co_{0.5}Cr_{0.5})_2$ alloy. In the experimental section, non-homogenized (no oxidation) $Zr(Co_{0.5}Cr_{0.5})_2$ samples, were utilized in the reactor volume calculations. These samples absorbed hydrogen quite readily, with hydrogen capacities of $H/M > 0.5$. The annealed samples, on the other hand, absorbed no hydrogen even after two activation attempts. The effect of contaminants on zirconium binary and pseudobinary compounds has not been reported elsewhere. However, other hydriding alloys, for example FeTi, are susceptible to poisoning (28,29,38,56,57, 58,59). The reaction kinetics and hydrogen capacity are decreased substantially in the presence of O_2 , H_2O and CO .

The difference in maximum capacities between the results presented here and in the literature, can also be attributed to differences in hydriding pressures. The maximum hydriding pressure available for this study was 400 KPa gauge. Pressures of 4000-6000 KPa gauge are reported in the literature, consequently higher capacities can be attained. However, the true useable portion of the P-C-T diagram only extends up to a few hundred KPa, as this is the relatively flat portion of the curve.

A phenomenon common to all the alloys studied is incomplete desorption. During the desorption cycle only 65-80% of the stored hydrogen is released. This type of behaviour has been reported previously for only one

zirconium pseudobinary, $(Zr_x Ti_{1-x})Cr_2$ (61,62), although no reason has been given. Incomplete desorption has also been observed for the $LaNi_5$ compound (43) and has been attributed to the formation of a stable fixed hydride. This explanation may have some merit when analyzing $Zr(B_x B'_{1-x})_2$ compounds. The equilibrium pressures, even for the higher 'x' values, are quite low at lower hydrogen concentrations. Consequently, a very stable hydride, requiring high temperatures for subsequent release, may be formed. If this is indeed the case, then the actual useable hydrogen capacity could only be considered as that amount that is cyclable, i.e., the maximum amount of hydrogen absorbed minus the quantity retained after desorption.

CHAPTER 6

Conclusions

- 1) The alloys utilized in this study, i.e., $Zr(Fe_xCr_{1-x})_2$, $Zr(Fe_xMn_{1-x})_2$, $Zr(Co_xCr_{1-x})_2$ and $Zr(Co_xMn_{1-x})_2$ ($x = 0.4, 0.5, 0.6$), all had two phase microstructures. The phases were identified as the cubic and hexagonal Laves phases.
- 2) The hexagonal and cubic Laves phases appeared to be of the same composition.
- 3) Hydrogen absorption increased the volume of the unit cell without changing the lattice structure. Consequently, hydrogen occupied interstitial sites in the lattice. This increase in unit cell volume is roughly proportional to the hydrogen capacity.
- 4) Hydrogen capacities and hydride stabilities decreased with increasing 'x' in all cases.
- 5) Hydriding properties, in general, were affected by oxidation in varying degrees. Hydrogen capacities were reduced substantially in most cases, although $Zr(Fe_xCr_{1-x})_2$ ($x = 0.4, 0.5, 0.6$), $Zr(Co_{0.4}Cr_{0.6})_2$ and $Zr(Co_{0.4}Mn_{0.6})_2$ exhibited good poisoning resistance. Hydrogen capacities for these alloys approached or attained $1.0 \text{ H-atoms F.U.}^{-1}$.
- 6) Both Laves phases, present in the alloys, hydrided to approximately the same level.
- 7) Complete desorption was not obtained for any of the alloys. The amount desorbed was in the 65-80% range of the quantity absorbed.

CHAPTER 7

Future Research

Further research is required on these pseudobinary compounds in order to learn more about their kinetics, cyclability, capacities and poisoning resistance.

1) A new hydriding/dehydriding apparatus should be constructed, or at least the old one modified. A schematic drawing of a new proposed apparatus is shown in Figures 31 and 32. The entire system would be constructed of stainless tubing, valves and fittings. The system would be able to withstand hydrogen pressures in excess of 6000 kPa. Dynamic pressure measurements could be made with the aid of pressure transducers, enabling kinetic studies to be undertaken. A very sensitive furnace, with an automatic temperature controller, would allow desorption isotherms to be obtained and hysteresis effects to be studied.

2) The effect of contaminants on hydriding properties could be further studied. Hydrogen of varying purities (containing known quantities of O_2 , H_2O , CO , etc.) could be utilized in an attempt to better understand the effect of impurities.

3) Desorption properties of the pseudobinary alloys require further investigation. Desorption isotherms, as well as desorption capacities, need to be examined and obtained. This would give a better idea as to the true cyclable hydrogen capacity and optimum desorption temperatures.

4) The effect of microstructure on hydriding properties could be investigated. The number and type of phases, phase distribution and grain size may affect hydriding kinetics and capacity.

5) Other compositions of these pseudobinary alloys as well as substitution with other alloying elements would be of interest. Hydrogen capacities, 'plateau' pressures and alloy cost would be varied with element substitution.

6) In situ hydriding studies would be extremely useful in examining activation effects, hydriding and dehydriding mechanisms, poisoning effects, etc. This could be achieved by hydriding inside a high voltage electron microscope. The actual hydriding/dehydriding process could be viewed while it is happening.

REFERENCES

1. LeRoy, Rodney L., Hydrogen in Metals, Annual Volume (1978) p. 1.
2. Bamberger, C.E. and Devan, J.H., Metallurgical Transactions, Volume 9A (1978) p. 201.
3. Gregory, D.P. and Pangborn, J.B., "Hydrogen Fuel Technology Session," 26th Power Sources Symposium, (1974) p. 1.
4. Mathis, David A., Hydrogen Technology For Energy, Noyes Data Corporation, New Jersey, U.S.A., 1976.
5. Edeskuty, F.J. and Williamson, Jr., K.D., Hydrogen: Its Technology and Implications, Volume 2 (1977) p. 51.
6. Toepler, J., Bernauer, O. and Buchner, H., Journal of Less-Common Metals, Volume 74 (1980) p. 385.
7. Folonari, C., Iemmi, G., Manfredi, F. and Rolle, A., Journal of Less-Common Metals, Volume 74 (1980) p. 371.
8. Holleck, G.L., Driscoll, J.R. and Paul, B.E., Journal of Less-Common Metals, Volume 74 (1980) p. 379.
9. Nomura, Kei and Ishido, Yoshihiko, Energy Conversion, Volume 19 (1979) p. 49.
10. Libowitz, G.G. and Blank, Z., Solid State Chemistry, (1976) p. 271.
11. Lynch, F.E., Journal of Less-Common Metals, Volume 74 (1980) p. 411.
12. Swisher, J.H., Journal of Less-Common Metals, Volume 74 (1980) p. 301.
13. Hord, J. and Parrish, W.R., Hydrogen: Its Technology and Implications, Volume 5 (1979) p. 3.
14. Westlake, D.G., Satterwrite, C.B. and Weaver, J.H., Physics Today, November (1978) p. 32.
15. Piercy, G.R., Hydrogen in Metals, Annual Volume (1978) p. 11.
16. Reilly, J.J., Hydrogen: Its Technology and Implications, Volume 2 (1977) p. 13.

17. Switendick, A.C., Solid State Communications, Volume 8 (1970) p. 1463.

18. Weaver, J.H. and Peterson, D.T., Journal of Less-Common Metals, Volume 74 (1980) p. 207.
19. Ward, J.W., Journal of Less-Common Metals, Volume 73 (1980) p. 183.
20. Buchner, H., International Journal of Hydrogen Energy, Volume 3 (1978) p. 385.
21. Flanagan, Ted B., Journal of Physical Chemistry, Volume 79 (1975) p. 444.
22. Van Mal, H.H., Buschow, K.H.J. and Miedema, A.R., Journal of Less-Common Metals, Volume 35 (1974) p. 65.
23. Miedema, A.R., Buschow, K.H.J. and Van Mal, H.H., Journal of Less-Common Metals, Volume 49 (1976) p. 473.
24. Gruen, D.M. and Mendelsohn, M., Journal of Less-Common Metals, Volume 55 (1977) p. 149.
25. Larsen, J.W. and Livesay, B.R., Journal of Less-Common Metals, Volume 73 (1980) p. 79.
26. Suda, S., Kobayashi, N. and Yoshida, K., Journal of Less-Common Metals, Volume 73 (1980) p. 119.
27. Goodell, P.D., Sandrock, G.D. and Huston, E.L., Journal of Less-Common Metals, Volume 73 (1980) p. 135.
28. Schlapbach, L., Journal of Less-Common Metals, Volume 73 (1980) p. 145.
29. Kuijpers, F.A. and van Mal, H.H., Journal of Less-Common Metals, Volume 23 (1971) p. 395.
30. Lundin, C.E. and Lynch, F.E., Hydrides for Energy Storage, Pergamon Press (1977) p. 395.
31. Libowitz, G.G., Hayes, H.F. and Gibb, T.R.P., Inorganic Chemistry, Volume 62 (1957) p. 76.
32. Flanagan, Ted B., Bowerman, B.S. and Biehl, G.E., Scripta Metallurgica, Volume 14 (1980) p. 443.
33. Irvine, S.J.C. and Harris, I.C., Hydrides For Energy Storage, Pergamon Press (1977) p. 431.
34. Ivey, D.G. and Northwood, D.O., Storing Energy in Metal Hydrides: A Review of the Physical Metallurgy, Journal of Materials Science, Submitted for publication, Oct. 1981.

35. Ivey, D.G., Northwood, D.O., Chittim, R.I. and Chittim, K.J., Metal Hydrides for Energy Storage, Journal of Materials for Energy Systems, Accepted for publication, Sept. 1981.
36. Ivey, D.G. and Northwood, D.O., Metal Hydrides for Energy Storage, Canadian Metallurgical Quarterly, In Press, Nov. 1981.
37. Lakner, J.F., Uribe, F.S. and Steward, S.A., Journal of Less-Common Metals, Volume 72 (1980) p. 87.
38. Switendick, A.C., Theoretical Studies of Hydrogen In Metals: Current Status and Further Prospects, Sandia Laboratories Report, SAND 78-0250, 1978.
39. Van Vucht, J.H.N., Phillips Research Reports, Volume 25 (1970) p. 133.
40. Stafford, S.W., Acta Metallurgica, Volume 22 (1974) p. 1463.
41. Schlapbach, L., International Journal of Hydrogen Energy, Volume 4 (1979) p. 21.
42. Sandrock, G.D. and Goodell, P.D., Journal of Less-Common Metals, Volume 73 (1980) p. 161.
43. Cohen, R.L., West, K.W. and Wernick, J.H., Journal of Less Common Metals, Volume 70 (1980) p. 229.
44. Mendelsohn, M.H. and Gruen, D.M., Nature, Volume 269 (1977) p. 45.
45. Mendelsohn, M.H., Gruen, D.M. and Dwight, A.E., Materials Research Bulletin, Volume 13 (1978) p. 1221.
46. Büschow, K.H.J., Journal of Less-Common Metals, Volume 42 (1975) p. 163.
47. Reilly, J.J., Inorganic Chemistry, Volume 13 (1974) p. 218.
48. Bowman, R.C., International Journal of Hydrogen Energy, Volume 2 (1977) p. 309.
49. Strickland, S., International Journal of Hydrogen Energy, Volume 2 (1977) p. 309.
50. Henriksen, D.L., Mackay, D.B. and Anderson, V.R., 1st World Hydrogen Energy Conference, Volume 7C (1976) p. 1.

51. Johnson, D.G. and Pangborn, J.B., Journal of Less-Common Metals, Volume 73 (1980) p. 127.

52. Fischer, P., Materials Research Bulletin, Volume 13 (1978) p. 931.
53. Reilly, J.J., 1st World Hydrogen Energy Conference, Volume 4 (1979) p. 29.
54. Rudman, P.S., Journal of Less-Common Metals, Volume 58 (1978) p. 231.
55. Shaltiel, D., Journal of Less-Common Metals, Volume 53 (1977) p. 117.
56. Pebler, A. and Gulbrahsen, E.A., Transactions of the AIME, Volume 239 (1967) p. 1593.
57. Didisheim, E.J., Journal of Less-Common Metals, Volume 73 (1980) p. 355.
58. Fruchart, D., Journal of Less-Common Metals, Volume 73 (1980) p. 363.
59. Friauf, J.B., Physical Review, Volume 29 (1927) p. 34.
60. Friauf, J.B., Journal of American Chemistry Society, Volume 49 (1927) p. 3107.
61. Wiswall, R., Hydrogen in Metals II, Volume 29 (1978) p. 201.
62. Jacob, I., Solid State Communications, Volume 23 (1977) p. 669.
63. Mendelsohn, M.H. and Gruen, D.M., Journal of Less-Common Metals, Volume 78 (1981) p. 275.
64. Jacob, I., Journal of Less-Common Metals, Volume 73 (1980) p. 369..
65. Oesterreicher, H., Materials Research Bulletin, Volume 13 (1978) p. 83.
66. Reilly, J.J. and Wiswall, R., Inorganic Chemistry, Volume 6 (1967) p. 2220.
67. Karty, A., Grunzweig-Genossar, J. and Rudman, Journal of Applied Physics, Volume 50 (1979) p. 7200.
68. Seiler, A., Journal of Less-Common Metals, Volume 73 (1980) p. 193.

69. Vizeholm, B., Kjoller, J. and Larsen B., Journal of Less-Common Metals, Volume 74 (1980) p. 341.

70. Douglass, D.L., Metallurgical Transactions, Volume 6A (1975) p. 2179.
71. Schefer, J., Journal of Less-Common Metals, Volume 74 (1980) p. 65.
72. Mintz, M.H., Journal of Less-Common Metals, Volume 74 (1980) p. 263.
73. Pezat, M., Daniel, B. and Hagenmuller, P., Journal of Less-Common Metals, Volume 74 (1980) p. 427.
74. Kierstead, H.A., Journal of Less-Common Metals, Volume 71 (1980) p. 311.
75. Dunlap, B.D., Viccaro, P.J. and Shenoy, G.K., Journal of Less-Common Metals, Volume 74 (1980) p. 75.
76. Van Essen, R.H. and Buschow, K.H.J., Journal of Less-Common Metals, Volume 70 (1980) p. 189.
77. Kierstead, Henry A., Journal of Less-Common Metals, Volume 73 (1980) p. 61.
78. Magee, Charles B., Journal of Less-Common Metals, Volume 78 (1981) p. 119.
79. Shaltiel, D., Journal of Less-Common Metals, Volume 73 (1980) p. 329.
80. Shoemaker, D.P. and Shoemaker, C.B., Journal of Less-Common Metals, Volume 68 (1979) p. 43.
81. Shaltiel, D., Journal of Less-Common Metals, Volume 62 (1978) p. 407.
82. Johnson, J.R., Journal of Less-Common Metals, Volume 73 (1980) p. 345.
83. Oesterreicher, H. and Bittner, H., Journal of Less-Common Metals, Volume 73 (1980) p. 339.
84. Rumball, W.M., Journal of Less-Common Metals, Volume 20 (1970) p. 191.
85. Edwards, A.R., Metallurgical Transactions, Volume 3, (1972) p. 1365.

Table 1
Summary of Hydrating Behaviour of Metallic Hydride Systems (19)

Observation	Electropositive Metals	Electronegative Metals
Hydride Location Electrical Conductivity Activation Energy for Dissociation Poisoned by Hydride	Tetrahedral Sites Increases upon Hydrating Appreciable Electrophilic Molecules (e.g., SO ₂ , CO ₂ and HCl) Is Autocatalytic	Octahedral Sites Decreases upon Hydrating Nil Electrophobic Molecules (e.g., NH ₃ and pyridine) Poisons reaction

Table 2
Summary of Hydriding Alloys and Their Properties

Alloy Type	Quantity of Hydrogen Absorbed		Kinetics	Stability of Hydride	Cycling Degradation	Hysteresis	Resistance to Poisoning	Cost
	M/N	wt%						
<p>AB₅</p> <p>Example</p> <p>LaNi₅</p> <p>LaCo₅</p> <p>CaCo₅</p> <p>LaMn₃Co₂-x</p>	1.0 up to 1.5	1.4t to max 1.9t	Rapid kinetics, of the order of a few seconds due to surface segregation. Heat transfer controlled. No activation required.	Relatively stable. ΔH -7kcal/mole; 1/3 changes, up or down, with alloy substitutions. P _{eq} ~2.2 atm. at R.T. for LaNi ₅ .	May be degradation after 300-600 cycles due to formation of stable hydrides (LaNi ₃)	Moderate hysteresis at low temperatures.	Good resistance to H ₂ O and O ₂ poisoning. Susceptible to CO poisoning, partial reactivation possible.	Quite expensive because of cost of La and Ni.
<p>AB</p> <p>Example</p> <p>FeTi</p> <p>ZrNi</p> <p>TiX₁</p> <p>Fe_{1-x}Ni_xTi</p>	1.0	1.8t max.	Moderate kinetics partially controlled by heat transfer. Needs activation for surface segregation.	Stability varies from ΔH -7.0 kcal/mole for FeTi based alloys to ΔH -11.0 to -19.0 kcal/mole for other AB compounds. P _{eq} 4-5 atm. at R.T.	No evidence as yet, but no high cycle experiments have been done.	Pronounced hysteresis in FeTi however can be reduced by addition of Mn.	General poor resistance to poisoning for FeTi. Especially susceptible to CO. Partial reactivation possible. Addition of Mn gives better Co resistance.	Relatively inexpensive. Fe fairly cheap.
<p>AB₂</p> <p>Example</p> <p>ZrV₂</p> <p>ZrCr₂</p> <p>ZrNi₂</p> <p>LaNi₂</p> <p>Zr(Fe_{1-x}V_x)₂</p> <p>Zr(Co_{1-x}Cr_x)₂</p>	From 1.0 up to 2.0	From 1.5 to 2.0t	Rapid kinetics. No activation necessary in most cases. Not much data on kinetics, however.	Generally quite stable. ΔH -18.0 kcal/mole for binaries. Pseudobinary decrease stability to acceptable levels.	No evidence as yet, but no high cycle experiments have been done.	Low hysteresis in binary compounds. Moderate hysteresis in pseudobinary.	No reported poisoning problems, but little work has been done in this area.	Quite expensive because of cost of Zr metal.

continued...

Table 2 (Continued)

Alloy Type	Quantity of Hydrogen Absorbed		Kinetics	Stability of Hydride	Cycling Degradation	Hysteresis	Resistance to Poisoning	Cost
	H ₂ /N	wt%						
Mg-Compounds Example Mg Mg ₂ Ni Mg ₂ Cu	1.3 up to 3.0	From 3.5% up to 6.7%	Sluggish kinetics. Activation is necessary and difficult. Rate limited by diffusion of H atoms (when activated). If segregation stops rate limited by dissociative chemisorption and associative desorption. Ni, Cu, etc. are added as catalysts.	Very stable. $\Delta H = 10.0$ kcal/mole. $P_{eq} = 1$ atm at 300°C.	Cycling may cause reduction in desorption rate of Mg-Mg ₂ Ni	None reported	Very susceptible to poisoning by O ₂ , H ₂ O, CO, etc.	Relatively inexpensive because of high Mg content.
AB ₂ + A ₂ B ₇ Example K ₂ CO ₃ VFe ₃ Co ₂ Co ₇ Th ₂ Fe ₇	Max. of 1.4 for AB ₂ Max. of 0.67 for A ₂ B ₇	Max. of 1.6% Generally much less though.	Not reported.	Quite stable. AB ₂ compounds are more stable than A ₂ B ₇ compounds.	Not reported.	Little or no hysteresis.	Not reported.	Not too expensive since Co and Fe are majority metals in most cases.

Table 3

Hydrides of Zirconium Binaries and Pseudobinaries

Compound	Hydrides	Hydrogen to Metal Ratio	ΔH (kcal/mole H_2)	Equilibrium Plateau Pressure* (atm)	Reference
ZrNi ₅					
ZrNi	ZrNiH & ZrNiH ₃	1.47	-18.4	---	31
ZrCo	ZrCoH _{2.6}	1.3	-18.0	---	31
TiCr ₂	TiCr ₂ H _{3.84}	1.28	---	1 (-55°C)	82
ZrV ₂	ZrV ₂ H ₆	2.0	-48.0	10 ⁻⁸	55, 58
ZrCr ₂	ZrCr ₂ H _{3.8}	1.3	-11.0	10 ⁻⁸	55, 58
ZrMn ₂	ZrMn ₂ H _{3.6}	1.2	-12.7	---	65
ZrFe ₂	---	.2	---	---	55
ZrCo ₂	---	.2	---	---	55
ZrMo ₂	ZrMo ₂ H _{0.78}	.26	---	---	56
LaNi ₂	LaNi ₂ H _{4.5}	1.5	---	---	83
La _{2.75} Mg _{0.25} Ni ₂	La _{2.75} Mg _{0.25} Ni ₂ H _{4.1}	1.4	---	---	83
La _{0.4} Mg _{0.6} Ni ₂	La _{0.4} Mg _{0.6} Ni ₂ H _{2.9}	1.0	---	---	83
Ti _{0.6} Zr _{0.4} Mn ₂	Ti _{0.6} Zr _{0.4} Mn ₂ H _{0.9}	0.3	---	20 (140°C)	65

* given at room temperature unless specified

Table 3 (Continued)

Compound	Hydrides	Hydrogen to Metal Ratio	ΔH (kcal/mole H ₂)	Equilibrium Plateau Pressure (atm)	Reference
Ti _{0.4} Zr _{0.6} Mn ₂	Ti _{0.4} Zr _{0.6} Mn ₂ H _{1.1}	0.36	---	8.0 (140°C)	65
Ti _{0.2} Zr _{0.8} Mn ₂	Ti _{0.2} Zr _{0.8} Mn ₂ H _{1.2}	0.4	---	1.8 (140°C)	65
Zr(Fe _{0.5} Cr _{0.5}) ₂	Zr(Fe _{0.5} Cr _{0.5}) ₂ H _{3.2}	1.07	-11.5	0.0012	55
Zr(Fe _{0.75} V _{0.25}) ₂	Zr(Fe _{0.75} V _{0.25}) ₂ H _{3.2}	1.07	-7.7	0.25	55
Zr(Fe _{0.5} Cr _{0.5}) ₂	Zr(Fe _{0.5} Cr _{0.5}) ₂ H _{3.4}	1.13	-11.8	0.1	55
Zr(Fe _{0.75} Cr _{0.25}) ₂	Zr(Fe _{0.75} Cr _{0.25}) ₂ H _{2.85}	0.95	-5.8	5.5	55
Zr(Fe _{0.4} Mn _{0.6}) ₂	Zr(Fe _{0.4} Mn _{0.6}) ₂ H _{3.2}	1.07	-7.9	0.4	55
Zr(Fe _{0.5} Mn _{0.5}) ₂	Zr(Fe _{0.5} Mn _{0.5}) ₂ H _{2.9}	0.97	-7.2	0.65	55
Zr(Co _{0.5} V _{0.5}) ₂	Zr(Co _{0.5} V _{0.5}) ₂ H _{3.7}	1.23	-11.8	0.0023	55
Zr(Co _{0.75} V _{0.25}) ₂	Zr(Co _{0.75} V _{0.25}) ₂ H _{3.0}	1.0	-8.2	1.5	55
Zr(Co _{0.5} Cr _{0.5}) ₂	Zr(Co _{0.5} Cr _{0.5}) ₂ H _{3.2}	1.07	-9.6	0.7	55
Zr(Co _{0.25} Mn _{0.75}) ₂	Zr(Co _{0.25} Mn _{0.75}) ₂ H _{3.4}	1.13	-10.6	0.08	55
Zr(Co _{0.4} Mn _{0.6}) ₂	Zr(Co _{0.4} Mn _{0.6}) ₂ H _{3.1}	1.03	-8.6	0.5	55
Zr(Co _{0.5} Mn _{0.5}) ₂	Zr(Co _{0.5} Mn _{0.5}) ₂ H _{3.1}	1.03	-8.3	1.2	55

Table 4List of Metals Used, in the Forms and Purities Received

Element	Purity (%)	Form
Zirconium	99.9	Ingot Crystal Bar
Iron	99.95	5/8" Rod
Cobalt	99.9	Broken Cathodes
Manganese	99.99	Flakes
Chromium	99.999	Pellets

Table 5
List of Twelve Alloys Utilized in Hydriding Experiments

Alloy	Number of Grams of Each Constituent				
	Zr	Fe	Co	Mn	Cr
Zr(Fe _{0.4} Cr _{0.6}) ₂	17.389	8.504			11.900
Zr(Fe _{0.5} Cr _{0.5}) ₂	20.640	12.660			11.786
Zr(Fe _{0.6} Cr _{0.4}) ₂	21.132	15.502			9.628
Zr(Fe _{0.4} Mn _{0.6}) ₂	18.733	9.156		13.544	
Zr(Fe _{0.5} Mn _{0.5}) ₂	18.148	11.150		10.948	
Zr(Fe _{0.6} Mn _{0.4}) ₂	19.324	14.180		9.320	
Zr(Co _{0.4} Cr _{0.6}) ₂	18.681		9.648		12.779
Zr(Co _{0.5} Cr _{0.5}) ₂	21.325		13.775		12.157
Zr(Co _{0.6} Cr _{0.4}) ₂	20.716		16.047		9.463
Zr(Co _{0.4} Mn _{0.6}) ₂	21.452		11.098	15.497	
Zr(Co _{0.5} Mn _{0.5}) ₂	19.406		12.530	11.695	
Zr(Co _{0.6} Mn _{0.4}) ₂	19.847		15.392	9.570	

Table 6

Typical Results for Volume Calculation of Reactor, Using Ideal Gas Equation ($PV=nRT$), ($R=8.31441 \text{ J.mol}^{-1} \cdot \text{K}^{-1}$)

Sample	Sample Weight (g)	Initial H ₂ Pressure (Kpa gauge)	Final H ₂ Pressure (Kpa gauge)	Weight of H ₂ (g)	Volume of Reactor (m ³)	Temperature (K)
Zr(Co _{0.5} Cr _{0.5}) ₂	6.1245	95	-50	2.43×10^{-2}	209×10^{-6}	300
Zr(Co _{0.5} Cr _{0.5}) ₂	3.5205	95	-42	2.31×10^{-2}	209.2×10^{-6}	299
Zr(Co _{0.5} Cr _{0.5}) ₂	4.4805	147	-25	2.89×10^{-2}	208.9×10^{-6}	299
Zr(Co _{0.5} Cr _{0.5}) ₂	3.8385	147	-20	2.8×10^{-2}	209.1×10^{-6}	300

Table 7
Values of 'a' for the Two Calibration Curves of Figure 20

Test Number	Temperature Range (k)	Number of Moles	Slope (kPa.k ⁻¹)	'a'
5	295-420	1.29×10^{-2}	215.5	0.4200
5	405-656	1.29×10^{-2}	177.22	0.3453
6	295-430	1.69×10^{-2}	274.5	0.4083
6	420-560	1.69×10^{-2}	225.0	0.3347

Table 8
Lattice Parameters for the Twelve Alloys

Alloy	Lattice Parameter		
	Hexagonal		Cubic
	'a' (Å)	'c' (Å)	'a' (Å)
Zr(Fe _{0.4} Cr _{0.6}) ₂	5.05	8.26	7.20
Zr(Fe _{0.5} Cr _{0.5}) ₂	5.045	8.20	7.12
Zr(Fe _{0.6} Cr _{0.4}) ₂	5.02	8.22	7.01
Zr(Fe _{0.4} Mn _{0.6}) ₂	5.012	8.19	7.02
Zr(Fe _{0.5} Mn _{0.5}) ₂	5.03	8.19	6.96
Zr(Fe _{0.6} Mn _{0.4}) ₂	5.00	8.166	6.93
Zr(Co _{0.4} Cr _{0.6}) ₂	5.04	8.25	7.14
Zr(Co _{0.5} Cr _{0.5}) ₂	5.01	8.18	7.07
Zr(Co _{0.6} Cr _{0.4}) ₂	5.025	8.18	7.07
Zr(Co _{0.4} Mn _{0.6}) ₂	5.00	8.19	7.05
Zr(Co _{0.5} Mn _{0.5}) ₂	5.00	8.16	7.085
Zr(Co _{0.6} Mn _{0.4}) ₂	4.97	8.14	7.03

Table 9
Effect of Hydriding on Lattice Parameters

Alloy	Lattice Parameters							
	Original (Å)		Hydrided (Å)		Percent Change			
	Hexagonal	Cubic	Hexagonal	Cubic	Hexagonal	Cubic	Hexagonal	Cubic
Zr(Fe _{0.4} Cr _{0.6}) ₂	a=5.05 c=8.26	a=7.20	a=5.21 c=8.77	a=7.41	a=3.17 c=6.17	a=2.92		
Zr(Fe _{0.5} Cr _{0.5}) ₂	5.045 8.20	7.12	5.31 8.74	7.50	5.25 6.34	5.34		
Zr(Fe _{0.6} Cr _{0.4}) ₂	5.02 8.22	7.01	5.061 8.241	7.08	0.82 0.26	1.0		
Zr(Co _{0.4} Cr _{0.6}) ₂	5.04 8.25	7.14	5.31 8.80	7.62	5.36 6.67	6.72		
Zr(Co _{0.4} Mn _{0.6}) ₂	5.00 8.19	7.05	5.276 8.904	7.56	5.52 8.72	7.23		

Table 10

Comparison of X-Ray Results From This Work with Results of Shaltiel et al. (55)

Alloy	Lattice Parameters (Å)			
	This Work		Shaltiel et al. (55)	
	Cubic	Hexagonal	Cubic	Hexagonal
Zr(Fe _{0.4} Cr _{0.6}) ₂	a=7.20	a=5.05 c=8.26	a=	a= c=
Zr(Fe _{0.5} Cr _{0.5}) ₂	7.12	5.045 8.20		5.034 8.219
Zr(Fe _{0.6} Cr _{0.4}) ₂	7.01	5.02 8.22		5.02 8.22
Zr(Fe _{0.4} Mn _{0.6}) ₂	7.02	5.012 8.19		5.012 8.188
Zr(Fe _{0.5} Mn _{0.5}) ₂	6.96	5.03 8.19		5.006 8.178
Zr(Fe _{0.6} Mn _{0.4}) ₂	6.93	5.00 8.166		4.998 8.166
Zr(Co _{0.4} Cr _{0.6}) ₂	7.14	5.04 8.25		
Zr(Co _{0.5} Cr _{0.5}) ₂	7.07	5.01 8.18		5.034 8.22
Zr(Co _{0.6} Cr _{0.4}) ₂	7.07	5.025 8.18		
Zr(Co _{0.4} Mn _{0.6}) ₂	7.05	5.00 8.19		5.00 8.19
Zr(Co _{0.5} Mn _{0.5}) ₂	7.085	5.00 8.16		5.00 8.16
Zr(Co _{0.6} Mn _{0.4}) ₂	7.03	4.97 8.14	7.03	

Table 11

$\Delta H'$ Values For Partially and Totally Occupied Interstitial Sites
in AB_2H_x Hydrides (79)

Interstitial Site	Occupancy	$\Delta H'$ Kcal. (mol H ₂) ⁻¹				
		ZrCr ₂	ZrMn ₂	ZrFe ₂	ZrCO ₂	
AB ₃	1	-18.5	-17.9	-14.9	-15.6	
	0.5	-22.7	-21.8	-17.4	-18.4	
	0.25	-25.3	-24.3	-19.1	-20.3	
	0	-25.4	-24.3	-19.1	-20.3	
A ₂ B ₂	1	-8.1	-7.9	-6.8	-7	
	0.5	-16.2	-15.8	-13.8	-14.3	
	0.333	-22.2	-21.7	-19.1	-19.7	
	0.167	-36.4	-35.8	-32.6	-33.3	
	0.083 _A	-44	-43.3	-39.8	-40.6	
0	-49	-48.3	-44.8	-45.6		

Table 12
 Comparison of Volume Changes with Final Hydrogen Capacity

Alloy	Original Volume		Volume After Hydrating		% Change		Final Hydrogen Capacity H/M
	Hexagonal	Cubic	Hexagonal	Cubic	Hexagonal	Cubic	
Zr(Fe _{0.4} Cr _{0.6}) ₂	182.4Å ³	373.2Å ³	206.2Å ³	406.9Å ³	13.05	9.02	0.93
Zr(Fe _{0.5} Cr _{0.5}) ₂	180.74	360.9	213.4	421.9	18.08	16.9	0.75
Zr(Fe _{0.6} Cr _{0.4}) ₂	179.4	344.5	182.8	354.9	1.89	3.02	0.49
Zr(Co _{0.4} Cr _{0.6}) ₂	180.0	364.0	214.9	442.5	19.38	21.56	1.0
Zr(Co _{0.4} Mn _{0.6}) ₂	177.3	350.4	214.6	432.1	21.06	23.31	0.910

Table 13

List of Maximum Hydrogen Capacities in Terms of
H/M Ratios

Alloy Type	Value of x					
	0.4		0.5		0.6	
	Zr(Fe _x Cr _{1-x}) ₂	0.230	1.20*	0.830	1.20*	0.790
Zr(Fe _x Mn _{1-x}) ₂	0.240	1.10*	0.153	1.10*	0.118	1.07*
Zr(Co _x Cr _{1-x}) ₂	1.0	1.20*	0.0	1.20*	0.370	1.07*
Zr(Co _x Mn _{1-x}) ₂	0.910	1.30*	0.395	1.20*	0.276	1.07*

* Values obtained from references (52,59,76).

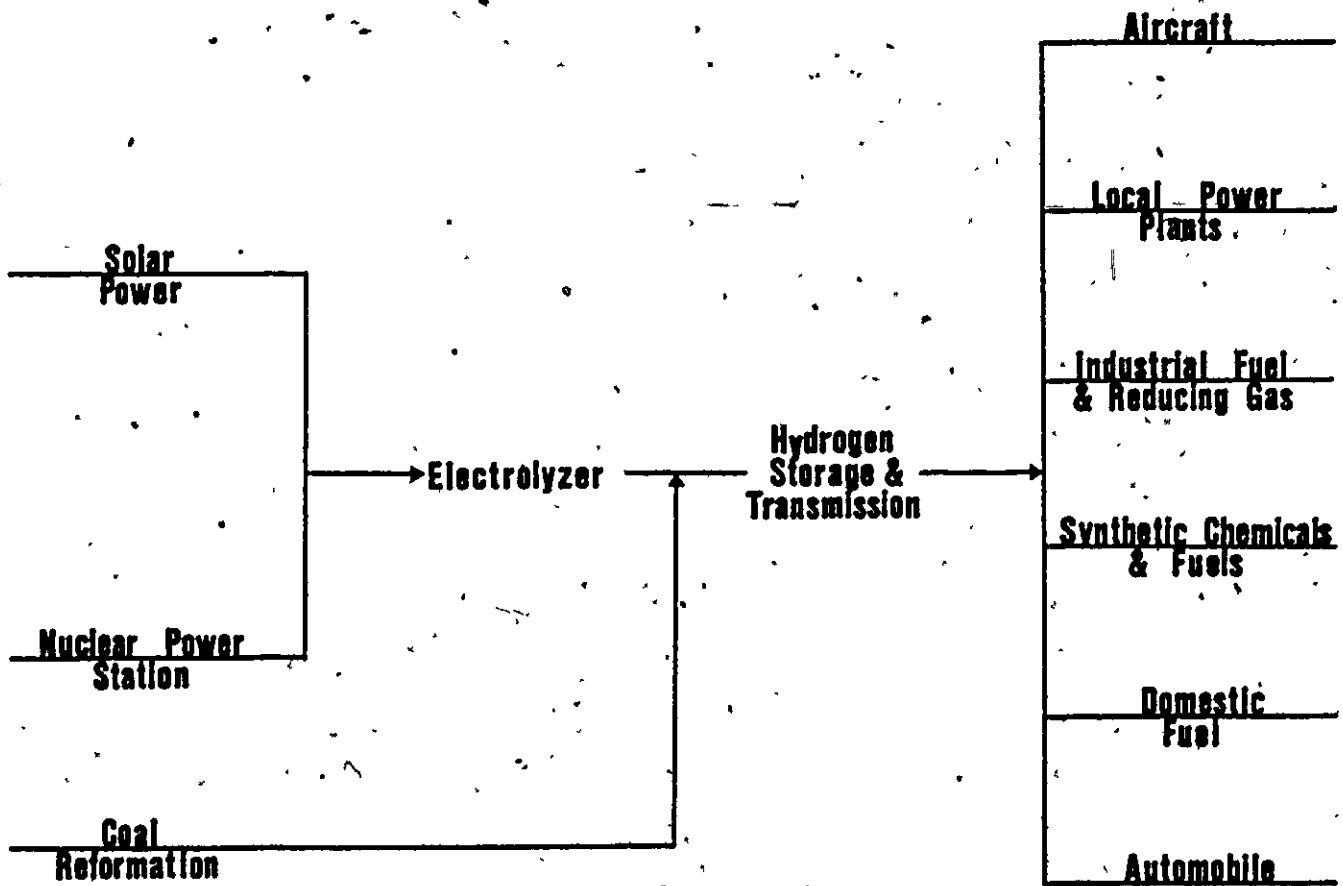


Figure 1 Schematic representation of the Hydrogen System (1).

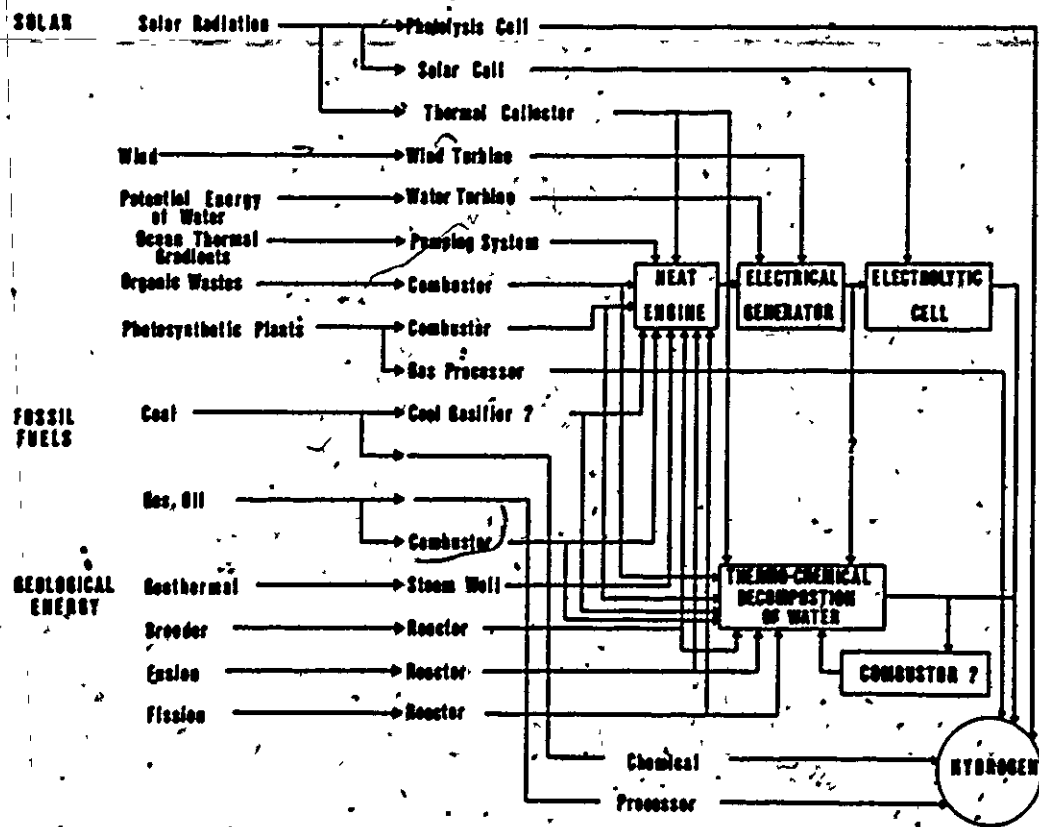


Figure 2 Summary of methods for hydrogen production (4).

	IA																0	
1	H																He	
2	LiH	BeH											B	C	N	O	F	Ne
3	NaH	MgH ₂											AlH ₃	Si	P	S	Cl	Ar
			IIIA	IVA	VA	VIA	VIIA	VIII	IX	X	XI	XII						
4	KH	CaH ₂	ScH ₂	TiH ₂	VH VH ₂	CrH CrH ₂	Mn	Fe	Co	NiH	CuH	ZnH ₂	Ga	Ge	As	Se	Br	Kr
5	RbH	SrH ₂	YN ₂ YN ₃	ZrH ₂	NbH NbH ₂	Mo	Tc	Ru	Rh	PdH	Ag	CdH ₂	In	Sn	Sb	Te	I	Xe
6	CsH	BaH ₂	LaH ₃	HfH ₂	TaH	W	Re	Os	Ir	Pt	Au	Hg	Tl	Pb	Bi	Po	At	Rn
7	Fr ?	Ra ?	AcH ₂															

CoH ₃	PtH ₃	NdH ₃	PuH ₂ PuH ₃	SmH ₂ SmH ₃	EuH ₂	GdH ₂ GdH ₃	TbH ₂ TbH ₃	DyH ₂ DyH ₃	HoH ₂ HoH ₃	ErH ₂ ErH ₃	TmH ₂ TmH ₃	YbH ₂ YbH ₃	LuH ₂ LuH ₃
TmH ₂ ThH ₃	PuH ₃	UH ₃	NpH ₂ NpH ₃	PuH ₂ PuH ₃	AmH ₂ AmH ₃	Cm	Bk	Cf	Es	Fm	Md	No	Lr
						?	?	?	?	?	?	?	?

Figure 3 Periodic Table showing occurrence of binary hydrides. The underlined compounds cannot be prepared by a direct reaction (16).

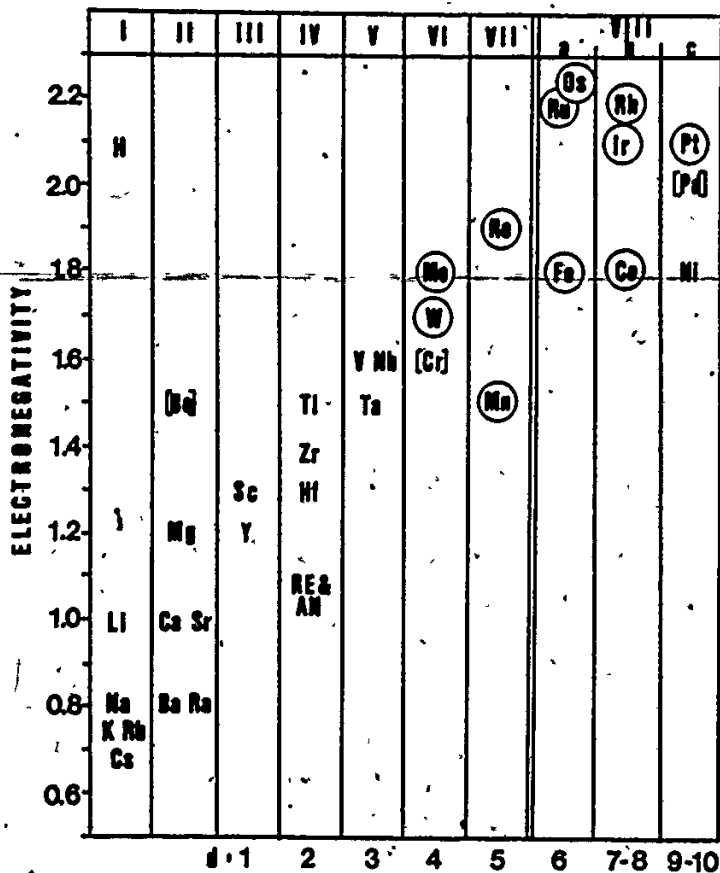


Figure 4 Relative electronegativities of the transition metals, the rare earths (RE), the actinides and hydrogen. Electronegativity is the ability of an atom in a molecule or solid to attract bonding electrons to itself. The values are calculated from the Pauling relationship, $\Delta_{A-B} = 96.5 (X_A - X_B)^2$, where Δ_{A-B} is the excess binding energy (KJ/mol of bonds) and X_A and X_B are electronegativities of A and B.

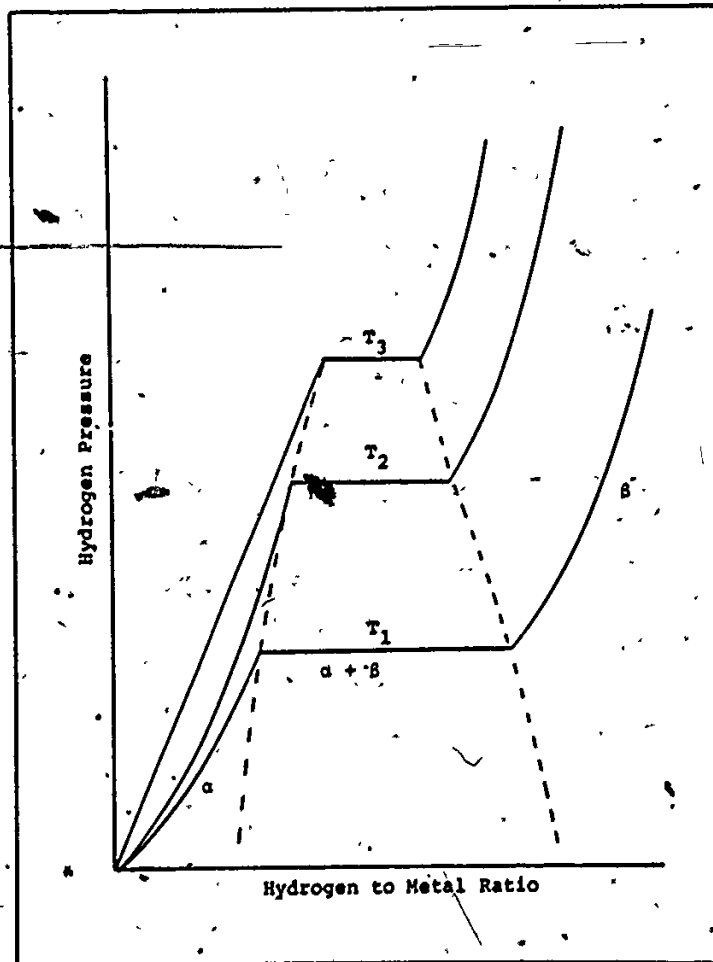


Figure 5 Pressure-composition-isotherm (P-C-T) diagram showing the relationship between the equilibrium hydrogen pressure and the hydrogen concentration.

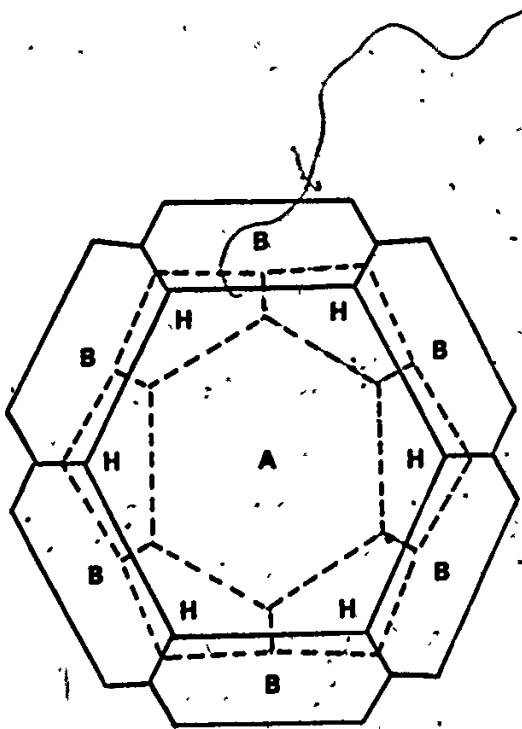


Figure 6 Atomic cells in an intermetallic compound of two metals, A and B, with and without hydrogen present. The atomic cells of hydrogen are indicated by broken lines. Upon hydrogen absorption, the lattice is increased, which is not shown here (22).

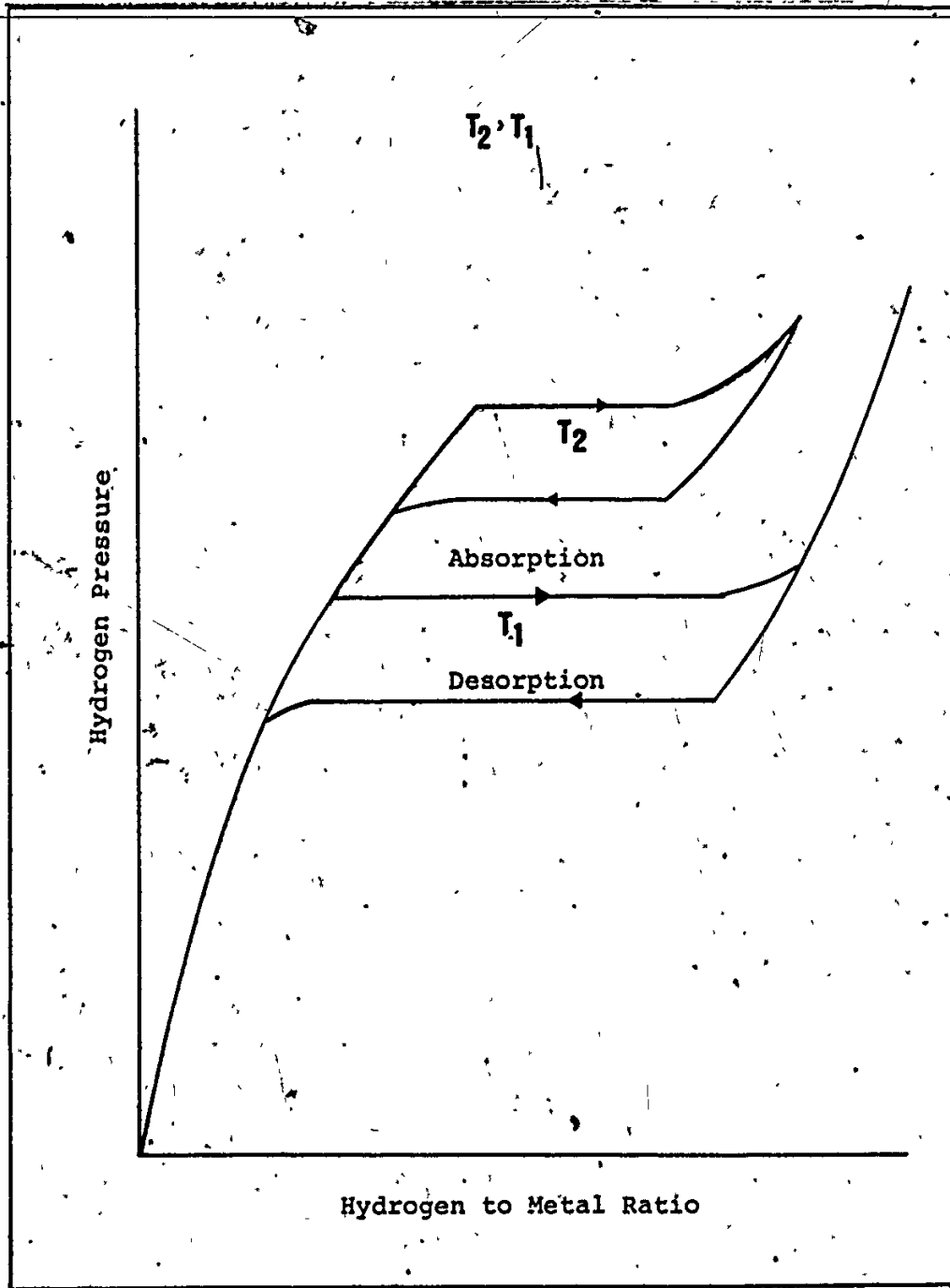


Figure 7 P-C-T diagram showing hysteresis in a metal-hydrogen system (16).

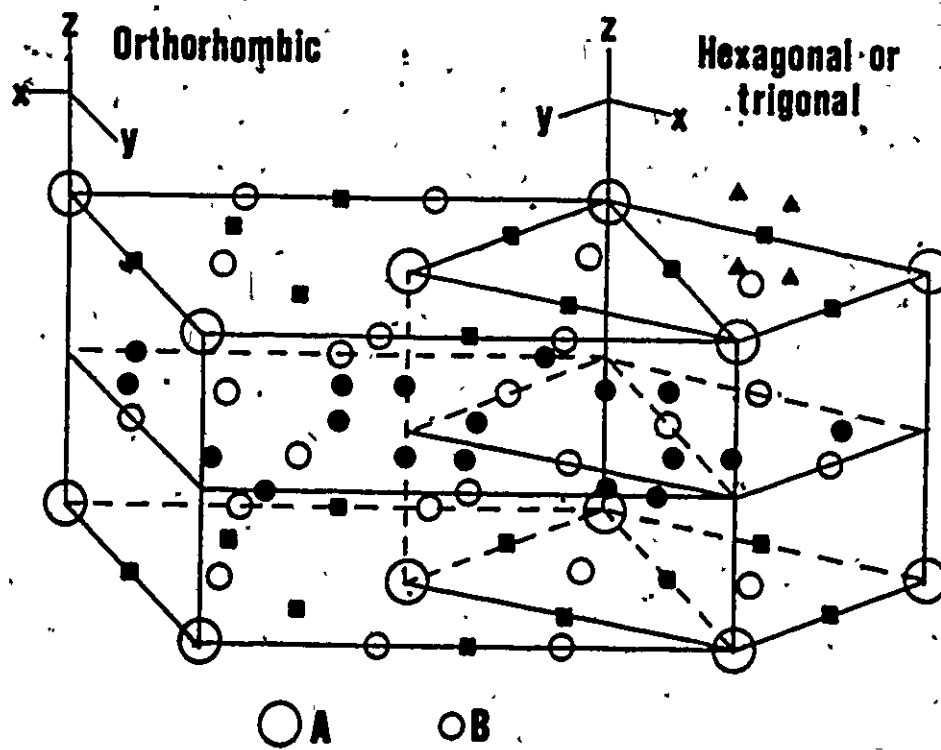


Figure 8 The AB₅ structure shown in both the hexagonal (right) and orthorhombic (left) lattices. Also shown are tetrahedral (●) and octahedral (■) hydrogen sites and their possible degeneracies (▲) (37).

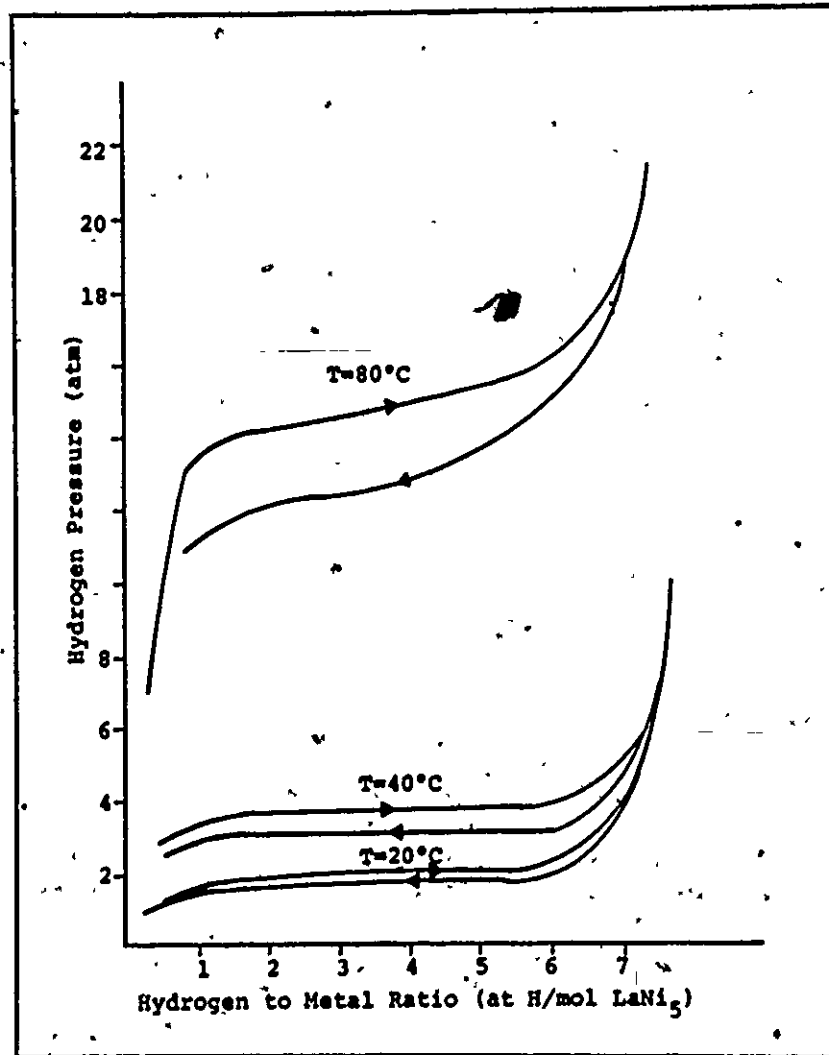


Figure 9 P-C-T plot for the LaNi₅-H system (39). Note that hysteresis is small at low temperatures.

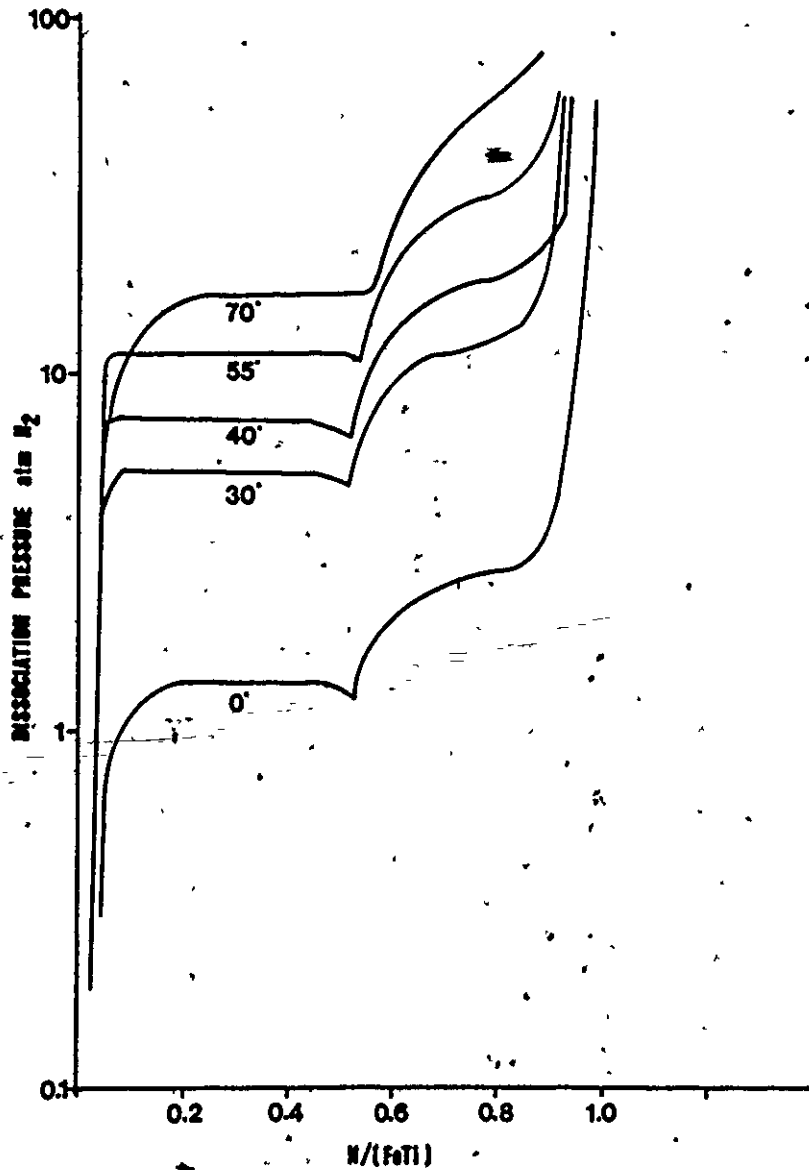


Figure 10 P-C-T plot for the FeTi-H system (47).

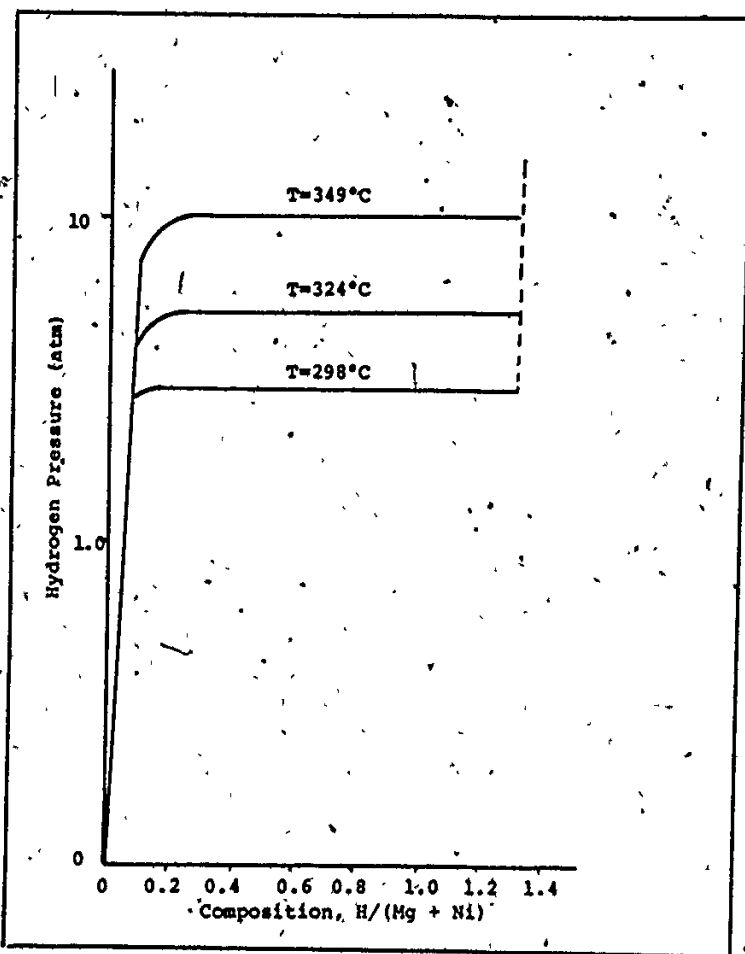


Figure 11 P-C-T plot for the Mg₂Ni-H system (16).

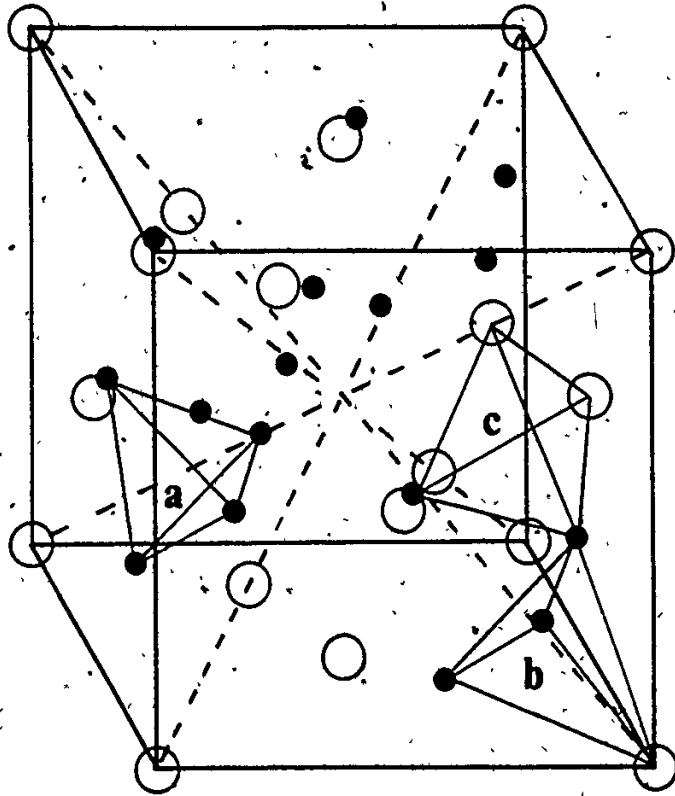


Figure 12. The cubic (C15) Laves phase is shown. The A atoms are shown as open circles and the B atoms as solid ones. The three types of interstitial sites are given: a) B₄ sites, b) AB₃ sites and c) A₂B₂ sites (81).

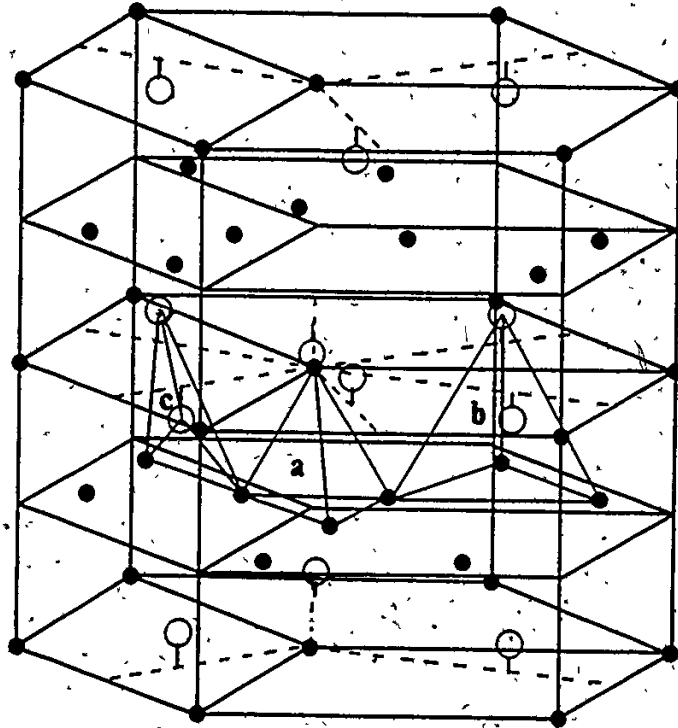


Figure 13 The hexagonal (C14) Laves phase is given. The solid circles represent B atoms and the open circles A atoms. The interstitial sites are shown: a) B₄ sites; b) AB₃ sites and c) A₂B₂ sites (81).

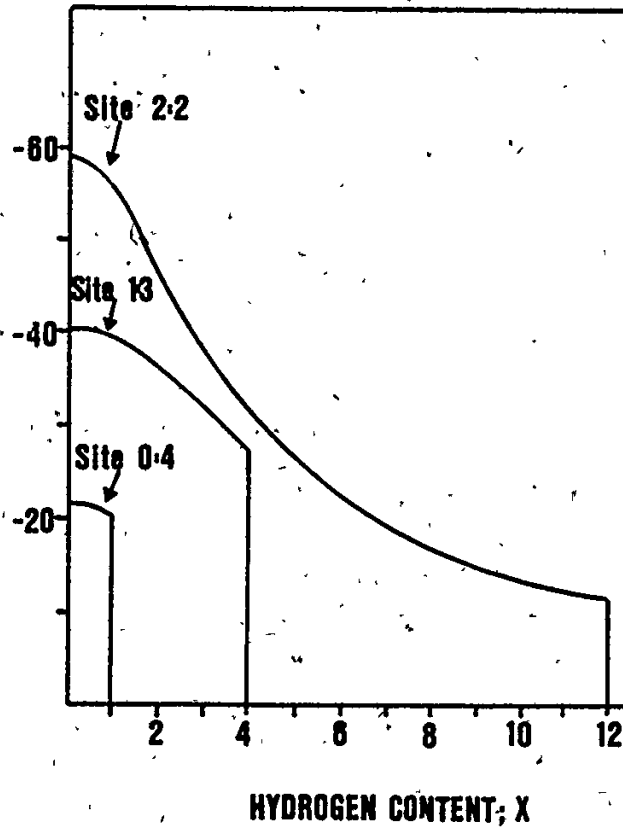
$\Delta H'$ (kcal/mole H_2)

Figure 14 The calculated heats of formation as a function of the hydrogen concentration are shown for the three types of tetrahedral sites in ZrV_2 . At the concentration ~ 2.5 , the 2-2 (A_2B_2) and the 1-3 (AB_3) interstices are competitive with respect to hydrogen occupation (62).

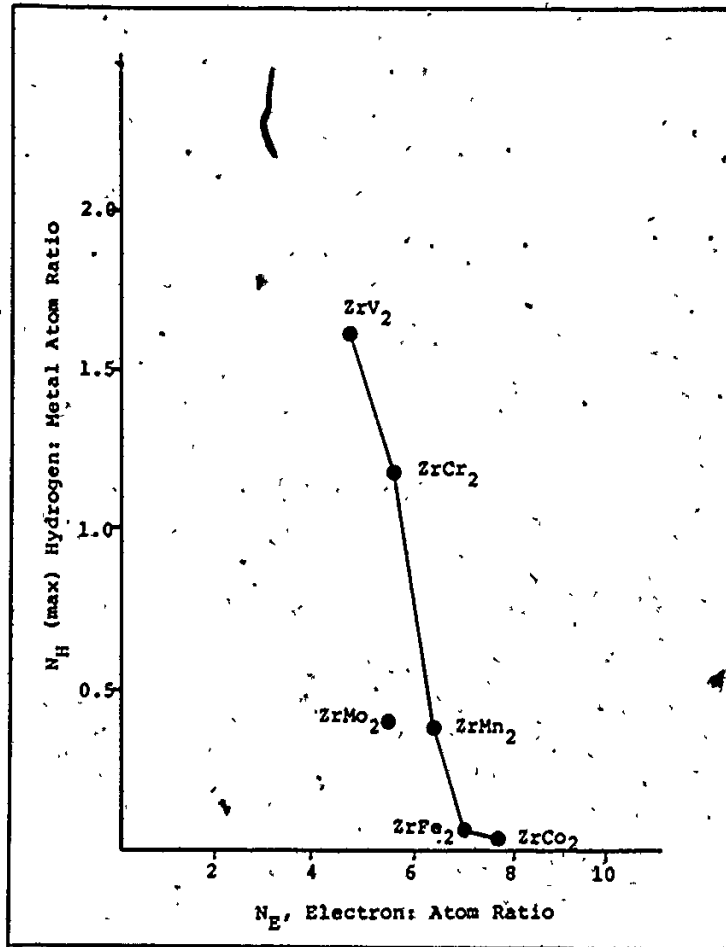


Figure 15 Plot of hydrogen concentration against electron concentration (57).

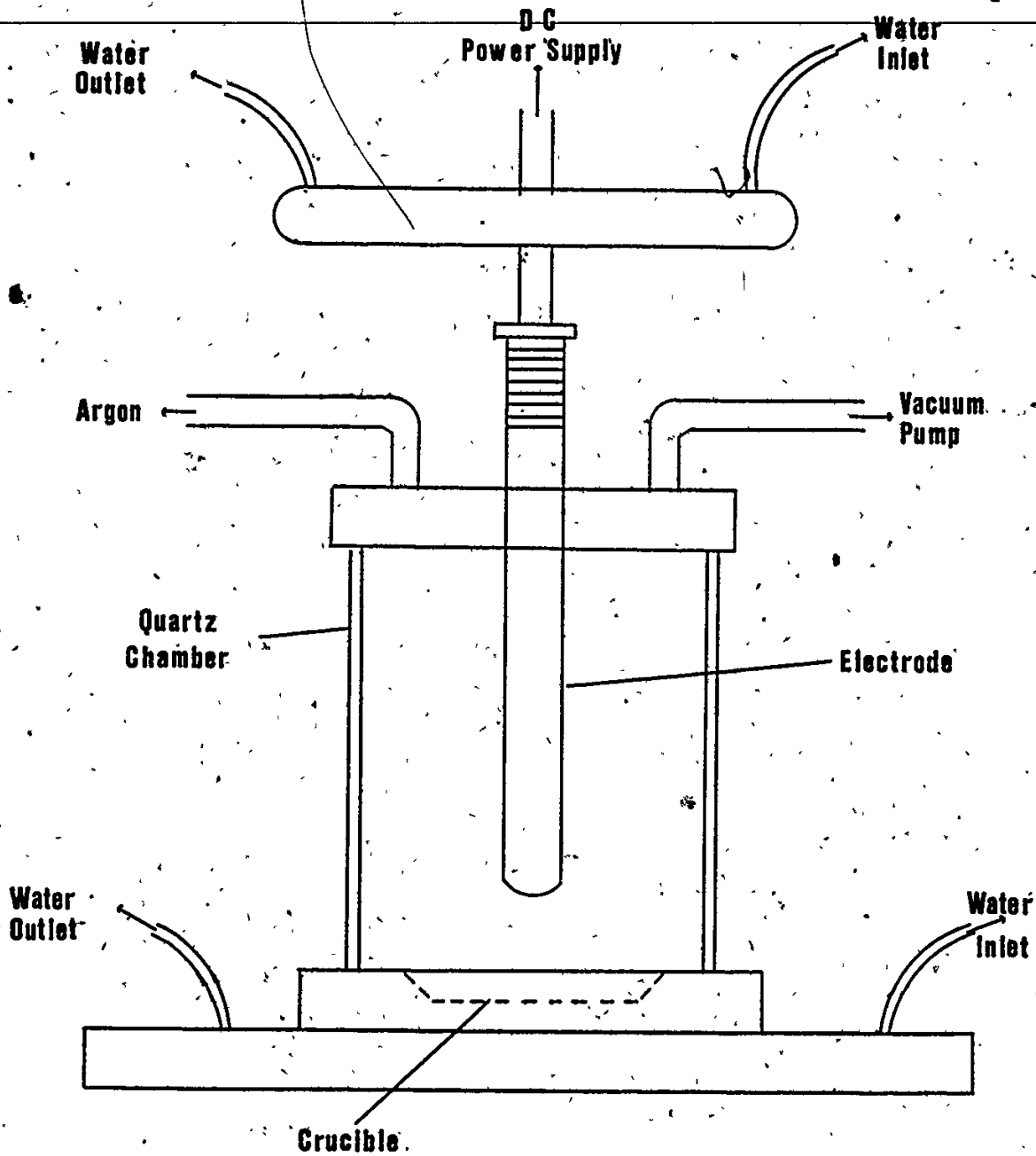


Figure 16 Schematic drawing of vacuum arc furnace, showing main components.

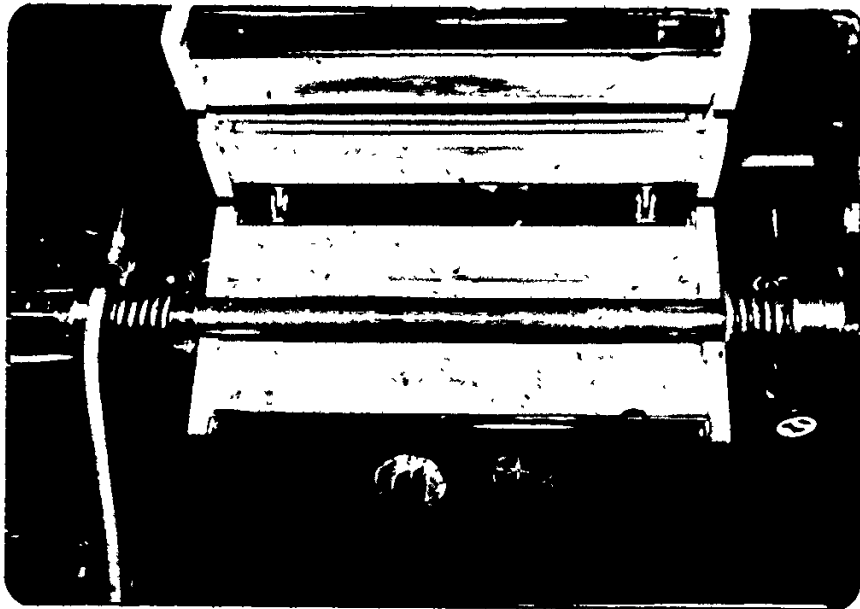


Figure 17 Photograph of the reactor vessel, surrounded by a tube furnace. The dimensions and description are given in the text.

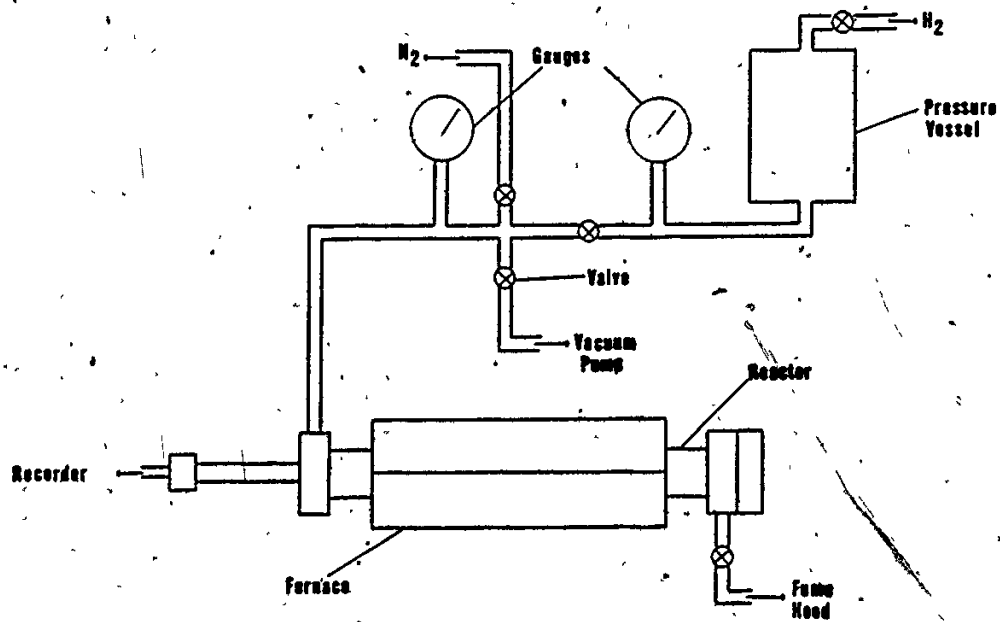


Figure 18a Schematic drawing of Hydriding/Dehydriding apparatus, illustrating key components.

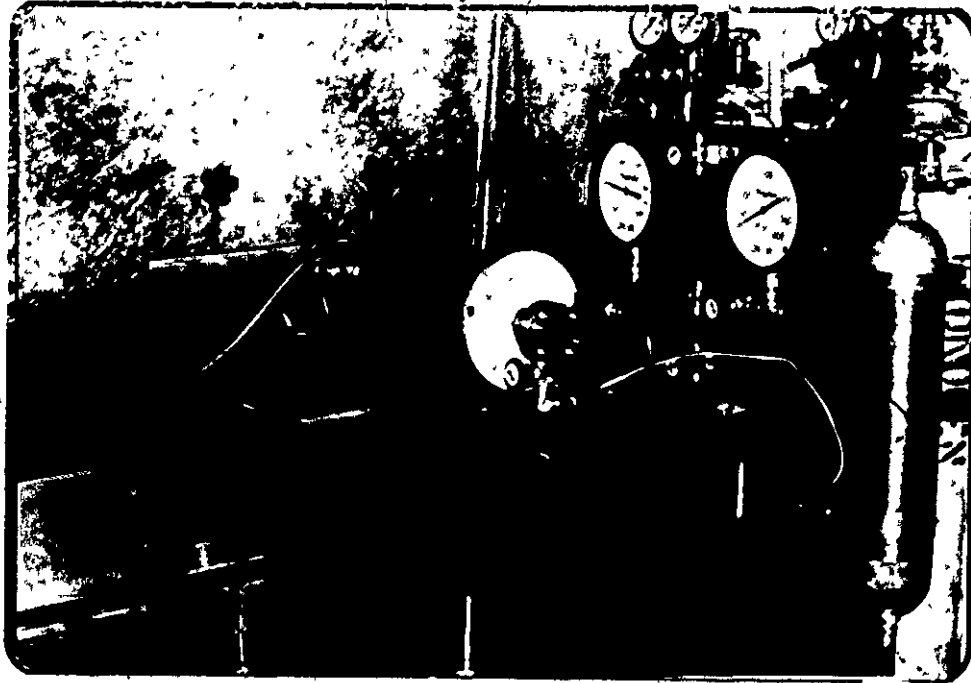


Figure 18b Photograph of apparatus shown in Figure 18a.

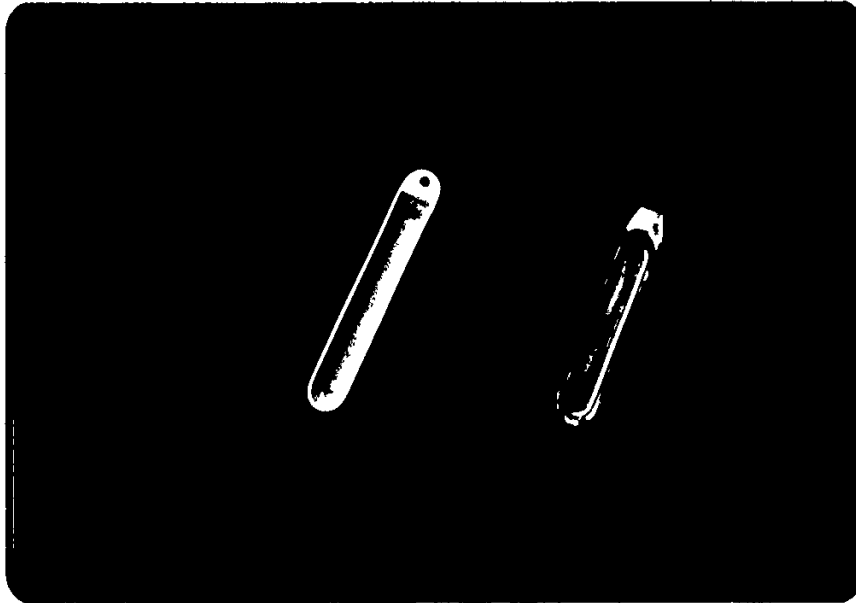


Figure 19 Photograph of the ceramic (left) and nickel-alloy (right) crucibles utilized in this study.

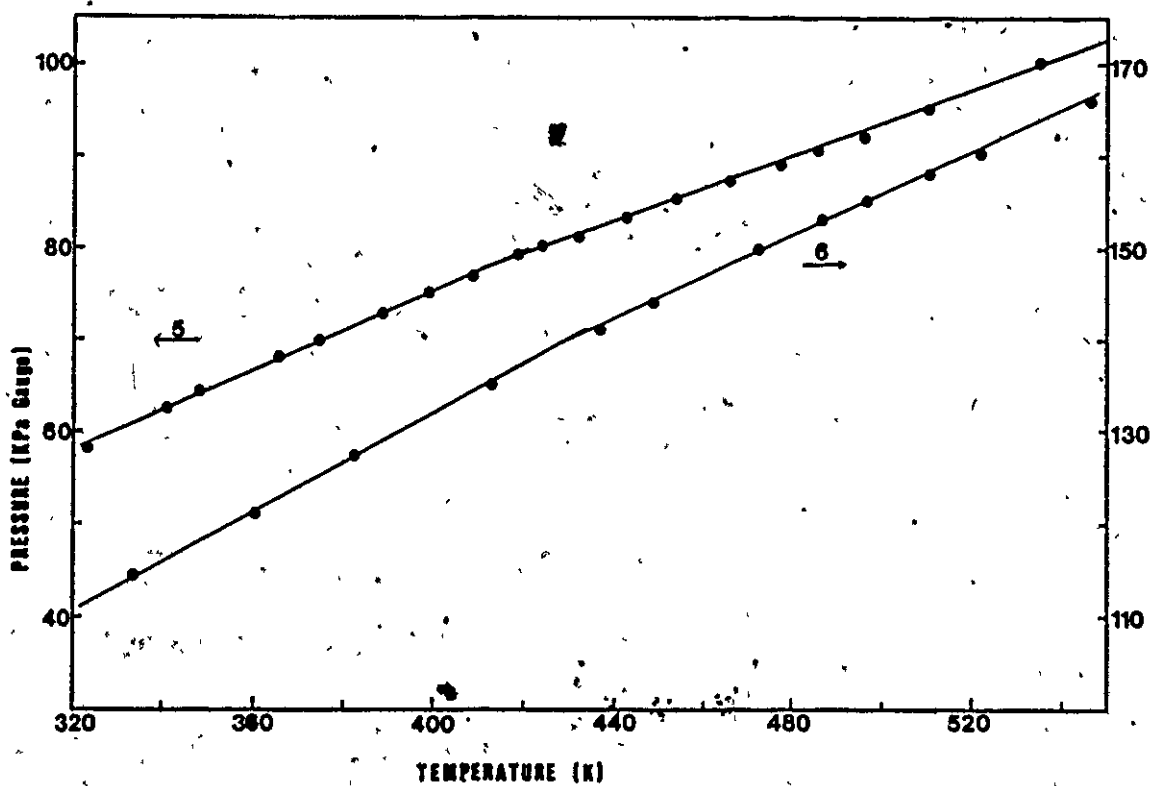


Figure 20 Calibration curves for determining the relationship between pressure, temperature and number of moles of gas in the reactor system. The two curves shown are for the 5th and 6th experimental runs.

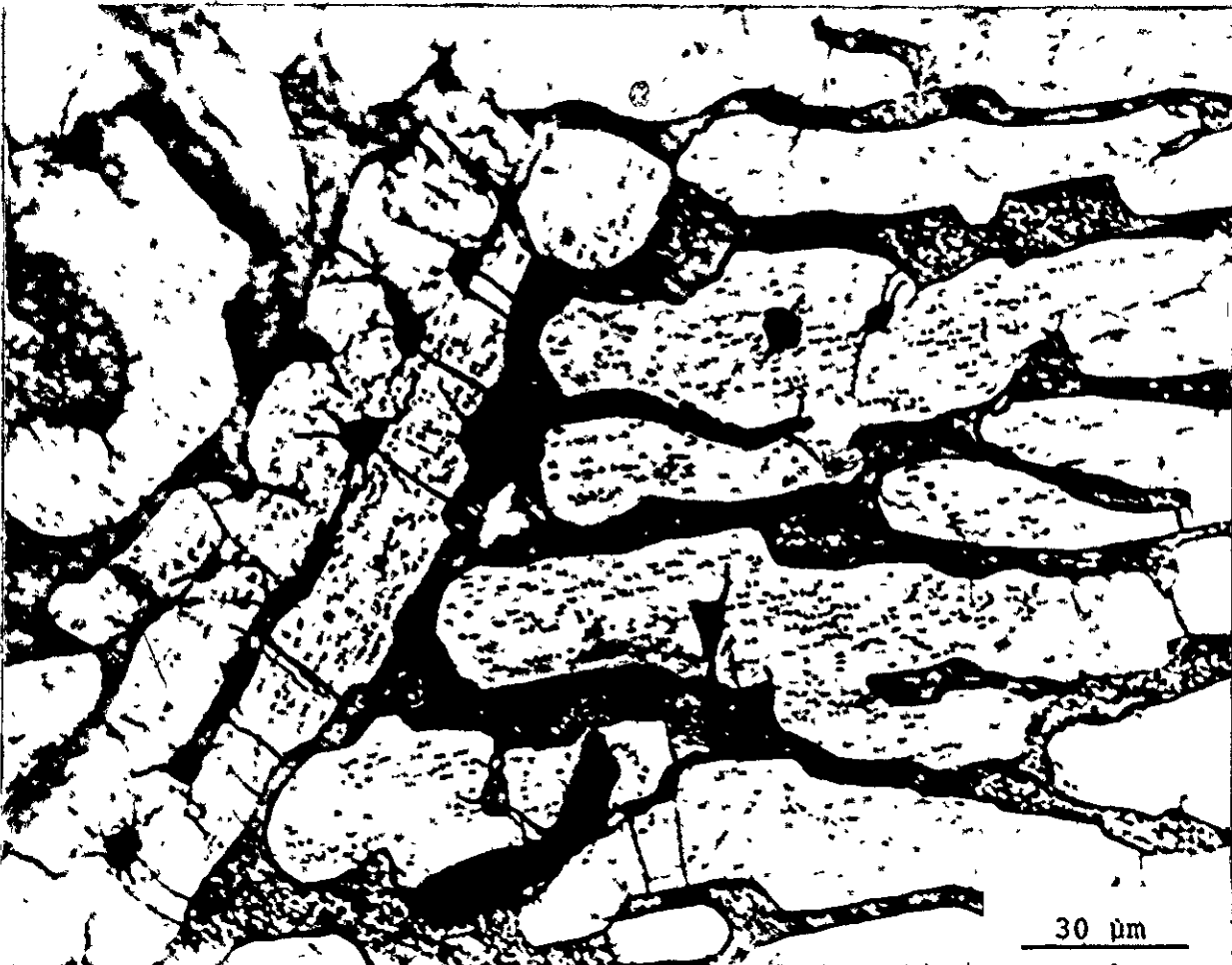


Figure 21 Optical micrograph of the microstructure of the $Zr(Fe_{0.5}Mn_{0.5})_2$ alloy, showing the two-phase region and the difference in etching. Also evident are elongated grains, characteristic of a cast structure.

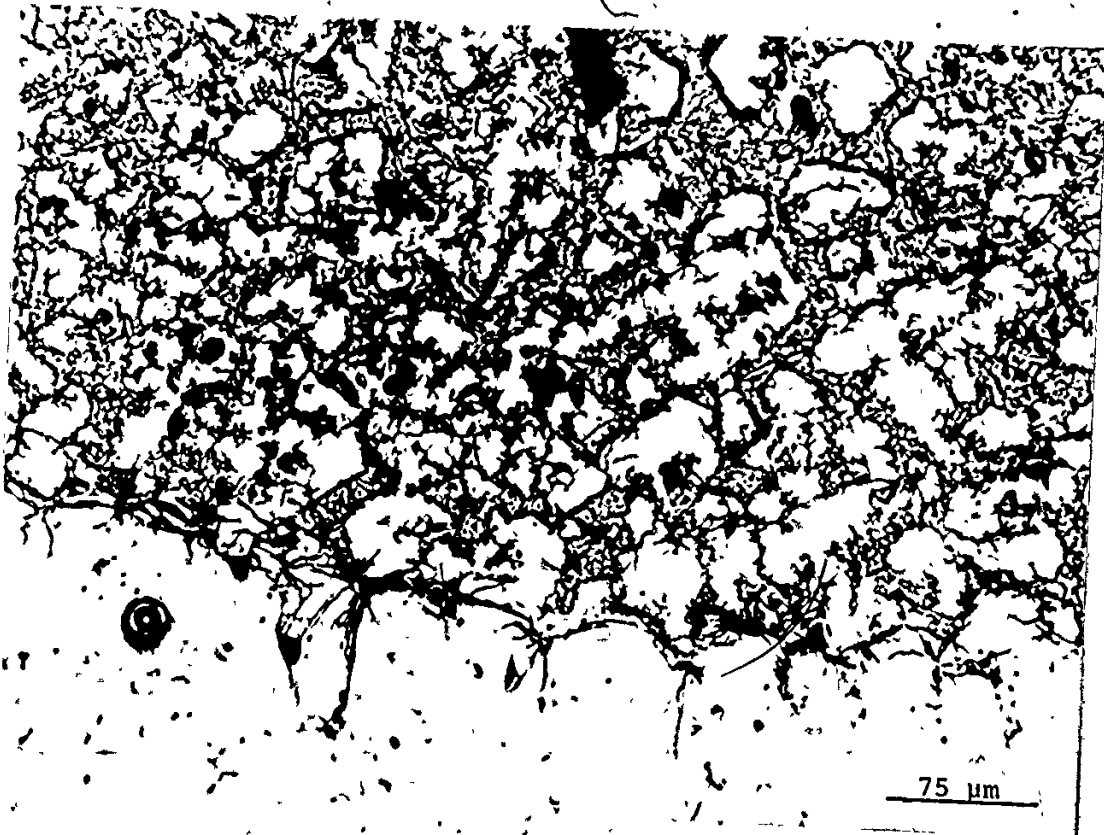


Figure 22 Optical micrograph of $Zr(Mn_{0.5}Co_{0.5})_2$ alloy, illustrating the phase separation.

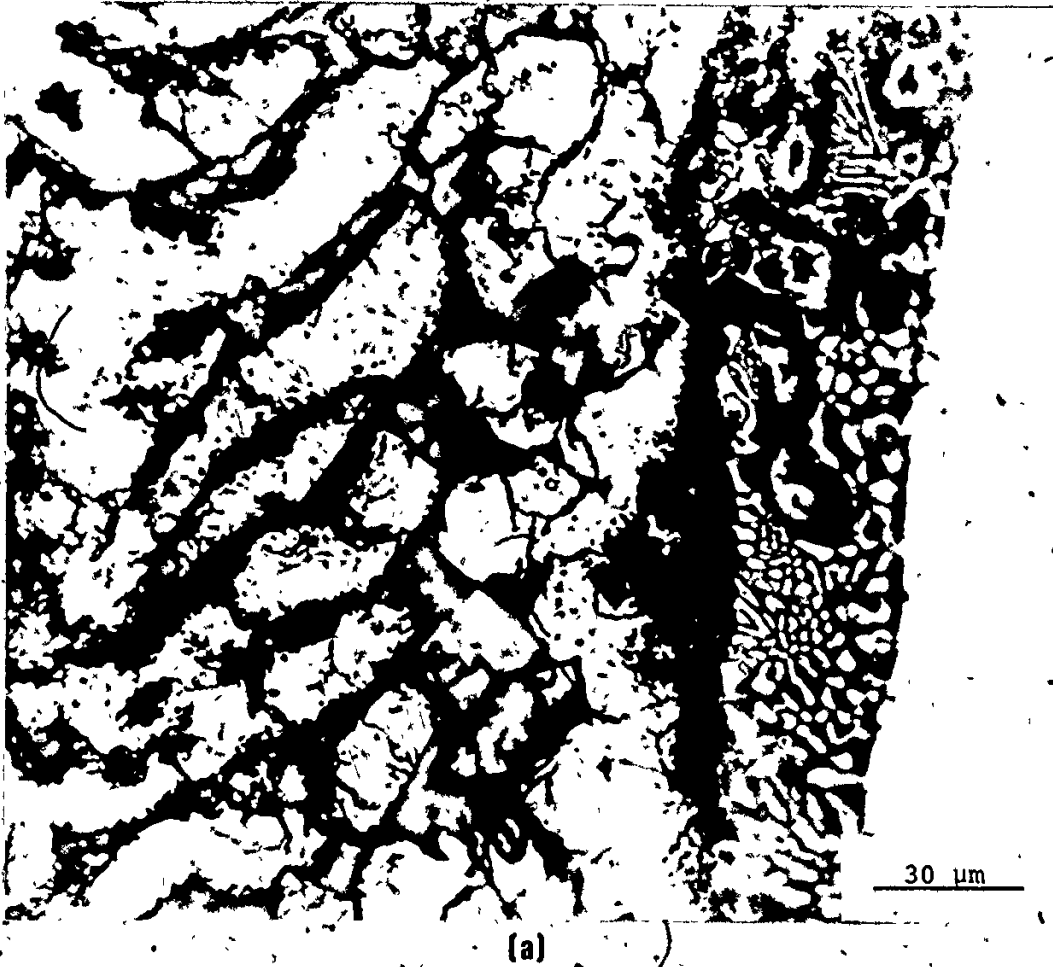
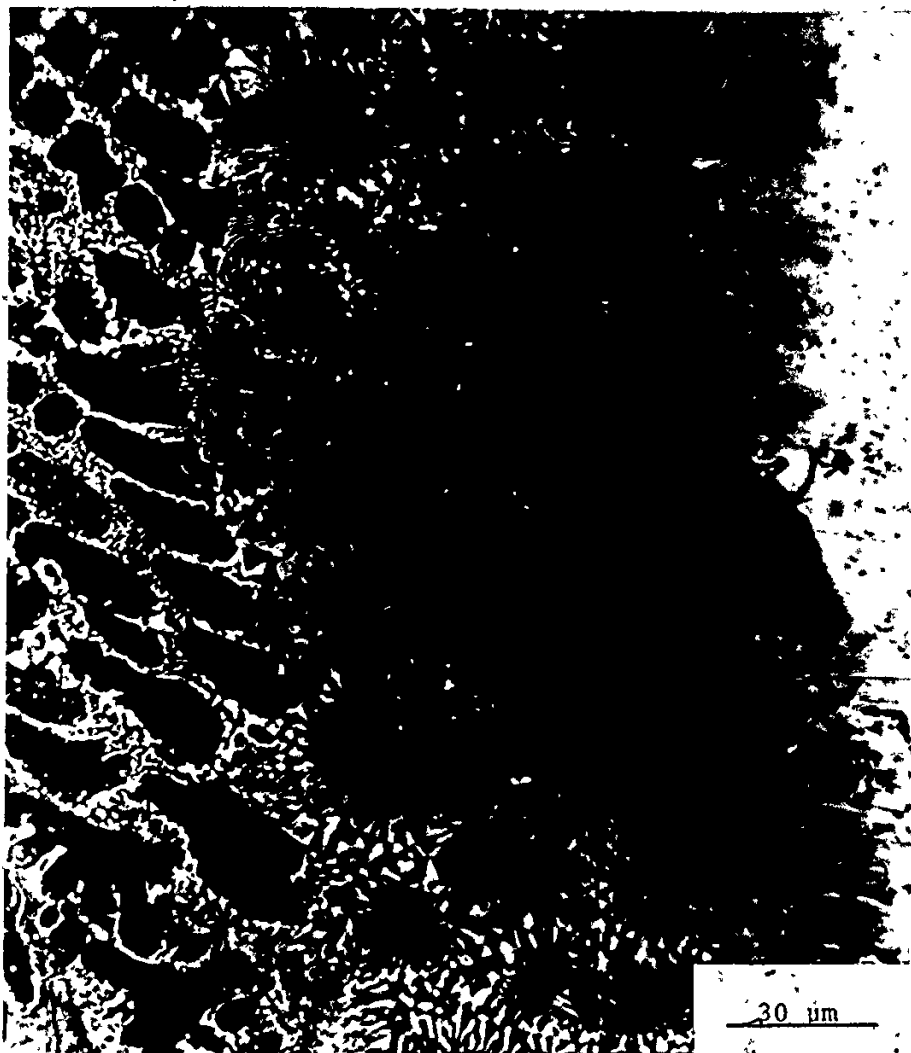


Figure 23 Optical micrographs of a) $\text{Zr}(\text{Co}_{0.4}\text{Co}_{0.6})_2$ and b) $\text{Zr}(\text{Fe}_{0.5}\text{Cr}_{0.5})_2$ samples, showing the rim structure between the phase separation. The rim structure is composed of the two phases, finely distributed.

5



(b)

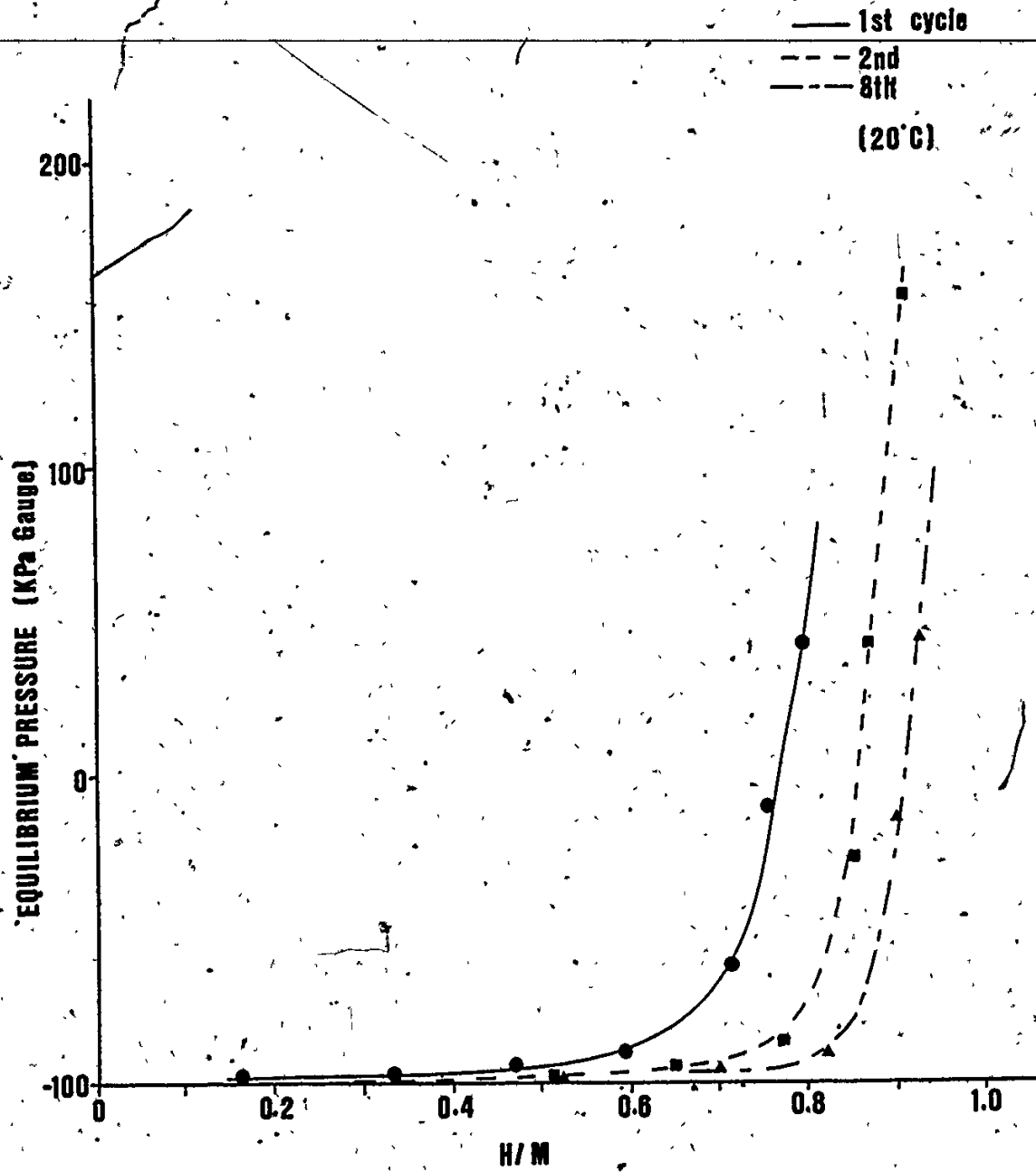


Figure 24 P-C-T plot for the $\text{Zr}(\text{Fe}_{0.4}\text{Cr}_{0.6})_2\text{-H}$ system.

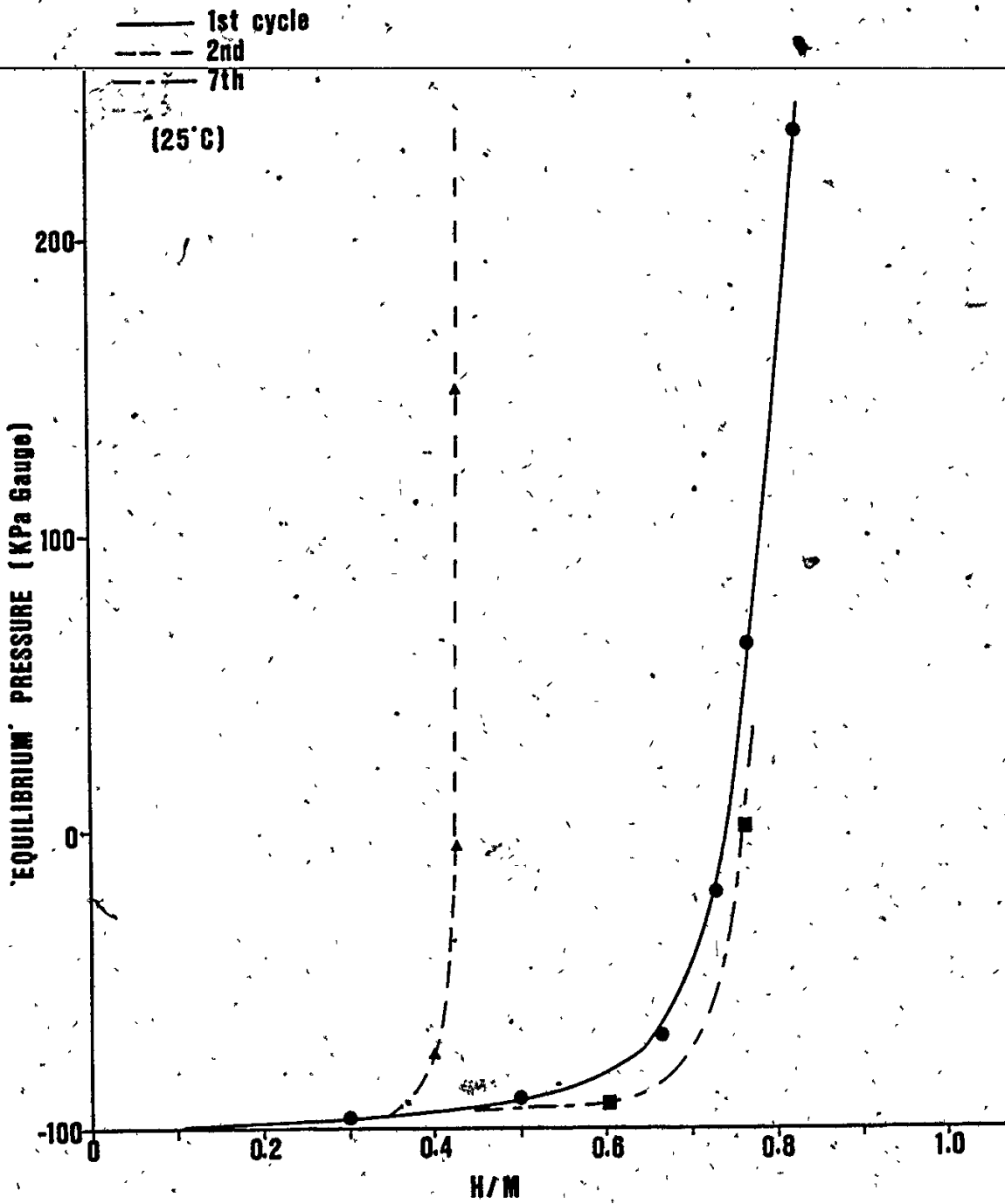


Figure 25 P-C-T plot for the $Zr(Fe_{0.5}Cr_{0.5})_2-H$ system.

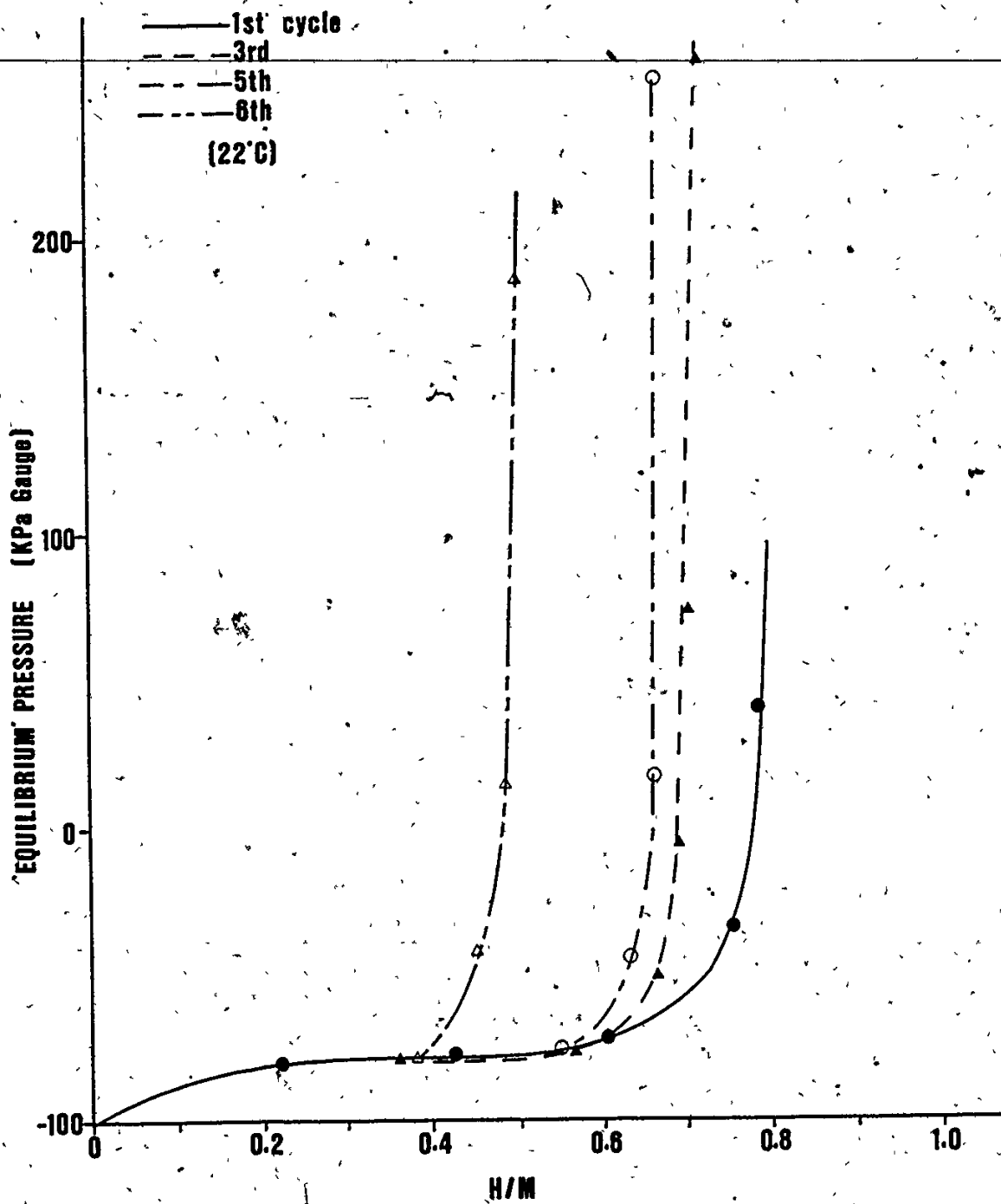


Figure 26 P-C-T plot for the $\text{Zr}(\text{Fe}_{0.6}\text{Cr}_{0.4})_2\text{-H}$ system.

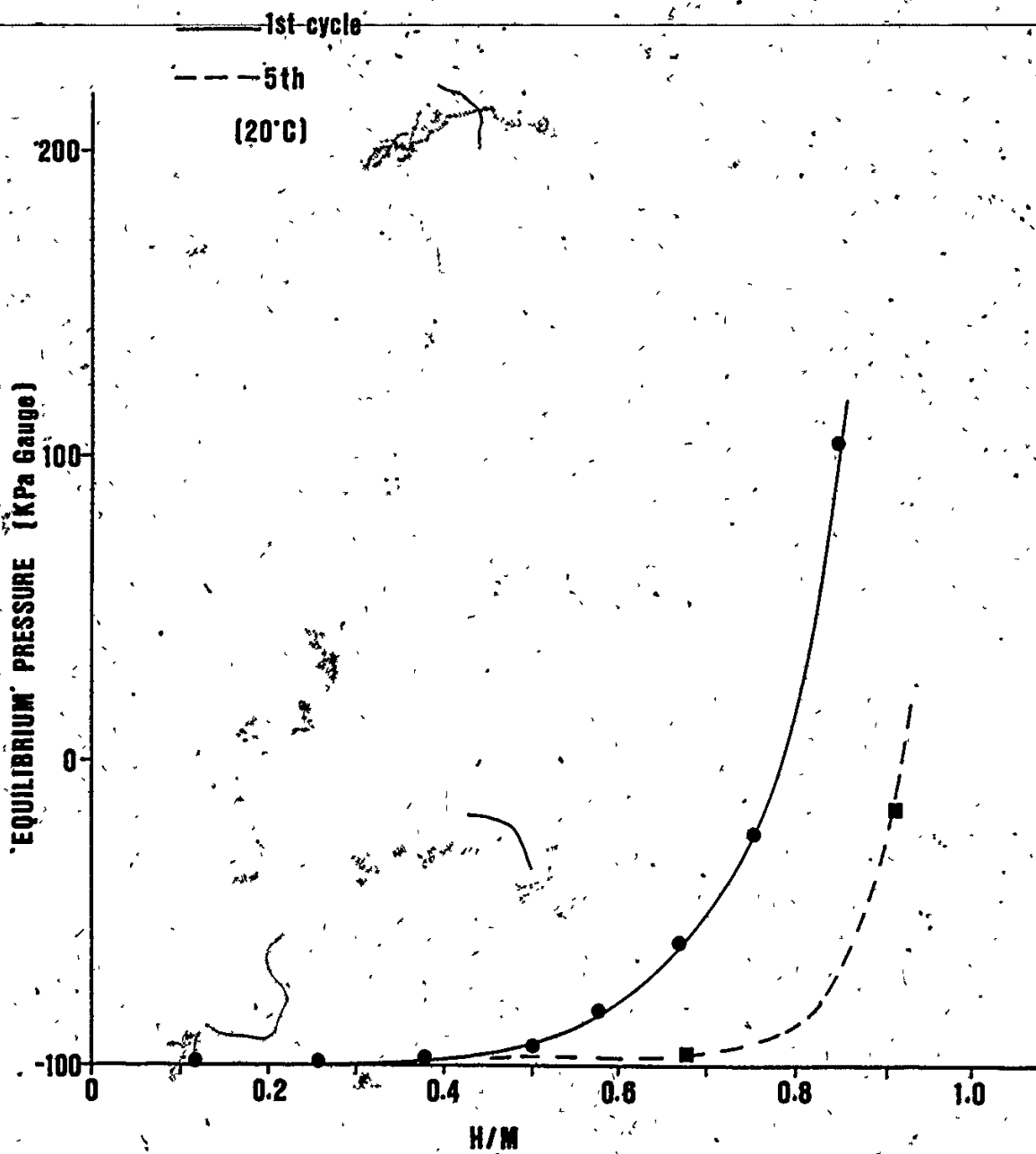


Figure 27 P-C-T plot for the $\text{Zr}(\text{Co}_{0.4}\text{Mn}_{0.5})_2\text{-H}$ system.

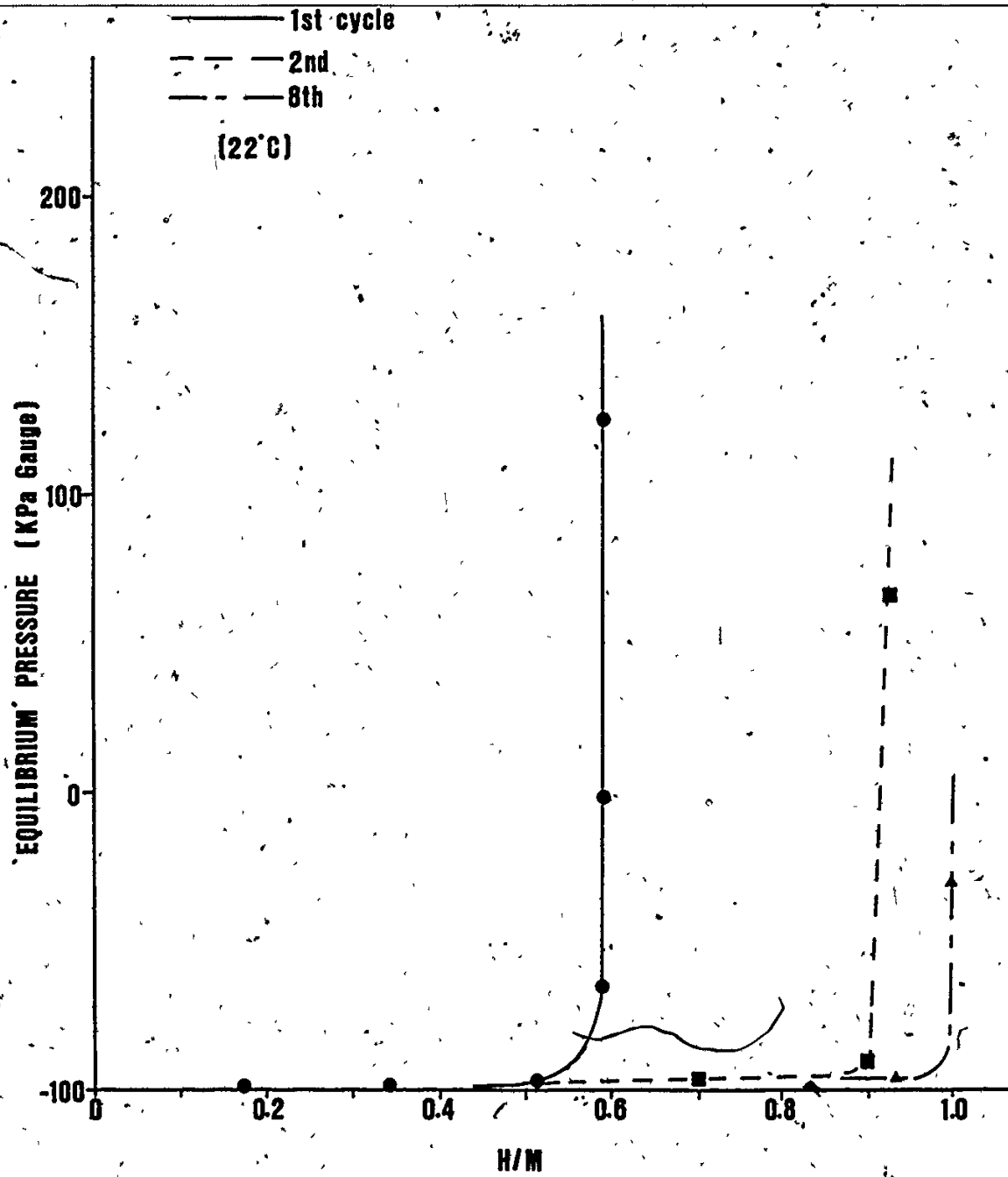


Figure 28 P-C-T plot for the $\text{Zr}(\text{Co}_{0.4}\text{Cr}_{0.6})_2\text{-H}$ system.

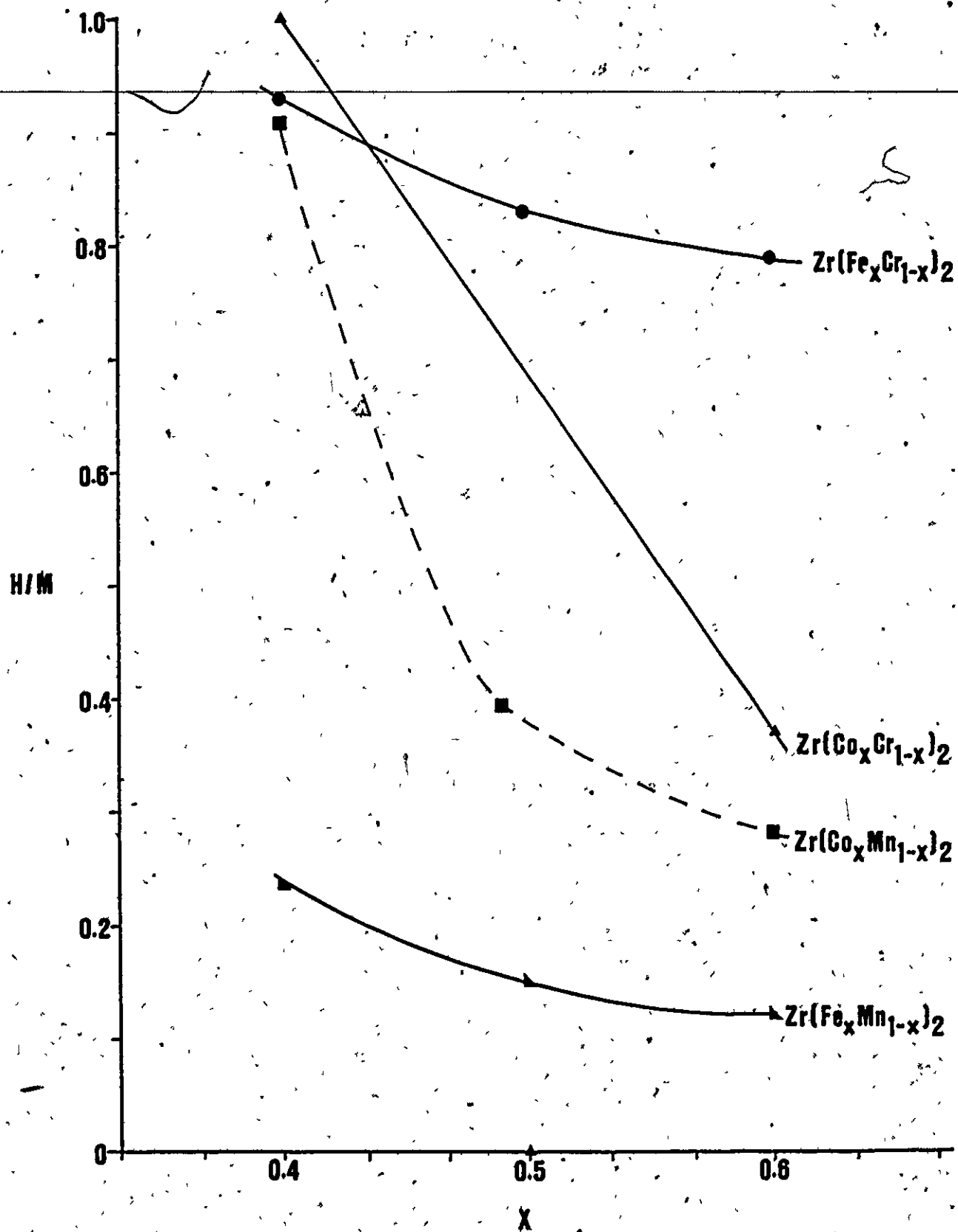


Figure 29 Plots of H/M ratio vs. 'X' for $Zr(B_x B'_{1-x})_2$ where $B=Fe, Co$ and $B'=Cr, Mn$.

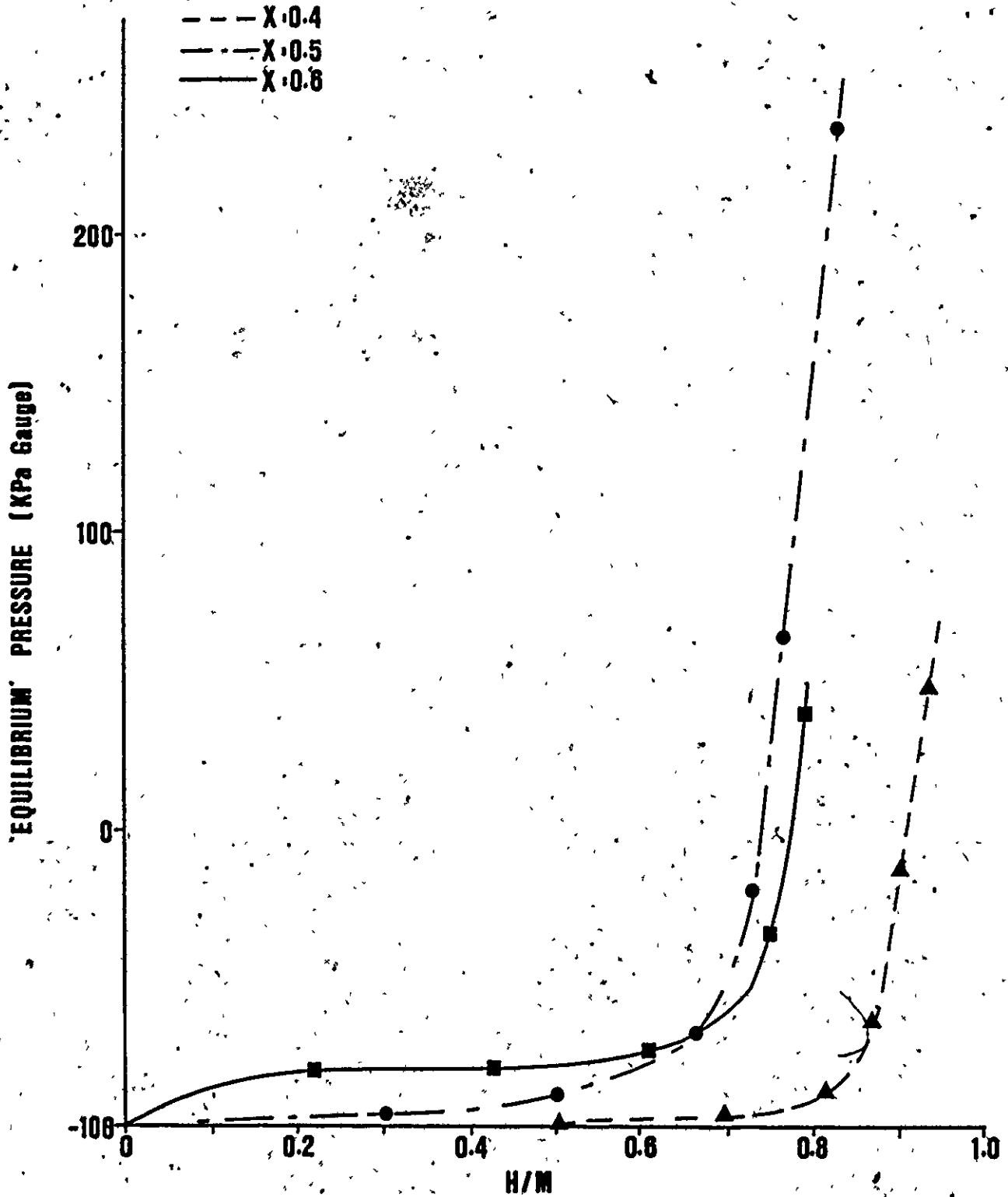


Figure 30 P-C-T plots for the $Zr(FexCr_{1-x})_2$ alloys. Note the increase in 'plateau' pressure and decrease in H/M ratio as 'x' increases.

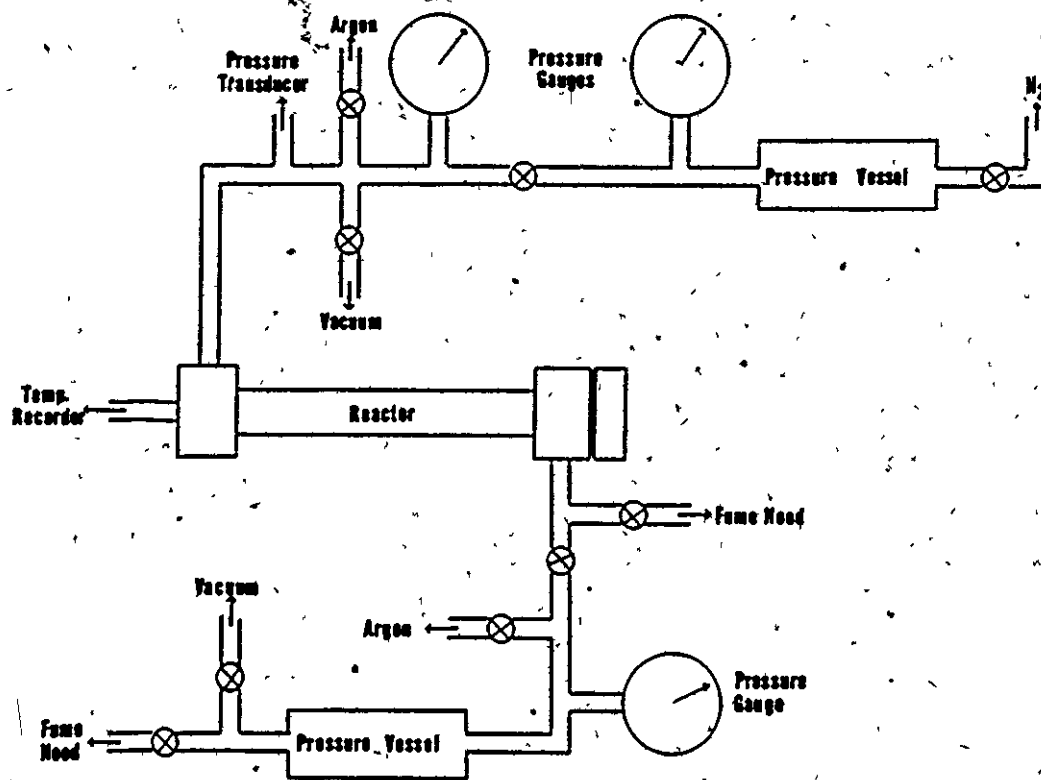


Figure 31 Schematic diagram of proposed hydriding system, showing major components.

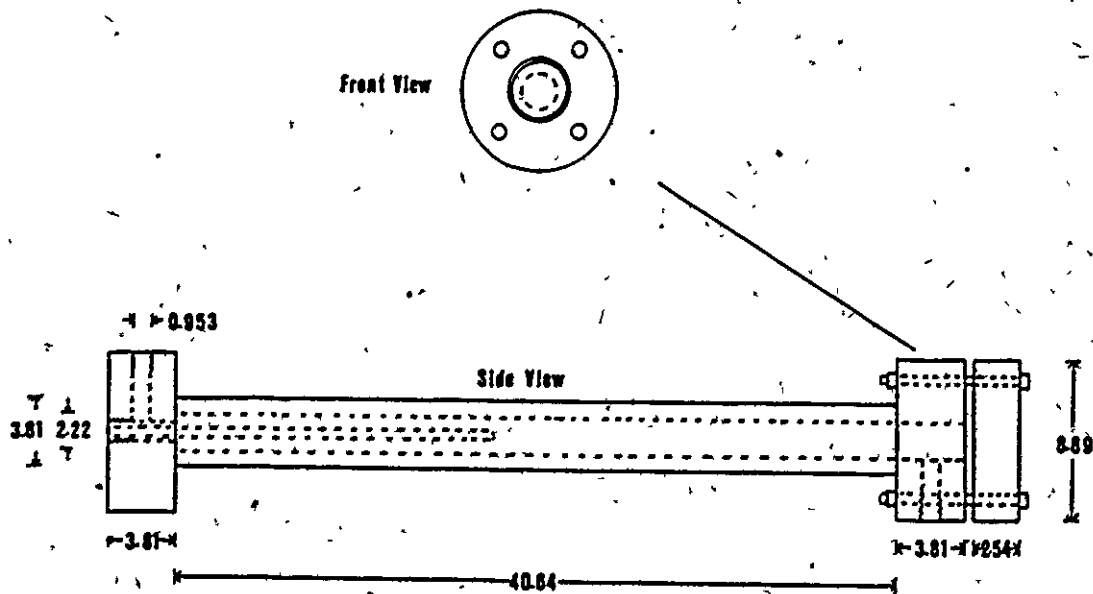


Figure 32 Schematic drawing of reactor design.
Dimensions are in centimeters.

APPENDIX A

Calculation of the Effect of Sample Size on
Reactor Volume

Atomic weights and densities were utilized in calculating the volume occupied by a hydriding sample in the reactor system. Calculations were done on one alloy type, i.e., $Zr(Co_{0.5}Cr_{0.5})_2$, and it was assumed that this would be representative of all the alloys employed in this research. The atomic weights and densities for zirconium, chromium and cobalt are given in Table A.1 and a typical calculation is shown below:

1) Molecular weight of $Zr(Co_{0.5}Cr_{0.5})_2$

$$= \frac{1}{3} \text{ atomic wt Zr} + \frac{1}{3} \text{ atomic wt Cr} \\ + \frac{1}{3} \text{ atomic wt Co}$$

$$= \frac{1}{3} (91.22 + 51.996 + 58.93)$$

$$= 67.382 \text{ g/mole}$$

2) Density of $Zr(Co_{0.5}Cr_{0.5})_2$

$$= \frac{1}{3} \text{ density Zr} + \frac{1}{3} \text{ density Co} \\ + \frac{1}{3} \text{ density Cr}$$

$$= \frac{1}{3} (6.49 + 7.20 + 8.9)$$

$$= 7.53 \text{ g/cm}^3$$

$$= 7.53 \times 10^6 \text{ g/m}^3$$

3) Volume of $Zr(Co_{0.5}Cr_{0.5})_2$ per mole

$$= \frac{\text{molecular wt}}{\text{density}}$$

$$= \frac{67.382 \text{ g/mole}}{7.53 \times 10^6 \text{ g/m}^3}$$

$$= 8.948 \times 10^{-6} \text{ m}^3/\text{mole}$$

$$= 9.0 \times 10^{-6} \text{ m}^3/\text{mole} \quad (9.0 \text{ cm}^3/\text{mole})$$

4) The maximum amount of weight deviation is 5.0 grams,
hence the maximum volume change

$$= 9.0 \times 10^{-6} \text{ m}^3/\text{mol} \times \frac{5 \text{ g}}{67.382 \text{ g/mol}}$$

$$= 6.68 \times 10^{-7} \text{ m}^3$$

$$\sim 1.0 \times 10^{-6} \text{ m}^3 \quad (1.0 \text{ cm}^3)$$

or

$$\frac{1.0 \times 10^{-6} \text{ m}^3}{209.0 \times 10^{-7} \text{ m}^3} \times 100$$

$$< 0.5\%$$

Table A.1Densities and Atomic Weights For Zirconium,
Chromium and Cobalt

Element	Atomic Weight (g/mole)	Density (g/cm ³)
Zr	91.22	6.49
Cr	51.996	8.90
Co	58.93	7.20

20-293

CALCULATED PATTERN-PEAK HEIGHT

2.15	2.33	1.32	100	60	40	d A	1/1 ₀	h k l	d A	1/1 ₀	h k l
<p><chem>Mn2Zr12N</chem> Manganese Zirconium Ref. Wallmann, Z. Krist., 102, 391 (1941)</p> <p>Sys. Hexagonal S.G. P6₃/mmc (194) 2 4 a₀ 5.038 b₀ c₀ 8.250 Z 12 Ref. 1944.</p> <p>Scale factor (Integrated Intensities) 1.7982</p>											
d A	1/1 ₀	h k l	d A	1/1 ₀	h k l						
2.320	20	110	1.375	30	004,302						
2.327	60	103	1.316	40	305						
2.150	100	112	1.260	30	220						
2.109	20	201	1.164	20	215,206						
1.414	10	213									

FORM CP
V

Copyright © Joint Committee on Powder Diffraction Standards

6-0613

d	2.17	2.94	2.33	4.14	ZnO ₂ (Low Temp.)	
1/1 ₀	100	80	80	20	Orthorhombic ZnO ₂ 2:1	
Ref. Dts. 1/2 Visual	A	Ch. mt.	Tuner			
Ref. ROSTONER, J. METALS 2, 304 (1953)			Calc. 4 mm. abs. 1			
Sys. Hexagonal	S.G.					
a ₀ 3.079 b ₀ c ₀ 4.279	A	C				
Ref. 1918.						
to 2θ	D	mp	Color	Sign.		
Ref.						
STRUCTURE: MnZnO TYPE						
TRANSITION TO THE P.6. CUBIC HIGH TEMP. PHASE						
(MnO ₂) OCCURS AT 200-224°C.						
	d A	1/1 ₀	h k l	d A	1/1 ₀	h k l
	4.144	20	002			
	2.791	30	003			
	2.543	40	100			
	2.330	80	100			
	2.301	30	100			
	2.166	100	112			
	2.129	80	201			
	2.044	60	004			
	1.977	20	202			
	1.867	40	104			
	1.681	30	210			
	1.648	30	212			
	1.612	10	304			
	1.609	80	300			
	1.627	80	213			
	1.396	80	302			
	1.323	80	308			
	1.299	80	214			
	1.274	80	220			
	1.213	20	116			

447

Appendix C

Crystallographic Results

Target: Mo

Wavelengths: $\lambda_{K\alpha_1} = 0.7093\text{\AA}$

$\lambda_{K\alpha_2} = 0.7135\text{\AA}$

$\bar{\lambda} = \frac{2K\alpha_1 + K\alpha_2}{3} = 0.7107\text{\AA}$

Target: Cu

Wavelengths: $\lambda_{K\alpha_1} = 1.5405\text{\AA}$

$\lambda_{K\alpha_2} = 1.5453\text{\AA}$

$\bar{\lambda} = \frac{2K\alpha_1 + K\alpha_2}{3} = 1.542\text{\AA}$

Required Equations

$\lambda = 2d \sin\phi$ (Bragg equation)

or,

$d = \frac{\lambda}{2\sin\phi}$

Hexagonal System:

$d_{hkl} = \frac{1}{(4/3 \cdot \frac{h^2 + hk + k^2}{a^2} + \frac{l^2}{c^2})^{1/2}}$

Cubic System:

$d_{hk} = \frac{a}{(h^2 + k^2 + l^2)^{1/2}}$

1) Sample 12 Zr(Fe_{0.6}Cr_{0.4})₂ (Mo-target)

ϕ (°)	Intensity	d (Å) (From Bragg Relation)	hkl Hexagonal	* Cubic	d (Å) (From Lattice Parameters) Hexagonal	Cubic
8.80	3	2.323	103		2.318	
9.30	9	2.200	200		2.174	
9.65	1	2.120	112	311	2.142	2.114
9.90		2.067	201		2.101	
10.15	9	2.016	004	222	2.055	2.024
10.50		1.950	202		1.922	
11.0		1.862	104		1.858	
12.85		1.598	210	331	1.643	1.608
13.35		1.539	212		1.526	
13.65		1.506	204		1.493	
14.30		1.439	300	422	1.449	1.431
14.65	5	1.405	213		1.409	
15.05	6	1.369	302	333, 511	1.367	1.349
15.70	1	1.313	205		1.311	
16.10		1.281	214		1.283	
16.40	4	1.259	220	440	1.255	1.239
17.40		1.188	116	531	1.203	1.185
18.70		1.108		620		1.108

Lattice Parameters

Hexagonal: a = 5.02Å, c = 8.22Å

Cubic: a = 7.01Å

Sample 11 Zr(Fe_{0.5}Cr_{0.5})₂ (Mo-target)

ϕ (°)	Intensity	d (Å) (from Bragg Equation)	hkl		d (Å) (From Lattice Parameters)
			Hexagonal	Cubic	
8.80	5	2.323	103		2.317
9.50	2	2.153	112	222	2.148
10.0	1	2.046	004		2.050
10.53	8	1.945	202		1.928
12.30		1.668	210	331	1.651
14.25		1.444	300	422	1.456
14.65		1.405	213		1.413
14.95		1.377	302	511, 333	1.372
15.6	4	1.321	205		1.312
15.73		1.311	214		1.286
16.4		1.259	220	440	1.261
17.0	6	1.215		531	
17.50	7	1.182	116		1.180
17.63		1.174	215, 206		1.164, 1.159
18.43		1.124		620	
19.03		1.090		533	
22.03		0.948		642	
22.9	3	0.913		553, 731	

Lattice ParametersHexagonal: $a = 5.045\text{\AA}$, $c = 8.20\text{\AA}$ Cubic: $a = 7.12\text{\AA}$

Sample 10 Zr(Fe_{0.4}Cr_{0.6})₂ (Mo-target)

ϕ (°)	Intensity	d (Å) (From Bragg Equation)	hkl Hexagonal	Cubic	d (Å) (From Lattice Parameters) Hexagonal Cubic
8.75		2.336	103		2.330
9.425	1	2.170	112	311	2.154
9.65		2.120	201		2.114
9.90	6	2.067	004	222	2.065
10.58	12	1.936	202		1.933
10.98		1.867	104		1.867
12.30		1.668	210	331	1.653
13.63		1.508	204		1.501
14.13		1.456	300	422	1.458
14.43	4	1.426	213		1.417
14.80	8	1.391	302	333	1.375
15.55	3	1.326	205	511	1.318
15.95		1.293	214		1.290
16.25		1.270	220	440	1.263
16.80	5	1.229	116		1.209
18.18	7	1.139		620	1.139
18.40	9	1.126			1.110
18.68	2	1.110		533	1.110
19.15		1.083		622	1.085

Lattice ParametersHexagonal: $a = 5.05 \text{ \AA}$, $c = 8.26 \text{ \AA}$ Cubic: $a = 7.20 \text{ \AA}$

Sample 9 Zr(Fe_{0.6}Mn_{0.4})₂ (MO-target)

ϕ (°)	Intensity	d (Å) (From Bragg Equation)	hkl Hexagonal Cubic	d (Å) (From Lattice Parameters) Hexagonal Cubic
8.30	11	2.462	110 220	2.497 2.450
8.80	7	2.323		
8.95	3	2.284		
9.45		2.164		
9.75	1	2.098	103 311	2.304 2.089
10.05	2	2.036	112 222	2.164 2.001
13.05		1.574	201 331	2.131 1.590
14.68	4	1.403	213 422	1.402 1.415
15.10	4	1.364	006,302	1.361,1.360
15.58		1.323		
15.85	6	1.301	205 333	1.304 1.334
16.55	8	1.247	220	1.250
17.0		1.215		
17.55		1.178		
17.90	9	1.156	440 531	1.225 1.171
19.03	10	1.090	215,206 620	1.156,1.152 1.096

Lattice Parameters

Hexagonal: a = 5.00 Å, c = 8.166 Å

Cubic: a = 6.930 Å

Sample 8 Zr (Fe_{0.5}Mn_{0.5})₂ (Cu-target)

ϕ (°)	Intensity	d (Å) (From Bragg Equation)	hk ℓ Hexagonal Cubic	d (Å) (From Lattice Parameters) Hexagonal Cubic
18.0	4	2.495	110	2.515
18.30	5	2.455		2.460
21.10	2	2.142	112	2.143
21.50	3	2.104	201	2.105
28.90		1.595	213	2.099
33.05	1	1.414	006, 302	1.597
34.25		1.370		1.421
34.88		1.348		1.365, 1.369
35.90	6	1.315	205	1.339
37.75	7	1.259	220	1.309
38.85	9	1.229		1.258
40.50		1.187		
42.15		1.149	206, 215	1.230
44.1	8	1.108		1.176
44.25	10	1.105		1.100

Lattice ParametersHexagonal: $a = 5.03\text{\AA}$, $c = 8.19\text{\AA}$ Cubic: $a = 6.96\text{\AA}$

Sample 7 Zr(Fe_{0.4}Mn_{0.6})₂ (Mo-target)

ϕ (°)	Intensity	d (Å) (From Bragg Equation)	hkl Hexagonal Cubic	d (Å) (From Lattice Parameters) Hexagonal Cubic
8.20		2.491		2.506
9.65	1	2.120	110 220	2.137
9.90		2.067	112 311	2.117
10.90	4	1.879	201 222	2.098
12.95		1.586		
14.45		1.424		
14.65		1.405	213 331	1.406
15.0		1.373	422	1.365, 1.364
15.6	2	1.321	005, 302 333	1.307
17.45		1.185	205	
17.75		1.166	531	1.187
20.65	3	1.094	215, 206 620	1.159, 1.155

Lattice Parameters

Hexagonal: a = 5.012Å, c = 8.190Å

Cubic: a = 7.02Å

Sample 6 Zr(Co_{0.5}Cr_{0.6})₂ (Cu-target)

ϕ (°)	Intensity	d (Å) (From Bragg Equation)	hk _l Hexagonal Cubic	d (Å) (From Lattice Parameters) Hexagonal Cubic
18.0	2	2.495	110*	2.505
19.6		2.298	103	2.309
21.25	1	2.127	112	2.136
21.75	2	2.081	201	2.097
22.0		2.058	004	2.045
22.20	6	2.041		
23.90		1.903	202	1.916
30.55		1.517	204	1.488
33.40	7	1.401	213	1.405
38.15	3	1.248	220	1.255
40.05		1.198	116	1.197
41.95	4	1.153	206, 215	1.153
44.55	5	1.099		1.250
46.2		1.068	622	1.195
				1.066

Lattice Parameters

Hexagonal: a = 5.01Å, c = 8.18Å

Cubic: a = 7.07Å

Sample 5: Zr(Co_{0.6}Mn_{0.4})₂ (Mo-target)

ϕ (°)	Intensity	d (Å) (From Bragg Equation)	hkl Hexagonal Cubic	d (Å) (From Lattice Parameters) Hexagonal Cubic
9.60	2	2.131	112	2.121
9.85	1	2.077	201	2.081
10.25	11	1.997		2.120
14.40	8	1.429	213	2.029
14.83	9	1.389	006, 302	1.435
15.28	3	1.349	511, 333	1.395
15.40	5	1.338		1.357, 1.353
16.08	7	1.283	205	1.298
16.63	4	1.242	220	1.243
17.53		1.180	440	1.243
18.93		1.156	531	1.188
19.35	6	1.096	215, 206	1.151, 1.148
19.58		1.072	620	1.112
22.25	10	1.061	533	1.072
		0.938	642	1.060
23.05		0.908	731, 553	0.939
				0.879

Lattice ParametersHexagonal: $a \approx 4.97\text{\AA}$, $c = 8.14\text{\AA}$ Cubic: $a = 7.03\text{\AA}$

Sample 4 Zr(Co_{0.4}Mn_{0.6}) (Mo-target)

ϕ (°)	Intensity	d (Å) (From Bragg Equation)	hkl Hexagonal Cubic	d (Å) (From Lattice Parameters) Hexagonal Cubic
8.73	4	2.343	103	2.309
9.35	5	2.187	200	2.165
9.63	1	2.125	112	2.134
9.95		2.057	201	2.093
12.73	3	1.613	213	1.617
14.43	9	1.426	006, 302	1.404
14.95	2	1.377	205	1.361
15.60	7	1.321	220	1.306
16.53	7	1.249	440	1.250
17.53	7	1.180	531	1.192
17.88	6	1.158	215, 206	1.158, 1.155
17.225		1.085	620	1.115

Lattice Parameters

Hexagonal: a = 5.00Å, c = 8.19Å

Cubic: a = 7.05Å

Sample 3 Zr(Co_{0.5}Mn_{0.5})₂ (Mo-target)

ϕ (°)	Intensity	d (Å) (From Bragg Equation)	hkl Hexagonal Cubic	d (Å) (From Lattice Parameters) Hexagonal Cubic
9.00	5	2.272	103	2.303
9.58	1	2.136	112	2.132
9.85	2	2.077	201	2.093
10.00	9	2.046	213	1.402
14.30	6	1.439	422	1.360, 1.361
15.15	3	1.360	511, 333	1.303
15.65	3	1.317	205	1.250
16.60	7	1.244	220	1.156, 1.152
18.40	10	1.126	215, 206	1.120
19.25	4	1.078	533	1.080
19.45	4	1.067	622	1.068
22.05	8	0.947	642	0.947
22.65	8	0.923	731, 553	0.922

Lattice Parameters

Hexagonal: a = 5.00Å, c = 8.16Å

Cubic: a = 7.085Å

Sample 2 Zr(Co_{0.6}Cr_{0.4})₂ (Mo-target)

ϕ (°)	Intensity	d (Å) (From Bragg Equation)	hk2 Hexagonal Cubic	d (Å) (From Lattice Parameters) Hexagonal Cubic
8.25		2.476		2.500
8.83		2.316	103	2.311
9.10	7	2.247		
9.50	3	2.153	112	2.141
9.60	3	2.131		
9.78	3	2.104	201	2.132
10.05	2	2.036	004	2.103
10.65		1.923	202	2.045
12.80	9	1.604	331	1.921
14.25	8	1.446	300	1.622
14.58		1.412	213	1.443
14.90		1.382	302	1.408
15.85	11	1.301	205	1.367
16.45	11	1.255	220	1.307
17.53	6	1.180		1.256
18.23	10	1.136	440	1.250
			531	1.195
			620	1.118

Lattice Parameters

Hexagonal: a = 5.025Å, c = 8.18Å

Cubic: a = 7.07Å

Sample 1 Zr(Co_{0.4}Cr_{0.6})₂ (Mo-target)

ϕ (°)	Intensity	d (Å) (From Bragg Equation)	hk ℓ Hexagonal Cubic	d (Å) (From Lattice Parameters) Hexagonal Cubic
8.05		2.538	110	2.520
8.73	11	2.343	103	2.327
9.40	4	2.176	200	2.182
9.68	2	2.114	112	2.150
9.93	7	2.062	004	2.063
11.0		1.862	104	1.865
13.40		1.533	212	1.532
14.13	5	1.456	300	1.455
14.45		1.424	213	1.415
14.98	8	1.375	302	1.372
15.60	6	1.321	205	1.316
16.10		1.281	214	1.288
16.25		1.270	220	1.260
17.55		1.178	116	1.207
17.80	10	1.162		
18.7	9	1.108		
19.2	1	1.081		
19.3	3	1.075		
23.75		0.882		
			533	1.089
			622	1.076
			800	0.893

Lattice Parameters

Hexagonal: $a = 5.04\text{\AA}$, $c = 8.25\text{\AA}$

Cubic: $a = 7.14\text{\AA}$

Hydrated SamplesSample 12A Zr(Fe_{0.6}Cr_{0.4})₂ (Mo-target)

ϕ (°)	Intensity	d (Å) (From Bragg Equation)	hkl		d (Å) (From Lattice Parameters)	
			Hexagonal	Cubic	Hexagonal	Cubic
8.83	5	2.316	103		2.328	
9.25	5	2.211	200		2.191	
9.58	1	2.136	112	311	2.156	2.136
9.68	2	2.114	201		2.118	
10.25	8	1.997	202	222	1.935	2.044
10.93		1.875	104		1.865	
12.65		1.623	210	331	1.657	1.624
13.35		1.539	212		1.537	
13.75	12	1.495	204		1.501	
14.15	13	1.454	300	422	1.461	1.445
14.55	11	1.414	213		1.419	
14.95	3	1.377	302	333, 511	1.377	1.363
15.60	4	1.321	205		1.317	
15.95		1.293	214		1.291	
16.40	5	1.259	220	440	1.265	1.252
16.83		1.228	116		1.207	
17.75	8	1.166		531		1.197
18.65	8	1.111		620		1.119

Lattice ParametersHexagonal: $a = 5.061\text{Å}$, $c = 8.241\text{Å}$ Cubic: $a = 7.08\text{Å}$

Sample 11A Zr(Fe_{0.5}Cr_{0.5})₂ (Mo-target)

ϕ (°)	Intensity	d (Å) (From Bragg Equation)	Hexagonal hkℓ	Cubic	d (Å) (From Lattice Parameters) Hexagonal Cubic
8.30	7	2.462	103		2.462
9.05	1	2.259	112	311	2.261
9.40		2.176	004		2.185
9.45		2.164			
9.55		2.142	202	222	2.165
10.23	2	2.002	104		2.035
12.13		1.692	212		1.974
13.35		1.539	300	422	1.615
13.73	3	1.498	213		1.533
14.15	6	1.454	302	511, 333	1.493
14.75	3	1.396	205		1.446
15.88	5	1.299	220		1.392
16.35		1.262	116	531	1.328
16.75	10	1.233	215, 206		1.277
17.65	40	1.172			1.233, 1.231
18.0	8	1.150		620	1.186
18.35		1.129		533	1.150
21.08	9	0.988		622	1.131
				642	1.002

Lattice Parameters

Hexagonal: $a = 5.31\text{\AA}$, $c = 8.74\text{\AA}$

Cubic: $a = 7.50\text{\AA}$

Sample 10A Zr(Fe_{0.4}Cr_{0.6})₂ (Mo-target)

ϕ (°)	Intensity	d (Å) (From Bragg Equation)	hk ℓ Hexagonal Cubic	d (Å) (From Lattice Parameters) Hexagonal Cubic
8.33	8	2.454	103	2.453
8.45	9	2.418		
9.03	1	2.265		
9.15	1	2.235	311	2.234
10.20	6	2.007		
10.45		1.959	202	2.006
12.10		1.695	104	1.972
12.58		1.632	210	1.705
13.13		1.565	212	1.589
13.30		1.545	204	1.572
13.68	4	1.503		
13.78	4	1.492	300	1.504
14.20	3	1.449	213	1.473
14.30		1.439	302	1.423
14.78	2	1.393		
15.35	7	1.342	205	1.385
15.63		1.319	214	1.346
15.93		1.295		
16.45		1.255	220	1.303
16.80	13	1.229	116	1.275
17.70	10	1.169	206, 215	1.227, 1.223
18.0	12	1.150		
18.75	14	1.105		
21.10	11	0.987	620	1.172
			511, 393	1.426
			440	
			531	
			422	
			331	

Lattice Parameters

Hexagonal: a = 5.21Å, c = 8.77Å

Cubic: a = 7.41Å

Sample 4B $Zr(Co_{0.4}Mn_{0.6})_2$ (Mo-target)

ϕ (°)	Intensity	d (Å) (From Bragg Equation)	hkl Hexagonal	Cubic	d (Å) (From Lattice Parameters) Hexagonal	Cubic
8.20	8	2.491	103		2.490	
8.95	1	2.284	112	311	2.269	2.279
9.25	10	2.211	201	222	2.213	
9.35	7	2.187	202		2.033	2.182
9.73		2.104	104		2.001	
10.23	2	2.002		422		1.543
13.35		1.539	300		1.523	
13.48	3	1.525	213		1.493	
13.58		1.514	302		1.474	
13.85	6	1.484		511, 333	1.454	1.455
14.15		1.454	205		1.405	
14.55	4	1.414	214		1.364	
15.13	5	1.362		440		1.336
15.28		1.349	220		1.319	
15.70	9	1.313	116	531	1.293	1.278
16.35	11	1.262		620		1.195
17.3	11	1.195		533		1.153
17.9		1.156		622		1.140
18.15		1.141				

Lattice Parameters

Hexagonal: $a = 5.276\text{Å}$, $c = 8.904\text{Å}$

Cubic: $a = 7.56\text{Å}$

Sample 1D Zr(Co_{0.4}Cr_{0.6})₂ (Mo-target)

ϕ (°)	Intensity	d (Å) (From Bragg Equation)	hkl Hexagonal Cubic	d (Å) (From Lattice Parameters) Hexagonal Cubic
8.30	7	2.462	103	2.473
8.88	3	2.303	200	2.300
9.08	1	2.253	112	2.273
9.15		2.235	201	2.225
9.30		2.200	004	2.200
10.23	6	2.002	202	2.038
10.40		1.968	104	1.985
11.43		1.794	210	1.738
12.70		1.616	212	1.617
13.25		1.550	204	1.590
13.55	4	1.517	300	1.533
14.08	2	1.461	302	1.448
14.70		1.400	220	1.398
15.35	5	1.342	220	1.328
16.5	10	1.251	116	1.284
16.98		1.217		
17.50	8	1.182	620	1.205
18.0	9	1.150	533	1.162
20.45		1.017	622	1.149
			642	1.018

Lattice Parameters

Hexagonal: a = 5.31Å, c = 8.80Å

Cubic: a = 7.62Å

VITA AUCTORIS

The author was born in Windsor, Ontario, Canada,
on November 26, 1957.

Education:

Secondary School Diploma, Level IV,
obtained at W.D. Lowe Secondary
School, Windsor, Ontario, Canada,
1975.

Secondary School Diploma, Level V,
obtained at W.D. Lowe Secondary
School, Windsor, Ontario, Canada,
1976.

B.A.Sc. in Engineering Materials,
obtained at the University of Windsor,
Windsor, Ontario, Canada, 1980.

Societies:

American Society for Metals (ASM)

American Institute of Mining, Metallur-
gical and Petroleum Engineers (AIME)

Canadian Institute of Mining and
Metallurgy (CIM)

Canadian Hydrogen Energy Society (CHES)

**Professional
Associations:**

Pending registration through residence
requirements for the Association of
Professional Engineers of Ontario
(APEO)

PUBLICATIONS

"Metal Hydrides for Energy Storage," D.G. Ivey and D.O. Northwood, Canadian Metallurgical Quarterly, In Press, November, 1981.

"Metal Hydrides for Energy Storage," D.G. Ivey, D.O. Northwood, R.I. Chittim, and K.J. Chittim, Journal of Materials for Energy Systems, Accepted for publication, October, 1981.

"Storing Energy in Metal Hydrides: A Review of the Physical Metallurgy," D.G. Ivey and D.O. Northwood, Submitted to Journal of Materials Science, October, 1981.

THESES CANADIENNES SUR MICROFICHE



National Library of Canada
Collections Development Branch

Canadian Theses on
Microfiche Service

Ottawa, Canada
K1A 0N4

Bibliothèque nationale du Canada
Direction du développement des collections

Service des thèses canadiennes
sur microfiche

NOTICE

The quality of this microfiche is heavily dependent upon the quality of the original thesis submitted for microfilming. Every effort has been made to ensure the highest quality of reproduction possible.

If pages are missing, contact the university which granted the degree.

Some pages may have indistinct print especially if the original pages were typed with a poor typewriter ribbon or if the university sent us a poor photocopy.

Previously copyrighted materials (journal articles, published tests, etc.) are not filmed.

Reproduction in full or in part of this film is governed by the Canadian Copyright Act, R.S.C. 1970, c. C 30. Please read the authorization forms which accompany this thesis.

THIS DISSERTATION
HAS BEEN MICROFILMED
EXACTLY AS RECEIVED

AVIS

La qualité de cette microfiche dépend grandement de la qualité de la thèse soumise au microfilmage. Nous avons tout fait pour assurer une qualité supérieure de reproduction.

S'il manque des pages, veuillez communiquer avec l'université qui a conféré le grade.

La qualité d'impression de certaines pages peut laisser à désirer, surtout si les pages originales ont été dactylographiées à l'aide d'un ruban usé ou si l'université nous a fait parvenir une photocopie de mauvaise qualité.

Les documents qui font déjà l'objet d'un droit d'auteur (articles de revue, examens publiés, etc.) ne sont pas microfilmés.

La reproduction, même partielle, de ce microfilm est soumise à la Loi canadienne sur le droit d'auteur, SRC 1970, c. C 30. Veuillez prendre connaissance des formules d'autorisation qui accompagnent cette thèse.

LA THÈSE A ÉTÉ
MICROFILMÉE TELLE QUE
NOUS L'AVONS REÇUE

metabolism in growing and developing cells, oligonucleotide maps and primary sequence data for the 25s, 17s and 5s RNA's was obtained (Batts-Young et al., 1980). This work concluded that the 5s rRNA sequence was unchanged and that no detectable changes could be observed in the 25s and 17s RNA in developing cells and in their vegetative counterparts. Although this work did not address itself to limited modifications such as methylation, it appears to rule out the idea of novel rRNA expression during development. In a related piece of work from the same laboratory, an extensive investigation was made into rRNA synthesis and degradation during cell differentiation (Mangiarotti et al., 1981). By using double labelling techniques these workers showed that the same fraction of old and new 60s ribosomal subunits, and old and new 40s subunits are found in polysomes during development. This contradicts earlier findings of Cocucci and Sussman (1961) and concludes that ribosomes synthesized during growth and differentiation are functionally indistinguishable. They also concluded that the rate of synthesis of rRNA during development is much slower than in growing cells and thus the replacement of vegetative stage ribosomes with those synthesized during differentiation is a slow and incomplete process. This conclusion is also in variance with Cocucci and Sussman (1970) who claimed that the majority of polysomes present during development contained new ribosomes. Mangiarotti

clearly lack hnRNA (Rosbach *et al.*, 1977; Timberlake, 1980), and thus is foundational for establishing Dictyostelium as a model for studying gene regulation in higher eukaryotes.

The messenger RNA (mRNA) of Dictyostelium is typically eukaryotic. It is transcribed from the DNA as a 500,000 dalton hnRNA species by an α -amanitin sensitive, DNA dependent RNA polymerase. The hnRNA is 70% transcribed from unique single copy regions on the DNA while 25% is transcribed from repetitive regions present in several hundred copies per genome (Firtel and Lodish, 1973). This repetitive region appears at the 5' end and is not conserved during processing. Another unique feature of the hnRNA molecule is the presence of a transcribed oligo (dT) region of about 25 base pairs (Jacobsen *et al.*, 1974). This region is conserved during processing and is localized near the 3' end of the molecule.

As is typical of eukaryotic mRNA the addition of a 3' poly (A) 'tail' and a 7-methyl-guanosine 'cap' completes the processing. The poly(A) 'tail' initially has a modal size length of about 110 to 115 nucleotides which shortens with ages to about 60 to 65 nucleotides (Palatnik *et al.*, 1979). Palatnik and coworkers have extensively examined the poly(A) metabolism and the role of the poly(A) tail. They conclude that it is unclear whether it has a significant regulatory role (Palatnik *et al.*, 1980). It does not play a role in the stability of the mRNA population as a whole, and does

Table 1. Quantitation of the polyadenylic acid containing RNA in the dormant spores of the cellular slime mold Dictyostellium discoideum

RNA (mg)	³ H-Poly(U) Hybridized			Poly(A) Hybridized		
	DPM (10 ⁻³)	uCi (10 ⁻³)	Moles (10 ⁻⁷)	Moles (10 ⁻⁷)	RNA (ug/mg) + Poly(A) RNA	
1. .021	17.0	7.73	1.55	1.55	0.24	2.84
.042	34.5	15.68	3.14	3.14	0.25	2.96
.084	59.1	26.87	5.37	5.37	0.21	2.49
2. .042	34.8	15.84	3.17	3.17	0.25	2.96
.084	64.1	29.13	5.83	5.83	0.23	2.73

Table 3. Comparison of charge ratios in dormant spores and vegetative amoebae of *Dictyostelium discoideum*

trNA Preparation	Activity (CPM/ug trNA)	Percent Charged
Control spore trNA	1939.8	20.8
Oxidized spore trNA	402.9	
Control vegetative trNA	1670.1	45.8
Oxidized vegetative trNA	764.5	

